THE UNIVERSITY OF MICHIGAN
OCT 28 1959
ENGINEERING LIBRARY

THE AERONAUTICAL QUARTERLY

A Journal devoted to Aeronautics and the Allied Sciences

Volume X AUGUST 1959 Part 3

CONTENTS

Trends in the Development of Liquid Propellant Rocket Engines — *E. G. D. Andrews and A. W. T. Mottram*

Quasi-Steady Derivatives for the Subsonic Flow past an Oscillating Aerofoil in a Porous Wind Tunnel — *D. G. Drake*

Plasto-Elastic Stress Distributions in Lugs — *H. Fessler and D. J. Haines*

Notes on Thin Wing Theory at Low Supersonic Speeds. Part I — *G. J. Hancock*

Symmetrically Loaded Circular Plates under the Combined Action of Lateral and End Loading — *R. Hicks*

The Drag of Ducted Bodies with Annular or Side Intakes in Supersonic Flow — *H. Portnoy*

Review of "The Potential Theory of Unsteady Supersonic Flow" by J. W. Miles — *L. E. Fraenkel*

LONDON

ROYAL AERONAUTICAL SOCIETY

4 HAMILTON PLACE W1

15/-

THE AERONAUTICAL QUARTERLY

Editorial Board

Dr. A. M. BALLANTYNE, T.D., B.Sc., Ph.D., Hon.F.C.A.I. F.I.A.S., F.R.Ae.S. (*Chairman*)

Mr. HAYNE CONSTANT, C.B., C.B.E., M.A., F.R.S., F.R.Ae.S.

Sir HAROLD ROXBEE COX, D.Sc., D.I.C., Ph.D., F.I.A.S., F.R.Ae.S.

Sir WILLIAM FARREN, C.B., M.B.E., M.A., D.Sc., F.R.S., Hon.F.I.A.S., Hon.F.R.Ae.S.

Sir ARNOLD HALL, M.A., F.R.S., F.R.Ae.S.

Sir BENNETT MELVILL JONES, C.B.E., A.F.C., M.A., F.R.S., Hon.F.I.A.S., Hon.F.R.Ae.S.

Sir ALFRED PUGSLEY, O.B.E., D.Sc., F.R.S., F.R.Ae.S.

Sir GEOFFREY TAYLOR, M.A., D.Sc., F.R.S., Hon.F.R.Ae.S.

Dr. P. B. WALKER, C.B.E., M.A., F.R.Ae.S.

Editor—E. C. PIKE, M.A., A.F.R.Ae.S.

Editorial Referees

Aerodynamics

(a) *General*

Sir LEONARD BAIRSTOW
Mr. D. KEITH-LUCAS
Prof. W. A. MAIR
Mr. L. F. NICHOLSON
Dr. R. C. PANKHURST
Mr. E. F. RELF
Prof. E. J. RICHARDS
Dr. B. THWAITES

(b) *Fluid Motion*

Dr. G. K. BATCHELOR
Mr. A. FAGE
Dr. D. W. HOLDER
Prof. L. HOWARTH
Dr. W. P. JONES
Dr. J. W. MACCOLL
Prof. J. H. PRESTON
Prof. H. B. SQUIRE
Prof. G. TEMPLE
Prof. G. N. WARD
Prof. A. D. YOUNG

(c) *Stability and Control*

Mr. L. W. BRYANT
Mr. S. B. GATES
Mr. H. B. IRVING
Mr. G. H. LEE
Mr. M. B. MORGAN
Mr. H. H. B. M. THOMAS

Helicopters and Propellers

Prof. J. A. J. BENNETT
Mr. P. BRETT
Mr. L. G. FAIRHURST
Mr. R. HAFNER
Dr. G. S. HISLOP
Capt. R. N. LIPTROT

Instruments and Electrical Equipment

Dr. G. E. BAIRSTO
Sir GEORGE GARDNER
Dr. C. S. HUDSON
Mr. C. N. JAQUES
Mr. F. W. MEREDITH

Aircraft Design

Mr. R. BOORMAN
Mr. R. M. CLARKSON
Mr. A. N. CLIFTON
Mr. H. H. GARDNER
Mr. H. KNOWLER
Mr. W. E. W. PETTER
Mr. F. H. POLLICUTT
Dr. A. E. RUSSELL
Mr. R. S. STAFFORD
Mr. W. H. STEPHENS

Radio and Radar

Mr. J. F. ATHERTON
Mr. B. G. GATES
Dr. R. L. SMITH ROSE
Dr. A. M. UTTLEY
Sir ROBERT WATSON-WATT

Aviation Medicine

Dr. K. G. BERGIN
Dr. A. BUCHANAN BARBOUR

Meteorology

Sir DAVID BRUNT
Mr. J. K. HARDY
Prof. P. A. SHEPPARD

Sound

Mr. W. MAKINSON
Mr. F. B. GREATREX
Mr. N. FLEMING

Aircraft Propulsion

Mr. A. D. BAXTER
Mr. A. V. CLEAVER
Sir A. H. ROY FEDDEN
Dr. S. HOOKER
Mr. A. R. HOWELL
Mr. W. H. LINDSEY
Mr. P. LLOYD
Dr. A. W. MORLEY
Dr. E. S. MOULT
Mr. N. S. MUIR
Mr. F. NIXON
Mr. F. M. OWNER
Mr. H. PEARSON
Sir DAVID PYE
Mr. H. SAMMONS
Prof. O. A. SAUNDERS
Prof. A. G. SMITH

Air Transport

Mr. A. C. CAMPBELL ORDE
Mr. P. G. MASEFIELD
Mr. N. E. ROWE
Mr. B. S. SHENSTONE
Mr. W. TYE

Aircraft Accessories

Mr. A. E. BINGHAM
Mr. W. C. CLOTHIER
Mr. H. G. CONWAY
Sir GEORGE DOWTY
Mr. R. GRAHAM
Mr. C. D. HOLLAND

Performance

Mr. H. DAVIES
Mr. D. R. NEWMAN
Mr. A. H. YATES

Flight Testing

Mr. R. R. DUDDY
Mr. P. A. HUFTON
Mr. E. T. JONES
Mr. S. SCOTT HALL
Mr. H. L. STEVENS

Structures

Prof. J. H. ARGYRIS
Mr. A. C. BROWN
Mr. H. L. COX
Mr. D. J. FARRAR
Prof. W. S. HEMP
Prof. R. HILL
Mr. H. B. HOWARD
Col. H. T. JESSOP
Mr. E. D. KEEN
Mr. F. A. KERRY
Dr. D. M. A. LEGGETT
Mr. R. L. LICKLEY
Prof. A. J. SUTTON PIPPARD
Prof. S. C. REDSHAW
Mr. R. H. SANDIFER
Sir RICHARD SOUTHWELL

Fuels and Oils

Mr. E. L. BASS
Dr. J. W. DRINKWATER
Prof. F. H. GARNER
Prof. W. E. GARNER
Dr. K. E. W. RIDLER
Dr. C. G. WILLIAMS

Materials

Dr. L. AITCHISON
Dr. N. P. ALLEN
Mr. G. FORREST
Prof. N. F. MOTT
Mr. L. ROTHERHAM
Dr. H. SUTTON
Dr. C. SYKES

Vibration and Flutter

Mr. E. G. BROADBENT
Prof. A. R. COLLAR
Prof. W. J. DUNCAN
Dr. R. A. FRAZER
Mr. H. TEMPLETON
Mr. M. O. W. WOLFE

Trends in the Development of Liquid Propellant Rocket Engines

E. G. D. ANDREWS, A.M.I.Mech.E., and A. W. T. MOTTRAM, B.Sc.

(*Bristol Siddeley Engines Limited*)

SUMMARY: The authors predict that rocket engines will fall into two categories. In both, combustion pressures will approach 200 atmospheres to attain optimum vehicle performance, balancing increased pumping losses and engine mass against increased expansion efficiency and reduced dissociation. For general purposes, engines will be intrinsically convenient: storable propellants will give specific impulses around 270 lb. sec./lb., and engine specific weights will be between 0·02 and 0·03. For exacting applications, the greatest overall convenience may necessitate using unpleasant propellants so as to obtain the highest performance. Immediate research into the use and handling of these is essential if future engine development is not to be hampered.

1. Introduction

The design of liquid propellant rocket engines is not yet a complete science, and many aspects of their design can still be resolved only by extensive development of actual components. Nevertheless, a clear pattern is beginning to emerge, and recent engines manufactured by widely scattered organisations have many features in common. An opinion that the art is reaching maturity might well be supported by the fact that many of these lend themselves fairly readily to the solution of problems posed by more exacting requirements. This seems to be an appropriate time, therefore, to determine the objectives to which our efforts should be directed in the future.

The relative importance of various engine characteristics in terms of overall vehicle performance has already been discussed by a number of authorities[1, 2]. The authors intend in this paper to consider the engine design rather than the vehicle performance; in this context the more important considerations are the attainment of

(*a*) the highest specific impulse,

(*b*) the highest propellant density,

(*c*) the lowest wet engine mass,

(*d*) the maximum operational convenience.

Received June 1959.

[The Aeronautical Quarterly, Vol. X, August 1959]

In any particular application there is an equivalence between specific impulse, propellant density and engine mass, this equivalence being heavily weighted in favour of high specific impulse. The wet engine mass has the least influence, but it is necessary to remember that when the limit has been reached in specific impulse and propellant density it is the only factor amenable to improvement.

There is no such equivalence in terms of operational convenience, which in the opinion of the authors may be the most important consideration.

2. The Highest Specific Impulse

The true dimension of specific impulse is velocity, and if consistent units were used the value obtained for this parameter would also be numerically identical with the mean velocity of the gases exhausted from the engine. In theory, the highest gas velocity is attained when the heat of reaction of the propellants is a maximum and is totally converted into kinetic energy, that is

$$\text{S.I.}_{\max} = \sqrt{\left(\frac{2HJ}{g}\right)},$$

where H is the heat of reaction and J is the mechanical equivalent of heat. Calculated values for some propellant combinations are shown in Table I.

These figures represent the theoretical limit of chemical rocket performance and are not attainable in practice, partly because of dissociation and partly because complete expansion of the exhaust gases cannot be achieved usefully.

At the pressures commonly used in rocket engines at the present time there is no great difference (about ten per cent) between the performance of the two bipropellant systems liquid oxygen/kerosine and hydrogen peroxide/kerosine. In considering future developments, however, it is important to note that approximately one third of the chemical energy of the liquid oxygen/kerosine combination is lost through dissociation whereas, owing to the large quantity of water

TABLE I

PERFORMANCE LIMIT FOR VARIOUS PROPELLANT COMBINATIONS

Oxidant	*Fuel*	*Mixture Ratio*	S.I.$_{\max}$ (lb. sec./lb.)
Oxygen	Hydrogen	8:1	574·8
Oxygen	Methane	4:1	481
Oxygen	Kerosine	3·43:1	466·5
Oxygen	Hydrazine	1:1	449
Fluorine	Hydrogen	9:1	900
Fluorine	Hydrazine	1·13:1	707
85% H.T.P.	Hydrogen	20:1	434·9
85% H.T.P.	Kerosine	8·56:1	376
100% H.T.P.	Hydrogen	17:1	470
100% H.T.P.	Kerosine	7·28:1	397·5

present in the decomposition products of hydrogen peroxide, the combustion temperature with kerosine is so low as to make dissociation effects less significant. Of the remaining energy from either combination, approximately half is lost through incomplete expansion through the nozzle.

To suppress dissociation it is essential to work with very high combustion pressures. To obtain high expansion efficiency it is essential to use very high expansion ratios and for operation near the ground at any rate this requires very high combustion pressures also. However the propellants have to be pumped into the combustion chamber (pressurised tanks and solid charges are not considered here) and high combustion pressures presuppose high pumping horsepowers. When considering optimum performance, therefore, it is necessary to determine the cycle efficiency, a practice which is almost unknown in the literature—Malina[3] making the only reference known to the authors.

In a regenerative cycle[4], the highest efficiency is attained with the highest possible combustion pressure, but in a cycle in which the turbine exhausts to atmosphere, the pumping losses are higher and there is an optimum combustion pressure[5].

Rough calculations made in the absence of precise data indicate that optimum combustion pressures are nearly an order higher than present practice, say 3000 lb./in.^{2} or so, depending on the propellants.

The difficulties of working with combustion pressures of this order are considerable. In the chamber itself the temperatures will be higher because of the effect of pressure on dissociation, the density will be higher and the velocity will be higher. Although the volume of the combustion chamber can probably be reduced roughly in inverse proportion to the square of the pressure[6], and hence the surface area to be cooled is reduced while the propellant flow available to cool it is increased per unit area, the increase in local heat transfer rate necessary to keep the wall cool is nevertheless large. Present cooling techniques may go some way towards solving these problems, but at the moment this seems doubtful, and completely new techniques may have to be developed.

Reference has been made to the reduction in combustion chamber volume: this probably means that the mass flow of propellants through it per unit cross-sectional area will be an order above the present levels, which may introduce new combustion problems.

At present the efficiencies of rocket components other than the combustion chamber are of small importance because the propellants expended in driving them are a negligible percentage of the total mass flow. Severe limitations on their efficiency are accepted for the sake of lightness and simplicity. Now pump inefficiency results in an increase in propellant temperature and is not in itself serious, but because the propellants used to drive the turbine are also used inefficiently the efficiencies of the pumps and turbine are important in an optimum cycle.

The problem of using as much as possible of the energy of the propellants that drive the turbine is similar to the problem of obtaining the highest gas velocity from the combustion chamber, and one may assume that the gas generator pressure will be similar to the combustion chamber pressure. Because it is normally necessary to obtain maximum turbine power at sea level, however, there is no point in attempting to use the same pressure ratio as in the combustion chamber nozzle which is usually over-expanded at sea level. Indeed to make most use of the residual energy in the exhaust gases it may be desirable to maintain at least a critical pressure ratio across the turbine exhaust, and to fit an expansion nozzle to obtain benefit at great altitudes. Even so the overall pressure ratio across the turbine is very great and cannot be employed in a single stage with reasonable efficiency, and at least two compounded stages must be used.

There are four principal reasons why a regenerative cycle does not appear to be suitable for this application. The first is that it would be prohibitively heavy to enclose the turbine discs in a casing capable of withstanding the combustion chamber pressure (with a two-stage independent turbine, the casing pressure of the high pressure stage is only a few per cent of the combustion chamber pressure because of the pressure drop across the inlet nozzles). The second is that the problem of sealing the turbine shaft against a pressure of several hundred atmospheres appears to be impracticable whereas with the system proposed the rotor assembly can be overhung from the low pressure stage and the pressure to be sealed need be no more than about 30 lb./in.^{2} The third reason is that a regenerative system imposes restrictions on the design of the combustion chamber and may not provide optimum conditions for obtaining high combustion efficiency. In practice it may be convenient to separate the turbo-pump unit from the combustion chamber in order to reduce the inertia of the parts that must be swivelled to control the vehicle: this is the fourth reason.

With conventional combustion chamber pressures, the two objections to the use of very high nozzle expansion ratios are the size of the nozzle required and the fact that the improved performance is not obtained at low altitudes. Using very high combustion chamber pressures, however, the cross-sectional area of the throat is reduced, roughly proportionally to the pressure; also, because of the increased gas velocity, the area at the end of the expansion cone is slightly reduced for the same back pressure. A pressure ratio ten times as high can thus be obtained with a nozzle very little longer than conventional nozzles, and an improvement in specific impulse of some 20 per cent may be obtainable from this cause alone. For better performance at high altitudes a greater expansion ratio is desirable, and because there are grounds for thinking that over-expansion in the nozzle at low altitudes can be suppressed by suitable design, it is probable that the full benefit of large nozzles can be realised even for ground launched vehicles. Using high combustion chamber pressures, the improvement in specific impulse obtained with increasing altitude is less than with current combustion chamber pressures.

The use of high energy propellants is, of course, subject to the same general design considerations. In the circumstances prevailing in the United Kingdom,

TABLE II

COMPARISON OF KEROSINE AND ALUMINIUM AS FUELS FOR USE WITH HYDROGEN PEROXIDE

Fuel	*Heat of Combustion*	
	B.t.u./lb. fuel	B.t.u./lb. mixture
Kerosine	19,000	4,285
Aluminium	10,300	5,450

the authors do not see much prospect of high energy oxidants being used in the near future. Quite apart from any technical considerations, the production of fluorine or ozone would have to be increased by several orders over the present levels. By the time that this amount of capital expenditure becomes worthwhile it is likely that the development of nuclear power will have reached the point where its application to rocket propulsion becomes feasible. In this respect, a propulsion system intermediate between the chemical and nuclear rockets seems to offer attractive possibilities. The difficulties associated with the transfer of heat at high temperatures from a nuclear reactor to the working fluid are formidable, and early nuclear rockets are expected to operate with gas temperatures well below those theoretically desirable. A chemical reaction subsequent to preheat of the propellants in an atomic reactor may offer a significant improvement in performance, while operating with the reactor temperature sufficiently low as to minimise the risk of radioactive contamination of the exhaust due to structural failure of the pile. The nuclear reactor could also provide power to drive the propellant pumps.

More proximately, the performance of chemical rockets can be increased by the use of higher energy fuels which may be already available in the United Kingdom or could be produced with less capital outlay than that required for high energy oxidants. Typical of these are metals such as aluminium and hydrazine, which is available as the hydrate in tonnage quantities. Aluminium metal, possibly in the form of a slurry, may be of particular benefit in hydrogen peroxide engines[7]. There are two reasons for this. First, although the heat of combustion of aluminium is low by comparison with that of kerosine, the reverse is true if the oxygen used in combustion is also taken into account (*see* Table II); thus, although aluminium has little merit as a heat source in an air-breathing engine, it has merit in a rocket engine. Secondly, the specific heat of aluminium oxide is low so that a large proportion of the heat of combustion is still available at the reaction temperature of hydrogen peroxide/kerosine. Because the large amount of water present has a relatively low molecular weight, the resulting increase in temperature may more than compensate for the inability of the aluminium oxide to do expansive work.

The choice is not limited to aluminium. There are numerous metals and alloys available, some of which have low melting points and high boiling points. They are excellent as coolants.

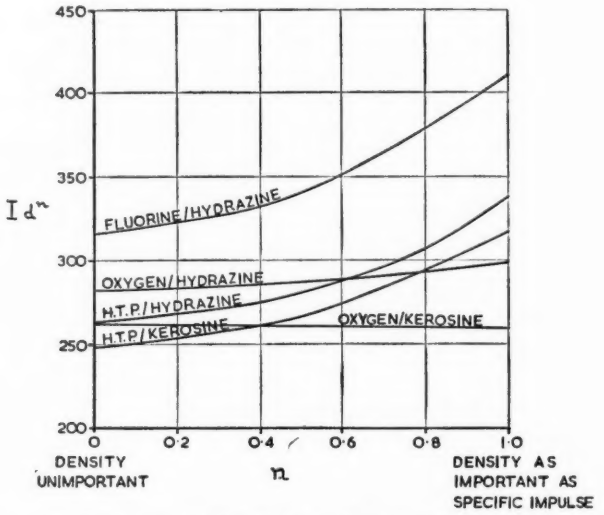

FIGURE 1. Performance index Id^n for various propellant combinations. Expansion from 500 lb./in.^{2} abs. to 14·7 lb./in.^{2} abs.

3. The Highest Propellant Density

The major importance of propellant density lies in its effect on the design of the complete rocket-propelled vehicle, where a large proportion of the "all-burnt" mass is taken up in the structure of the tanks and where aerodynamic drag may assume significant proportions. The relation between density and specific impulse is substantially fixed by the physical and chemical properties of the propellants and the question is one of choice. For this purpose the particular specification of the vehicle must be considered; there is no hard and fast rule applicable to all cases. Rough calculations show, however, that the specific impulse is between five and ten times as important as the density. A performance index Id^n, where I is the specific impulse and d the relative density, is plotted in Fig. 1. n is an arbitrary exponent which signifies the relative importance of d. The mixture ratio is assumed constant and the curves do not therefore represent optimum conditions. For this reason, the performance of hydrogen/oxidant combinations is not shown: because of the low density of liquid hydrogen, mixture ratio is a critical variable.

The effect of propellant density on the engine design is of more concern in the present context. In the light of the high chamber pressures which will be used, the power demanded by the propellant pumps will be of prime importance. For a given mass flow and supply pressure, the useful work done in pumping the propellants will be inversely proportional to the density. An increase in propellant density will therefore effect a corresponding decrease in turbo-pump power requirements. By way of illustration, the mean propellant density of hydrogen peroxide/kerosine is some 29 per cent greater than that of liquid oxygen/kerosine. This will have a significant effect on the size and weight of the

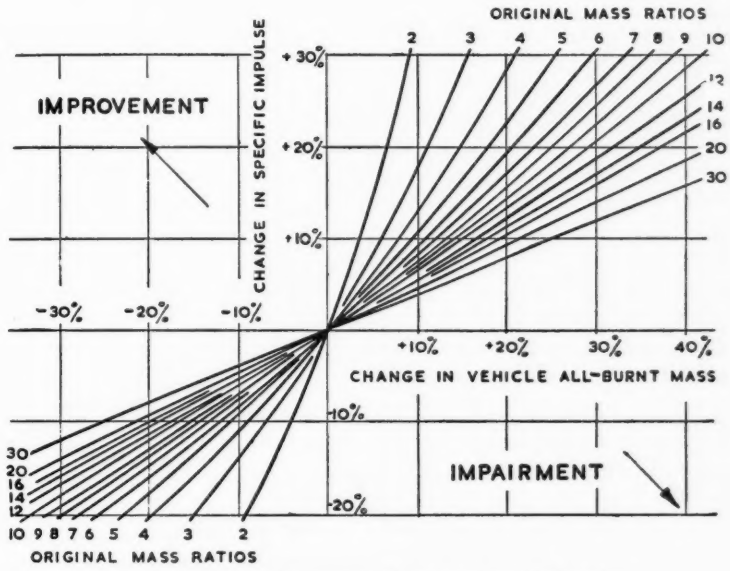

FIGURE 2. Relative importance of mass and specific impulse.

turbine. The pumps themselves will be reduced in size because of the higher density, and also to some extent because it should be possible to run them at higher rotational speeds, which will benefit the turbine also. Generally speaking, the propellant feed system will be the more compact the higher the density. This applies to pipes, valves and coolant passages as well as to the turbo-pump assembly.

The weight reduction that may be expected to accrue from these considerations will be offset to some extent by the fact that the optimum combustion pressure will be somewhat higher for the denser propellants. For this reason, it is difficult to determine the overall effect on engine weight of variations in density, without a design study beyond the scope of this paper.

4. The Lowest Wet Engine Mass

In rocket engineering the term weight is used loosely and it is nearly always mass that is implied. One exception to this is during a static launch when the thrust must exceed the weight of the loaded vehicle. We will therefore consider the means by which the mass of the engine may be made as small as possible at the time when the flame is extinguished. This distinction between wet engine mass and dry engine mass is important because the wet engine mass determines vehicle performance.

Consequent upon an increase in combustion pressure to increase the specific impulse, there will probably be some mass penalty. The effect of this on vehicle

performance is to detract from the benefits resulting from increased specific impulse, and in some conditions there may be no overall improvement. The relative importance of mass and specific impulse depends on the factors that are considered constant, but not all the combinations of these factors are capable of generalised presentation. If thrust and total impulse are considered to be constant, however, which is a realistic case in that it does not require complete redesign of the vehicle, the change of specific impulse which just offsets a change of "all-burnt" vehicle mass can be shown for various single-stage vehicles as in Fig. 2. In this figure the "original mass ratio" is that obtaining before the proposed changes are incorporated. The wet engine mass in current practice is usually from one to two per cent of the gross mass at launch. Taking a vehicle with a mass ratio of ten, an increase in specific impulse of ten per cent permits the wet engine mass to be approximately doubled before the vehicle performance is impaired.

It is for this reason that raising the combustion pressure to improve the specific impulse appears to be justified. Moreover the increase in engine mass resulting from these increased pressures is probably less than one might suppose at first sight.

Considering first the combustion chamber, the volume of the combustion zone is proportional to the time required for mixing and reaction. Because the combustion temperature and the concentration of the reactants are both increased as the chamber pressure is increased, the required time of stay of the gases in the combustion zone is reduced. Now for an ideal pressure vessel, its mass is proportional to the product of its volume and the design pressure: if, as happens in this case, the volume is reduced more rapidly than the pressure is increased, the mass of the combustion chamber itself is actually reduced.

With higher chamber pressures, increased expansion down to the same absolute back pressure is achieved by a short length of additional nozzle just downstream of the new throat; this is because the throat area is almost inversely proportional to the combustion pressure. Because the gas velocity is increased, the exhaust end of the expansion nozzle is slightly smaller in diameter at the same absolute pressure when the chamber pressure is raised.

One may safely say, therefore, that increase in chamber pressure should not appreciably change the mass of the chamber.

It is highly probable that the mass of the turbo-pump unit would be increased. The horsepower generated is proportional to the injection pressure of the propellants and it seems probable that the mass would be increased in somewhat similar proportion to the horsepower. Taking the mass of the turbo-pump unit in conventional rocket engines as one quarter of the engine mass, we may therefore assume that the total effect of increasing the combustion pressure by an order would be to increase the engine mass by a factor of about three.

As the pressure for optimum performance is approached, the engine mass increases more rapidly than the specific impulse increases, and the effect of this

change of mass must be taken into account in determining the optimum chamber pressure.

5. The Maximum Operational Convenience

Development of rocket engines to have the highest performance is essential, but it must never be forgotten that achievement of this is not an end in itself: in every case the engine is required to propel a vehicle to perform some mission, and each limitation on use that must be imposed in order to run the engine reduces the effectiveness of the vehicle. This is so, regardless of the mission for which the vehicle is designed, although the emphasis may change from one mission to another.

Convenience is a qualitative matter difficult to discuss without vagueness, but it is so important that reference to it must be made here.

Considerations of convenience begin with raw materials and end with completion of the mission. Inasmuch as convenience determines the amount of human effort required to fulfil the mission, either in terms of safety precautions, servicing, training, provision of fixed installations, size of vehicle, duplication of vehicles or research and development, the measure of convenience is the cost of the programme. Too little is known at present about the influence of technical decisions on the total cost for this to be a precise criterion, however, and considerable discretion must be exercised.

The authors believe that no engine characteristic is more important than reliability. This must be qualified. Absolute reliability, in the sense that without servicing nothing whatever can go wrong with any engine at any time during its rated life, can be guaranteed only by an infinite development expenditure—it is suggested that development cost is an inverse function of the statistical unreliability—even assuming that inspection techniques are adequate to ensure complete consistency between engines. In most cases it is cheaper to accept the probability of a few failures and allow for them by periodic inspection or provision of additional vehicles.

There are, however, some types of failure which are acceptable and some which are not. Because rocket engines are normally used on one mission only, some deterioration may be permissible provided no serious mechanical damage ensues. For ground launched applications, occasional failure to start may be permissible. For air launched applications, such as second or third stages, failure to start is as undesirable as complete shutdown of the engine, but even this is preferable to failures which create conditions in which explosions or detonations can occur. Failures of the latter type are quite intolerable, and all engines with which the authors have been associated have had control systems so interlocked that failures of that type were most unlikely. Other safety features were incorporated also to prevent serious failure, even though the additional parts did lower the theoretical reliability of the engines.

One of the most serious causes of engine failure is corrosion, which is most difficult to overcome completely. Techniques have been developed to circumvent this problem—the Gamma engine in Black Knight owes much of its reliability to these—and recent development in the use of non-metallic materials appears to offer hopes of overcoming the problem entirely. These, with other developments, indicate that rocket engines will become increasingly reliable, until the user need adopt no check firing procedures. This will represent a marked advance in operational convenience. It should perhaps be noted that for many applications engine reliability might well be increased if the user accepted the rocket engine as basically a one shot device: simply because it is possible to do so, he often requests that the engine be capable of repeated firings without stripping, and more elaborate control systems are often fitted to cater for this. Long life rocket engines can be, and have been, developed for suitable applications[1], however.

The oxidant used is often the cause of much inconvenience. By their nature, oxidants are unpleasant substances, and all oxidants have peculiar characteristics. The suitability of the oxidant for any particular mission may be more important than obtaining maximum performance. Thus for a defensive weapon the ability to maintain the vehicle in a state of instant readiness is the most important consideration, and solid propellant rockets are often used for this reason alone. The authors can see no reason why some liquid propellant combinations should not also be included in this category. Although liquid propellant rockets probably cannot be considered as serious rivals to solid propellant rockets if the burning time is less than six seconds, they become increasingly competitive as the duration is increased. They may be supplied as packaged units and serious development to this end is inevitable within the next few years.

For tactical weapons, mobility may be most important, and vehicles which weigh but a few hundred pounds when empty, and can be transported and erected on the launcher pad with comparatively light equipment, may be desirable. In such cases the safety and stability of the propellants may be the prime requirement, since the vehicles must be filled and sometimes emptied under difficult conditions.

Offensive weapons intended to act as deterrents fall into the same category as defensive weapons. It is difficult to justify the use of highly volatile propellants for any of these applications. Volatile propellants must be refrigerated continuously, and the rest of the vehicle must be heated. A serious penalty has also to be paid in performance for the weight of the lagging. It has been suggested that the time taken to fill the vehicle when required is acceptable because a longer period is required to prepare the guidance equipment. This may be true, but occasions can be foreseen in which the limitation could seriously reduce the effectiveness of the weapon. Oxidants which are suitable for these applications are oxides of nitrogen, nitric acid and hydrogen peroxide, and of these the last appears to have most in its favour.

It is probable that the most convenient propellants for vehicles which launch satellites and space probes are those with the maximum specific impulse, and the

limitations in convenience imposed by those propellants, which are usually volatile —and, in the case of fluorine compounds, toxic—must be offset as far as possible by consistency in performance of the engine.

Consistency of operation may be important also in engines for winged vehicles. For these, weight is of far less importance than for ballistic vehicles, and because the propellants constitute a much smaller proportion of the whole mass, the tendency to freeze the vehicle is reduced to manageable proportions. Volatile propellants may be acceptable, and because range is a function of specific impulse they may be essential.

As far as the engine is concerned, there is not much to choose between any of the oxidants: reliable engines can be made to burn any of them, though some are more amenable than others. Thus hydrogen peroxide engines are simple but the choice of materials is limited, and there are some problems connected with cooling the chamber. Many materials may be used with liquid oxygen, but ignition requires more equipment, and cooling problems in the chamber, and freezing problems elsewhere, may sometimes be ineluctable. The authors have no experience of the development of fluorine rockets, but expect that engines could be made reliable for this too, once a range of suitable materials and the practical characteristics of fluorine had been established by suitable research. Undoubtedly the extreme toxicity of fluorine would greatly hamper the rate of development of the engine until a technique had been found which would render it harmless without involving fire or explosion. The other objection to the use of fluorine, the toxicity of the exhaust, requires that vehicles be launched in remote places by remote control. These difficulties appear great, but the authors suspect that a certain amount of research into ways and means of overcoming them would show them to be not insuperable. Because of the increase in specific impulse obtainable by using fluorine, a satellite launcher need be only about one quarter the size of one burning liquid oxygen, and for such applications fluorine may perhaps be a convenient oxidant.

6. Conclusions

From this survey it appears that there are two parallel courses which must and will be followed, the two objectives being the best engines for general purposes and the best engines for very difficult, specialised applications.

The best engines for general purposes will have sea level specific impulses approaching 270 lb. sec./lb., attained by using near-optimum cycles with storable propellants, and the main emphasis will be on dependability. This might be achieved by using hydrogen peroxide with selected fuels, perhaps containing metals as slurries. Considerable research and development is needed to attain this objective, attention being given to high pressure combustion and cooling problems, component efficiencies, and the stability of the propellants. It is probable that such engines would have wet weights of about two or three per cent of their thrust.

For very difficult, specialised engines, the programme may be extended through liquid oxygen, liquid fluorine, mixed nuclear/chemical, and finally nuclear engines. Probably of these, liquid fluorine and nuclear engines would be used mainly for second and third stages of composite vehicles, while liquid oxygen and mixed nuclear/chemical engines would be useful for ground launched vehicles. For these engines convenience in handling must probably be sacrificed to some extent. Again, near-optimum cycles will be used. The research and development required will be far greater than for the conventional engines, and although development cannot be started until specific requirements are formulated, research activities cannot be delayed without making future development much more difficult.

Acknowledgment

The authors wish to thank the Directors of Bristol Siddeley Engines Limited for permission to publish this paper. The opinions expressed, however, are those of the authors and not necessarily those of the Company.

References

1. Allen, S. Rocket Engines. *Journal of the Royal Aeronautical Society.* Vol. 61, March 1957.

2. Allen, J. E. From Aviation to Astronautics. *Journal of the Royal Aeronautical Society.* Vol. 62, September 1958.

3. Malina, F. J. Characteristics of the Rocket Motor Unit Based on a Theory of Perfect Gases. *Journal of the Franklin Institute.* Vol. 230, No. 4, October 1940.

4. Sunley, H. L. G. British Patent Specification No. 702779, 1954.

5. Andrews, E. G. D. *High Altitude and Satellite Rockets.* A Symposium held at Cranfield, 18th—20th July 1957. Published by the Royal Aeronautical Society and the British Interplanetary Society. pp. 40, 41, 1958.

6. Sutton, G. P. *Rocket Propulsion Elements.* Second Edition. p. 193. Wiley, New York, and Chapman and Hall, London, 1949.

7. Gordon, J. S. High Temperature Chemistry as Applied to Metal-Based Propellants. *Jet Propulsion.* Vol. 28, p. 769, November 1958.

Quasi-steady Derivatives for the Subsonic Flow past an Oscillating Aerofoil in a Porous Wind Tunnel

D. G. DRAKE

(*Department of Applied Mathematics, University of Liverpool*)

SUMMARY: The compressible subsonic flow about an oscillating two-dimensional aerofoil in a wind tunnel with porous walls is considered. The porous wall is assumed to exhibit the property that the ratio of the normal velocity at the wall to the pressure drop across the wall is constant. The aerodynamic derivatives are found for quasi-steady pitching motion of the aerofoil. The dependence of the derivatives on Mach number and wall porosity is displayed graphically.

1. Introduction

A brief consideration of the problem of compressible subsonic flow about an oscillating two-dimensional aerofoil between porous walls has previously been given by the author[1]. In the present paper the analysis is extended and the aerodynamic derivatives for pitching motion about the mid-chord of the aerofoil are found when the motion may be considered quasi-steady.

The expressions for the derivatives include as special cases those of the closed tunnel and the open jet, corresponding to zero and infinite porosity respectively. The flow about an aerofoil at rest in a porous tunnel is also a special case of the problem and the results in this steady case are shown to be in agreement with those of Woods[2].

The possibility of the elimination or reduction of the interference effects of the tunnel walls on the lift and moment forces acting on the aerofoil is discussed in Section 4. Graphs are presented of the derivatives against the Mach number for various values of the porosity of the tunnel walls.

Consider a uniform stream of velocity U flowing past a thin aerofoil of chord c which lies midway between the walls of a two-dimensional porous wind tunnel of height b. Choose a co-ordinate system such that the x- and y-axes are parallel and normal to the walls respectively, with origin at the leading edge of the aerofoil when at zero incidence to the uniform stream. The co-ordinates x and y are assumed dimensionless, with the aerofoil chord c as the unit of length. Let the aerofoil perform simple harmonic oscillations of complex amplitude $-U\alpha(x)$ with angular frequency ω such that the normal velocity component is $-U\mathscr{R}[\alpha(x)\,e^{i\omega t}]$ where $\mathscr{R}$ denotes "real part of."

Received August 1958.

The restriction $|\alpha(x)| \ll 1$ allows the linearised theory to be used and, since the flow about the aerofoil is irrotational, the perturbation velocity vector $\mathbf{q}$ satisfies the condition

$$\text{curl } \mathbf{q} = 0. \quad . \quad . \quad . \quad . \quad . \quad . \quad (1)$$

Equation (1) implies the existence of a perturbation velocity potential such that

$$\mathbf{q} = Uc \text{ grad } \phi(x, y)\, e^{i\omega t}. \quad . \quad . \quad . \quad (2)$$

Linearising the equations of motion and continuity gives

$$p(x, y) - p_0 = -\rho_0 U^2 \mathscr{R}\{(\phi_x + ik\phi)\, e^{i\omega t}\}. \quad . \quad . \quad . \quad (3)$$

$$\text{and} \quad (M^2 - 1)\phi_{xx} + 2ikM^2\phi_x - k^2M^2\phi - \phi_{yy} = 0, \quad . \quad . \quad . \quad (4)$$

respectively, where M is the free stream Mach number, $k = \omega c/U$ is the frequency parameter, p is the pressure, p_0 is the free stream pressure and ρ_0 is the free stream density. The perturbation velocity potential ϕ is anti-symmetrical[3] in y and thus the pressure jump across the aerofoil is given by (3) as

$$p(x, 0-, t) - p(x, 0+, t) = 2\rho_0 U^2 \mathscr{R}\{\gamma(x)\, e^{i\omega t}\}, \quad . \quad . \quad (5)$$

$$\text{where} \quad \gamma(x) = \left(\frac{\partial}{\partial x} + ik\right)\phi(x, 0+). \quad . \quad . \quad . \quad . \quad (6)$$

Some assumption must be made concerning the nature of the flow through the porous wall. As in previous papers[1, 2, 4] the porous wall is assumed to exhibit the property that the normal velocity at the wall is proportional to the pressure drop across the wall. The constant of proportionality is taken as $\rho_0 U/\sigma$ with σ known as the "porosity." With the further assumption that the pressure outside the wall is the free stream pressure, the boundary conditions at the tunnel walls[1] are

$$\phi_y \pm \sigma(\phi_x + ik\phi) = 0, \quad y = \pm b/(2c) = \pm y_1 \text{ (say)}. \quad . \quad . \quad . \quad (7)$$

Also, the pressure along the centre line of the tunnel must be continuous except across the aerofoil and, since ϕ is anti-symmetrical in y, this implies

$$\phi_x + ik\phi = 0, \quad y = 0, \quad x < 0 \text{ and } x \geqslant 1. \quad . \quad . \quad . \quad (8)$$

The solution of (4) subject to the boundary conditions (7) and (8) is required. To this end the system (4), (7) and (8) may be subjected to the following Fourier transformation[1].

$$F(\nu)=\int_{-\infty}^{\infty} e^{-i\nu x} f(x)\,dx, \quad . \quad . \quad . \quad . \quad . \quad (9)$$

which leads to the integral equation

$$\alpha(x)=-\lim_{y\to 0+}\frac{\partial}{\partial y}\int_0^1 \phi_1(x-z,y)\,\gamma(z)\,dz \quad . \quad . \quad . \quad (10)$$

for the pressure jump function $\gamma(x)$, where $\phi_1(x, y)$ is the inverse transform of

$$\Phi_1(\nu, y)=\frac{\lambda\cosh\lambda(y_1-|y|)+i\sigma(\nu+k)\sinh\lambda(y_1-|y|)}{i(\nu+k)[\lambda\cosh(\lambda y_1)+i\sigma(\nu+k)\sinh(\lambda y_1)]}\operatorname{sgn} y \quad . \quad (11)$$

where $\operatorname{sgn} y=|y|/y$, and with

$$\lambda^2=\beta^2\left[\left(\nu-\frac{kM^2}{\beta^2}\right)^2-\frac{k^2M^2}{\beta^4}\right] . \quad . \quad . \quad . \quad (12)$$

For quasi-steady flow, neglecting terms of $O(k^2)$, the inverse transform of (11) is [1]

$$\phi_1(x,y)=\frac{\beta^2-\sigma ik(y_1-|y|)}{\beta^2-\sigma iky_1}e^{-ikx}\operatorname{sgn} y-\frac{\sigma iky\beta^2 e^{-ikx}}{[\beta^2-ik\sigma y_1]^2}-$$

$$-\sum_{n=0}^{\infty}\frac{e^{-a_n x/\beta}}{a_n y_1}\left(1+\frac{ik}{a_n\beta}\right)e^{-ikM^2x/\beta}\sin(a_n y)-$$

$$-\sum_{n=0}^{\infty}\frac{i\sigma k e^{-a_n x/\beta}}{a_n^2 y_1^2(\beta^2+\sigma^2)}\times\left[y\cos(a_n y)-\sin(a_n y)\left(\frac{x}{\beta}+\frac{2}{a_n}\right)\right], \quad (13)$$

where $a_n y_1=\tan^{-1}(\beta/\sigma)+n\pi$ with $0<\tan^{-1}(\beta/\sigma)\leqslant\pi$ and $x>0$.

The remainder of this paper is devoted to obtaining a solution of the integral equation (10) with ϕ_1 given by (13) and finding the quasi-steady derivatives for a particular prescribed motion of the aerofoil.

NOTATION

$A'=2\beta y_1$

b tunnel height

$C=0{\cdot}5772\ldots$, Euler's constant

C_l lift coefficient defined by (32)

C_m moment coefficient defined by (34)

c chord of aerofoil

f_1, f_2 defined by (29) and (30)

i imaginary unit

$k = \omega c/U$, frequency parameter

$l_\alpha, l_{d\alpha/dt}$ aerodynamic lift derivatives for pitching oscillations

M Mach number of free stream

$m_\alpha, m_{d\alpha/dt}$ aerodynamic moment derivatives for pitching oscillations

p pressure

p_0 free stream pressure

$\mathbf{q}$ perturbation velocity vector

$S(\varepsilon, \alpha)$ defined by (75)

$S'(\varepsilon, \alpha)$ defined by (98)

t time

U free stream

x, y non-dimensional (with respect to c) Cartesian co-ordinates

$y_1 = b/(2c)$

z dummy variable

α defined by (19)

α_0 amplitude of pitching oscillations

$\beta = (1 - M^2)^{1/2}$

$\gamma(x)$ pressure jump function defined by (6)

ε defined by (74)

θ defined by (23)

θ_1 defined by (24)

λ defined by (12)

ν Fourier transform variable

ρ density

ρ_0 free stream density

σ porosity

$\sigma' = 2\sigma y_1$, porosity parameter

ϕ non-dimensional (with respect to Uc) perturbation velocity potential

Φ_1 Fourier transform of ϕ_1

ϕ_1 defined by (13)

ω angular frequency

$\operatorname{sgn} y = |y|/y$

$\mathscr{R}$ "real part of"

$\frac{d}{d\alpha}\log\Gamma(\alpha)$ first logarithmic derivative of gamma function

$\frac{d^2}{d\alpha^2}\log\Gamma(\alpha)$ second logarithmic derivative of gamma function

2. Solution for the Pressure Jump Across the Aerofoil

In order to solve the integral equation (10) for γ it is necessary to know the form of $\alpha(x)$, together with the expression (13) for ϕ_1. The form of $\alpha(x)$ is determined if the mode of oscillation of the aerofoil is prescribed. The particular case considered is that of an aerofoil oscillating in pitch about the mid-chord of the aerofoil, when

$$\alpha(x) = \alpha_0\left[1 + ik\left(x - \frac{1}{2}\right)\right] . \quad . \quad . \quad . \quad . \quad (14)$$

Substituting for $\alpha(x)$ and ϕ_1, from (14) and (13), into (10) leads to

$$\alpha_0\left[1 + ik\left(x - \frac{1}{2}\right)\right] = -\int_0^1 \gamma(z)\left\{-\frac{1}{y_1}\sum_{n=0}^{\infty} e^{-a_n(x-z)/\beta}\left(1 + \frac{ik}{a_n\beta} + \frac{ikM^2}{\beta^2}(x-z)\right) + \right.$$

$$\left. + \frac{ik\sigma}{y_1^2(\beta^2+\sigma^2)}\sum_{n=0}^{\infty} e^{-a_n(x-z)/\beta} \times \left(\frac{x-z}{\beta a_n} + \frac{1}{a_n^2}\right)\right\} dz. \quad . \quad (15)$$

The assumption is made that the tunnel height is large compared with the chord of the aerofoil. Thus, terms dependent on negative powers of y_1 greater than two are neglected in (15). This assumption is usually made when calculating corrections to be applied to data obtained in subsonic tunnels.

Now, in the Appendix it is shown that

$$\sum_{n=0}^{\infty} e^{-a_n(x-z)/\beta} = \frac{1}{2}\left\{\frac{2\beta y_1}{\pi(x-z)} + \frac{2}{\pi}\tan^{-1}\left(\frac{\sigma}{\beta}\right) - \frac{\pi(x-z)}{12\beta y_1} + \right.$$

$$\left. + \frac{(x-z)}{\pi y_1\beta}\left[\tan^{-1}\left(\frac{\sigma}{\beta}\right)\right]^2\right\} + O\left(\frac{1}{y_1^2}\right) \quad . \quad . \quad (16)$$

$$\sum_{n=0}^{\infty} \frac{1}{a_n} e^{-a_n(x-z)/\beta} = \frac{y_1}{\pi}\left\{-\log\left[\frac{(x-z)\pi}{\beta y_1}\right] - \frac{d}{d\alpha}\log\Gamma(\alpha) - C + \frac{\pi}{\beta y_1}\left(\alpha - \frac{1}{2}\right)(x-z) - \right.$$

$$\left. - \left(\frac{\alpha^2-\alpha}{4} + \frac{1}{24}\right)\frac{(x-z)^2\pi^2}{\beta^2 y_1^2}\right\} + O\left(\frac{1}{y_1^2}\right) \quad . \quad . \quad (17)$$

$$\sum_{n=0}^{\infty} \frac{1}{a_n^2} e^{-a_n(x-z)/\beta} = \frac{y_1^2}{\pi^2}\left\{\frac{(x-z)\pi}{\beta y_1}\log\left[\frac{(x-z)\pi}{\beta y_1}\right] - \frac{(x-z)\pi}{\beta y_1} + \right.$$

$$\left. + \frac{\pi(x-z)}{\beta y_1}\left(\frac{d}{d\alpha}\log\Gamma(\alpha)+C\right) - \frac{\pi^2(x-z)^2}{2\beta^2 y_1^2}\left(\alpha-\frac{1}{2}\right) + \frac{d^2}{d\alpha^2}\log\Gamma(\alpha)\right\} + O\left(\frac{1}{y_1}\right) \quad (18)$$

$$\text{where} \quad \alpha = \frac{1}{\pi}\tan^{-1}(\beta/\sigma), \quad . \quad . \quad . \quad . \quad . \quad . \quad (19)$$

$$\text{and Euler's constant } C = 0{\cdot}5772 \ldots\ldots \quad . \quad . \quad . \quad . \quad . \quad (20)$$

and the logarithmic derivatives of the gamma function are defined by

$$\frac{d}{d\alpha}\log\Gamma(\alpha) = \sum_{n=1}^{\infty}\frac{\alpha}{n(\alpha+n)} - \frac{1}{\alpha} - C \quad . \quad . \quad . \quad . \quad . \quad (21)$$

$$\text{and} \quad \frac{d^2}{d\alpha^2}\log\Gamma(\alpha) = \sum_{n=0}^{\infty}\frac{1}{(\alpha+n)^2}. \quad . \quad . \quad . \quad . \quad . \quad . \quad (22)$$

The functions defined by (21) and (22) are tabulated in Ref. 5.

$$\text{Introducing } \theta \text{ and } \theta_1 \text{ by } z = \frac{1}{2}(1-\cos\theta). \quad . \quad . \quad . \quad . \quad . \quad . \quad (23)$$

$$\text{and} \quad x = \frac{1}{2}(1-\cos\theta_1), \quad . \quad . \quad . \quad . \quad . \quad . \quad (24)$$

and assuming that the pressure jump function γ may be expressed

$$\gamma(\theta) = (A_0 + ikB_0)\cot\frac{\theta}{2} + \sum_{n=1}^{\infty}(A_n + ikB_n)\sin n\theta, \quad . \quad . \quad (25)$$

where the A_n and B_n are independent of k, the integral equation (10) becomes

$$\alpha_0\left[1 - \frac{ik\cos\theta}{2}\right] = \frac{1}{2y_1}\int_0^{\pi}\left\{(A_0+ikB_0)\cot\frac{\theta}{2} + \sum_{n=1}^{\infty}(A_n+ikB_n)\sin n\theta\right\} \times$$

$$\times\left\{\sum_{n=0}^{\infty}\exp[-a_n(\cos\theta-\cos\theta_1)/\beta]\times\left[1+\frac{ik}{a_n\beta}+\frac{ikM^2(\cos\theta-\cos\theta_1)}{2\beta^2} - \right.\right.$$

$$\left.\left. - \frac{ik\sigma}{y_1(\beta^2+\sigma^2)}\left(\frac{(\cos\theta-\cos\theta_1)}{2\beta a_n}+\frac{1}{a_n^2}\right)\right]\right\}\sin\theta\, d\theta. \quad (26)$$

The expression (25) for the pressure jump function is such that the Kutta condition at the trailing edge is satisfied and has the proper type of singularity at the leading edge. Evaluating the integrals of (26) and equating the coefficients of $\cos n\theta_1$, $n \geqslant 0$, leads to two infinite sets of equations for A_n and B_n, $n = 0. \ldots \infty$.

These are easily solved and, to the order of approximation considered, give

$$\left.\begin{aligned} A_0 &= \frac{\alpha_0}{\beta}\left[1-\frac{\pi}{2\beta y_1}\left(\frac{1}{2}-\alpha\right)+\frac{3\pi^2}{16\beta^2 y_1^2}\left(\frac{1}{2}-\alpha\right)^2+\frac{\pi^2}{192\beta^2 y_1^2}\right], \\ A_1 &= -\frac{\alpha_0\pi^2}{8\beta^3 y_1^2}\left[\left(\frac{1}{2}-\alpha\right)^2-\frac{1}{12}\right], \\ A_n &= 0, \quad n\geqslant 2, \end{aligned}\right\} \quad . \quad . \quad . \quad (27)$$

$$\left.\begin{aligned} B_0 &= -\frac{1}{\beta}\left\{\frac{\pi}{4\beta y_1}\left(\frac{1}{2}-\alpha\right)\left[1-\frac{\pi}{2\beta y_1}\left(\frac{1}{2}-\alpha\right)\right]f_1-\right. \\ &\qquad \left.-\left[1-\frac{\pi}{2\beta y_1}\left(\frac{1}{2}-\alpha\right)+\frac{\pi^2}{192\beta^2 y_1^2}+\frac{3\pi^2}{16\beta^2 y_1^2}\left(\frac{1}{2}-\alpha\right)^2\right]\right\}, \\ B_1 &= -\frac{1}{\beta}\left\{\left[\frac{\pi^2}{8\beta^2 y_1^2}\left(\frac{1}{2}-\alpha\right)^2-\frac{\pi^2}{96\beta^2 y_1^2}\right]f_2-\right. \\ &\qquad \left.-\left[1+\frac{\pi^2}{192\beta^2 y_1^2}-\frac{\pi^2}{16\beta^2 y_1^2}\left(\frac{1}{2}-\alpha\right)^2\right]f_1\right\}, \\ B_2 &= -\frac{1}{\beta}\left\{\frac{\alpha_0\pi^2}{16\beta^4 y_1^2}\left(\frac{\alpha^2-\alpha}{4}+\frac{1}{24}\right)-\frac{\alpha_0\pi^2}{64\beta^4 y_1^2}\left[\left(\frac{1}{2}-\alpha\right)^2-\frac{1}{12}\right]+\right. \\ &\qquad \left.+\frac{\alpha_0 M^2\pi^2}{384\beta^4 y_1^2}-\frac{M^2\alpha_0\pi^2}{32\beta^4 y_1^2}\left(\frac{1}{2}-\alpha\right)^2+\frac{\sigma\alpha_0\pi}{32\beta^3 y_1^2(\beta^2+\sigma^2)}\left(\alpha-\frac{1}{2}\right)\right\} \\ B_n &= 0, \quad n\geqslant 3, \end{aligned}\right\} \quad . \quad . \quad . \quad (28)$$

where

$$f_1=\frac{\alpha_0}{2}+\frac{A_0}{2\beta}\left[1-\frac{\pi}{2\beta y_1}\left(\alpha-\frac{1}{2}\right)+\frac{\pi^2}{4\beta^2 y_1^2}\left(\frac{\alpha^2-\alpha}{4}+\frac{1}{24}\right)\right]+\frac{M^2A_0}{8\beta^2}\left[-\frac{2\pi}{y_1}\left(\frac{1}{2}-\alpha\right)+\right.$$
$$\left.+\frac{\pi^2}{24\beta y_1^2}-\frac{\pi^2}{2\beta y_1^2}\left(\frac{1}{2}-\alpha\right)^2\right]+\frac{\sigma\alpha_0\pi}{16\beta^3 y_1^2(\beta^2+\sigma^2)}\left(\alpha-\frac{1}{2}\right)-\frac{\sigma A_0}{4\beta y_1(\beta^2+\sigma^2)}. \quad (29)$$

$$f_2=-\frac{A_0}{2\beta}\left[-\log\left(\frac{\pi}{4\beta y_1}\right)-\frac{d}{d\alpha}\log\Gamma(\alpha)-C+\frac{\pi}{4\beta y_1}\left(\alpha-\frac{1}{2}\right)-\frac{\pi^2}{4\beta^2 y_1^2}\left(\frac{\alpha^2-\alpha}{4}+\frac{1}{24}\right)-\right.$$
$$-\frac{A_1}{2\beta}\left[-\frac{1}{2}\log\left(\frac{\pi}{4\beta y_1}\right)-\frac{1}{2}\frac{d}{d\alpha}\log\Gamma(\alpha)-\frac{C}{2}\right]-\frac{M^2A_0}{8\beta^2}\left[4\beta+\frac{\pi}{y_1}\left(\frac{1}{2}-\alpha\right)-\right.$$
$$\left.-\frac{\pi^2}{24\beta y_1^2}+\frac{\pi^2}{2\beta y_1^2}\left(\frac{1}{2}-\alpha\right)^2\right]-\frac{M^2A_1}{4\beta}+\frac{\sigma A_0\pi}{16\beta^2 y_1^2(\beta^2+\sigma^2)}\left(\alpha-\frac{1}{2}\right)+$$
$$\left.+\frac{\sigma A_0}{2\pi(\beta^2+\sigma^2)}\frac{d^2}{d\alpha^2}\log\Gamma(\alpha)-\frac{\sigma A_0}{8\beta y_1(\beta^2+\sigma^2)}+\frac{\sigma A_1}{4\pi(\beta^2+\sigma^2)}\frac{d^2}{d\alpha^2}\log\Gamma(\alpha)\right. . \quad (30)$$

Here A_0 and A_1 are given by (27). Thus, the pressure jump function γ is

$$\gamma(\theta)=(A_0+ikB_0)\cot\frac{\theta}{2}+(A_1+ikB_1)\sin\theta+ikB_2\sin 2\theta \quad . \quad (31)$$

where the A_n and B_n are given by (27) and (28).

3. Aerodynamic Derivatives

The lift coefficient C_l is related to the lift acting on the aerofoil by

$$C_l=\frac{\text{lift}}{\frac{1}{2}\rho_0 U^2 c} \quad . \quad . \quad . \quad . \quad . \quad . \quad . \quad . \quad (32)$$

and, from (5),

$$C_l=4\int_0^1 \gamma(z)\,dz. \quad . \quad . \quad . \quad . \quad . \quad . \quad . \quad (33)$$

Also, the moment coefficient C_m is derived from the moment about the mid-chord by

$$C_m=\frac{\text{moment}}{\frac{1}{2}\rho_0 U^2 c^2} \quad . \quad . \quad . \quad . \quad . \quad . \quad . \quad . \quad (34)$$

and, from (5),

$$C_m=4\int_0^1 (\tfrac{1}{2}-z)\,\gamma(z)\,dz. \quad . \quad . \quad . \quad . \quad . \quad . \quad (35)$$

Introducing the variable θ, which is related to z by (23), in (33) and (35) gives

$$C_l=2\int_0^\pi \gamma(\theta)\sin\theta\,d\theta \quad . \quad . \quad . \quad . \quad . \quad . \quad (36)$$

and

$$C_m=\int_0^\pi \gamma(\theta)\sin\theta\cos\theta\,d\theta. \quad . \quad . \quad . \quad . \quad . \quad (37)$$

On substituting for $\gamma(\theta)$ from (31) into (36) and (37), and evaluating the integrals, the lift and moment coefficients are

$$C_l=2\pi(A_0+ikB_0)+\pi(A_1+ikB_1) \quad . \quad . \quad . \quad (38)$$

and

$$C_m=\frac{\pi}{2}(A_0+ikB_0)+\frac{\pi}{4}ikB_2. \quad . \quad . \quad . \quad . \quad (39)$$

Since the terms $O(k^2)$ are neglected, it is convenient to write

$$C_l=\alpha_0[l_\alpha+ikl_{d\alpha/dt}+O(k^2)] \quad . \quad . \quad . \quad . \quad (40)$$

and

$$C_m=\alpha_0[m_\alpha+ikm_{d\alpha/dt}+O(k^2)] \quad . \quad . \quad . \quad . \quad (41)$$

Here l_α, $l_{d\alpha/dt}$, m_α and $m_{d\alpha/dt}$ are the aerodynamic derivatives and, in this quasi-steady case, are independent of the frequency parameter. Then, from (31), (36), (38) and (40), it is seen that

$$l_\alpha = \frac{2\pi}{\beta}\left[1 - \frac{1}{2\beta y_1}\tan^{-1}\left(\frac{\sigma}{\beta}\right) + \frac{1}{8\beta^2 y_1^2}\left(\tan^{-1}\left(\frac{\sigma}{\beta}\right)\right)^2 + \frac{\pi^2}{96\beta^2 y_1^2}\right]. \quad . \quad (42)$$

and $$l_{d\alpha/dt} = \frac{2\pi}{\beta\alpha_0}\left\{\left[\frac{1}{2} - \frac{1}{4\beta y_1}\tan^{-1}\left(\frac{\sigma}{\beta}\right) + \frac{3}{32\beta^2 y_1^2}\left(\tan^{-1}\left(\frac{\sigma}{\beta}\right)\right)^2 + \frac{\pi^2}{384\beta^2 y_1^2}\right] f_1 + \right.$$

$$\left. + \left[1 - \frac{1}{2\beta y_1}\tan^{-1}\frac{\sigma}{\beta} + \frac{1}{8\beta^2 y_1^2}\left(\tan^{-1}\left(\frac{\sigma}{\beta}\right)\right)^2 + \frac{\pi^2}{96\beta^2 y_1^2}\right] f_2\right\} \quad (43)$$

Similarly, from (31), (37), (39) and (41), the moment derivatives are

$$m_\alpha = \frac{\pi}{2\beta}\left[1 - \frac{1}{2\beta y_1}\tan^{-1}\left(\frac{\sigma}{\beta}\right) + \frac{3}{16\beta^2 y_1^2}\left(\tan^{-1}\left(\frac{\sigma}{\beta}\right)\right)^2 + \frac{\pi^2}{192\beta^2 y_1^2}\right] . \quad (44)$$

and $$m_{d\alpha/dt} = \frac{\pi}{2\beta\alpha_0}\left\{-\left[\frac{1}{4\beta y_1}\tan^{-1}\left(\frac{\sigma}{\beta}\right) - \frac{1}{8\beta^2 y_1^2}\left(\tan^{-1}\left(\frac{\sigma}{\beta}\right)\right)^2\right] f_1 + \right.$$

$$+ \left[1 - \frac{1}{2\beta y_1}\tan^{-1}\left(\frac{\sigma}{\beta}\right) + \frac{3}{16\beta^2 y_1^2}\left(\tan^{-1}\left(\frac{\sigma}{\beta}\right)\right)^2 + \frac{\pi^2}{192\beta^2 y_1^2}\right] f_2 -$$

$$\left. - \frac{\pi}{4\beta}\left\{\frac{M^2\pi^2}{384\beta^4 y_1^2} - \frac{M^2}{32\beta^4 y_1^2}\left(\tan^{-1}\left(\frac{\sigma}{\beta}\right)\right)^2 - \frac{\sigma}{32\beta^3 y_1^2(\beta^2+\sigma^2)}\tan^{-1}\left(\frac{\sigma}{\beta}\right)\right\}\right. . \quad (45)$$

The derivatives for the closed tunnel and the open jet are obtained from (42)–(45) on letting the porosity σ be zero and tend to infinity, respectively.

Considering the closed tunnel case ($\sigma = 0$), then,

$$\alpha = \left[\frac{1}{\pi}\tan^{-1}\left(\frac{\beta}{\sigma}\right)\right]_{\sigma=0} = \frac{1}{2} \quad . \quad . \quad . \quad . \quad . \quad (46)$$

and $$C + \left[\frac{d}{d\alpha}\log\Gamma(\alpha)\right]_{\alpha=\frac{1}{2}} = -2\log 2. \quad . \quad . \quad . \quad (47)$$

Thus, the aerodynamic derivatives for the closed tunnel $(l_\alpha)_c$ $(l_{d\alpha/dt})_c$, $(m_\alpha)_c$ and $(m_{d\alpha/dt})_c$ are

$$(l_\alpha)_c = \frac{2\pi}{\beta}\left[1 + \frac{\pi^2}{96\beta^2 y_1^2}\right] \quad . \quad . \quad . \quad . \quad . \quad (48)$$

$$(m_\alpha)_c = \frac{\pi}{2\beta}\left[1 + \frac{\pi^2}{192\beta^2 y_1^2}\right] \quad . \quad . \quad . \quad . \quad . \quad (49)$$

$$(l_{d\alpha/dt})_c = \frac{\pi}{\beta^3}\left[-\left(1+\frac{\pi^2}{48\beta^2 y_1^2}\right)\log\left(\frac{16\beta y_1}{\pi}\right)+\frac{1}{2}\left(3\beta^2-1\right)\left(1+\frac{\pi^2}{192\beta^2 y_1^2}\right)-\right.$$
$$\left.-\frac{\pi^2}{192\beta^2 y_1^2}\right]. \quad (50)$$

and
$$(m_{d\alpha/dt})_c = \frac{\pi}{4\beta^3}\left[-\left(1+\frac{3\pi^2}{192\beta^2 y_1^2}\right)\log\left(\frac{16\beta y_1}{\pi}\right)+(\beta^2-1)\left(1+\frac{3\pi^2}{384\beta^2 y_1^2}\right)-\right.$$
$$\left.-\frac{\pi^2}{192\beta^2 y_1^2}\right]. \quad (51)$$

These results are in agreement with those of Jones[6].

For the open jet ($\sigma \longrightarrow \infty$)

$$\alpha = \left[\frac{1}{\pi}\tan^{-1}\left(\frac{\beta}{\sigma}\right)\right]_{\sigma\to\infty} = 0 \quad . \quad . \quad . \quad . \quad (52)$$

and, using the relations

$$\frac{d}{d\alpha}\log\Gamma(\alpha) = \frac{d}{d\alpha}\log\Gamma(\alpha+1) - \frac{1}{\alpha} \quad . \quad . \quad . \quad . \quad (53)$$

and
$$\frac{d^2}{d\alpha^2}\log\Gamma(\alpha) = \frac{d^2}{d\alpha^2}\log\Gamma(\alpha+1) + \frac{1}{\alpha^2}, \quad . \quad . \quad . \quad (54)$$

the aerodynamic derivatives for the open jet $(l_\alpha)_o$, $(l_{d\alpha/dt})_o$, $(m_\alpha)_o$ and $(m_{d\alpha/dt})_o$, are

$$(l_\alpha)_o = \frac{2\pi}{\beta}\left(1-\frac{\pi}{4\beta y_1}+\frac{\pi^2}{24\beta^2 y_1^2}\right) \quad . \quad . \quad . \quad . \quad (55)$$

$$(m_\alpha)_o = \frac{\pi}{2\beta}\left(1-\frac{\pi}{4\beta y_1}+\frac{5\pi^2}{96\beta^2 y_1^2}\right) \quad . \quad . \quad . \quad . \quad (56)$$

$$(l_{d\alpha/dt})_o = \frac{2\pi}{\beta^2}\left\{1-\frac{\pi}{4\beta y_1}+\frac{\pi^2}{24\beta^2 y_1^2}\right\}\left\{\left[1-\frac{\pi}{4\beta y_1}+\frac{5\pi^2}{96\beta^2 y_1^2}\right]\times\right.$$
$$\times\left[\frac{\pi}{16 y_1}+\frac{1}{2\beta}\log\left(\frac{\pi}{4\beta y_1}\right)-\frac{M^2}{2\beta}+\frac{\pi^2}{192\beta^3 y_1^2}-\frac{M^2\pi^2}{96\beta^3 y_1^2}\right]-$$
$$-\frac{\pi^2}{192\beta^3 y_1^2}\log\left(\frac{\pi}{4\beta y_1}\right)+\left.\frac{\pi^2 M^2}{192\beta^3 y_1^2}\right\}+\frac{\pi}{2\beta^2}\left\{1-\frac{\pi}{4\beta y_1}+\frac{5\pi^2}{96\beta^2 y_1^2}\right\}\times$$
$$\times\left\{\left[1-\frac{\pi}{4\beta y_1}+\frac{5\pi^2}{96\beta^2 y_1^2}\right]\left[\frac{\pi}{4 y_1}+\frac{1}{\beta}+\frac{\pi^2}{96\beta^3 y_1^2}-\frac{M^2\pi^2}{48\beta^3 y_1^2}\right]+\beta\right\} \quad . \quad (57)$$

$$\text{and } (m_{d\alpha/dt})_0 = \frac{\pi}{2\beta^2}\left\{1-\frac{\pi}{4\beta y_1}+\frac{5\pi^2}{96\beta^2 y_1^2}\right\}\left\{\left[1-\frac{\pi}{4\beta y_1}+\frac{5\pi^2}{96\beta^2 y_1^2}\right]\times\right.$$

$$\times\left[\frac{\pi}{16y_1}+\frac{1}{2\beta}\log\left(\frac{\pi}{4\beta y_1}\right)-\frac{M^2}{2\beta}+\frac{\pi^2}{192\beta^3 y_1^2}-\frac{M^2\pi^2}{96\beta^3 y_1^2}\right]-\frac{\pi^2}{192\beta^3 y_1^2}\log\left(\frac{\pi}{4\beta y_1}\right)+$$

$$\left.+\frac{M^2\pi^2}{192\beta^3 y_1^2}\right\}-\frac{\pi}{4\beta^2}\left\{\frac{\pi}{8\beta y_1}-\frac{\pi^2}{32\beta^2 y_1^2}\right\}\left\{\left[1-\frac{\pi}{4\beta y_1}+\frac{5\pi^2}{96\beta^2 y_1^2}\right]\times\right.$$

$$\left.\times\left[\frac{\pi}{4y_1}+\frac{1}{\beta}+\frac{\pi^2}{96\beta^3 y_1^2}-\frac{M^2\pi^2}{48\beta^3 y_1^2}\right]+\beta\right\}+\frac{M^2\pi^3}{768\beta^5 y_1^2} \quad . \quad . \quad (58)$$

In Figs. 1 to 4, the derivatives l_a, m_a, $l_{d\alpha/dt}$ and $m_{d\alpha/dt}$ are plotted against the Mach number M for a tunnel height to chord ratio of five, *i.e.* $y_1=2{\cdot}5$, and for several values of the porosity parameter $\sigma'=2\sigma y_1$. These include the closed tunnel ($\sigma'=0$) and the open jet ($\sigma'=\infty$) curves.

The aerodynamic derivatives $(l_a)_u$, $(m_a)_u$, $(l_{d\alpha/dt})_u$ and $(m_{d\alpha/dt})_u$ for an unbounded stream are obtained on letting y_1 tend to infinity in (42)-(45), *i.e.*

$$(l_a)_u = 2\pi/\beta \quad . \quad . \quad . \quad . \quad . \quad . \quad (59)$$

$$(m_a)_u = \pi/(2\beta) \quad . \quad . \quad . \quad . \quad . \quad . \quad (60)$$

$$(l_{d\alpha/dt})_u = -\infty \quad . \quad . \quad . \quad . \quad . \quad . \quad (61)$$

$$\text{and} \quad (m_{d\alpha/dt})_u = -\infty. \quad . \quad . \quad . \quad . \quad . \quad . \quad (62)$$

It is clear from Figs. 3 and 4 and equations (61) and (62) that the values of the derivatives $l_{d\alpha/dt}$ and $m_{d\alpha/dt}$ for the closed tunnel and the open jet differ greatly from the unbounded stream values. Furthermore, the large differences in magnitude are not made smaller by using a porous wind tunnel. Thus, the effect of the tunnel walls on the derivatives $l_{d\alpha/dt}$ and $m_{d\alpha/dt}$ remains important at low frequency parameters.

4. Steady Case

The lift and moment coefficients of an aerofoil at rest in a subsonic tunnel with porous walls and at an incidence α_0 to the undisturbed stream are given by (40) and (41) with the frequency parameter k equal to zero. Then, letting $(C_l)_s$ and $(C_m)_s$ be the steady lift and moment coefficients,

$$(C_l)_s = \alpha_0 l_a$$

$$= \frac{2\pi\alpha_0}{\beta}\left[1-\frac{1}{2\beta y_1}\tan^{-1}\left(\frac{\sigma}{\beta}\right)+\frac{1}{8\beta^2 y_1^2}\left(\tan^{-1}\left(\frac{\sigma}{\beta}\right)\right)^2+\frac{\pi^2}{96\beta^2 y_1^2}\right] \quad (63)$$

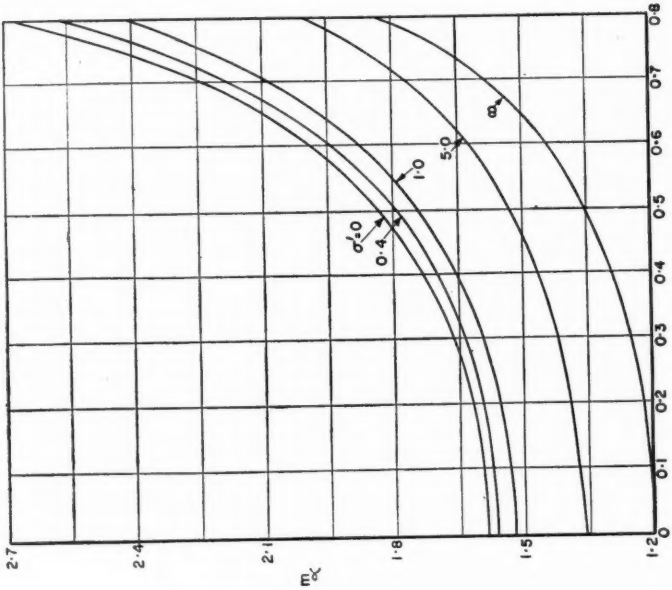

FIGURE 2. Derivative m_α against Mach number M. $\gamma_1 = 2{\cdot}5$.

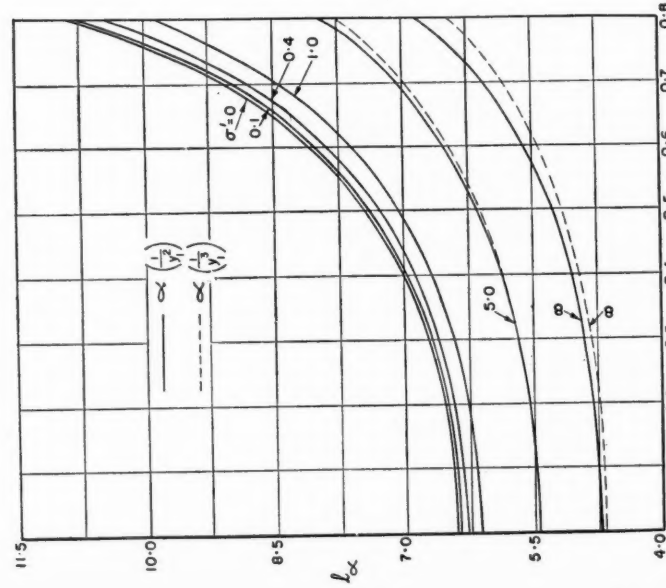

FIGURE 1. Derivative l_α against Mach number M. $\gamma_1 = 2{\cdot}5$.

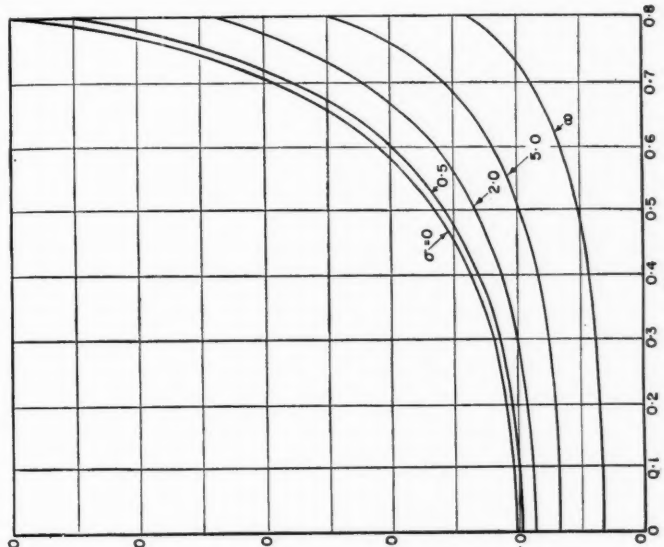

FIGURE 4. Derivative $m_{d\alpha/dt}$ against Mach number M. $y_1 = 2{\cdot}5$.

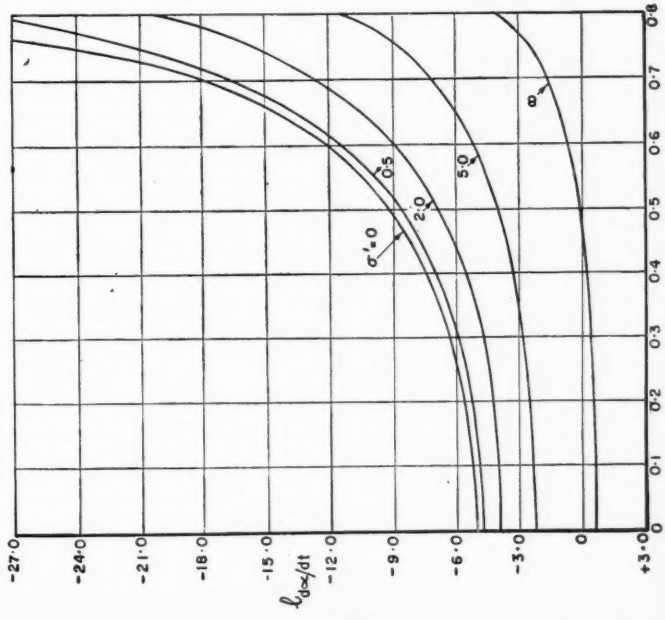

FIGURE 3. Derivative $l_{d\alpha/dt}$ against Mach number M. $y_1 = 2{\cdot}5$.

and $(C_m)_s = \alpha_0 m_a$

$$= \frac{\pi\alpha_0}{2\beta}\left[1 - \frac{1}{2\beta y_1}\tan^{-1}\left(\frac{\sigma}{\beta}\right) + \frac{3}{16\beta^2 y_1^2}\left(\tan^{-1}\left(\frac{\sigma}{\beta}\right)\right)^2 + \frac{\pi^2}{192\beta^2 y_1^2}\right] \quad (64)$$

These are in agreement with the steady results of Woods[2].

An informative method of displaying the dependence of the steady lift coefficient $(C_l)_s$ on the porosity, Mach number and the tunnel height to chord ratio is to plot $\beta(C_l)_s/(2\pi\alpha_0)$ against $A' = 2\beta y_1$ for different values of the porosity parameter $\sigma' = 2\sigma y_1$. This is done in Fig. 5 for several values of σ'. The difference in values of $\beta(C_l)_s/(2\pi\alpha_0)$ for a point on such a curve and a corresponding point on the curve $\beta(C_l)_s/(2\pi\alpha_0) = 1$ is a measure of the interference due to the tunnel walls on the lift coefficient. Thus, to measure interference-free steady lift coefficients in a porous tunnel, for a particular value of the tunnel height to chord ratio and over a range of Mach numbers, it is necessary for the porosity to be such that the curve coincides with $\beta(C_l)_s/(2\pi\alpha_0) = 1$. From (63), it is seen that this is the case if

$$\left[\tan^{-1}\left(\frac{\sigma}{\beta}\right)\right]^2 - 4\beta y_1 \tan^{-1}\left(\frac{\sigma}{\beta}\right) + \frac{\pi^2}{12} = 0. \quad . \quad . \quad . \quad (65)$$

To the approximation considered, (65) is satisfied if

$$\sigma' = \frac{\pi^2}{24} \simeq 0{\cdot}4. \quad . \quad . \quad . \quad . \quad . \quad . \quad (66)$$

Thus, the curve labelled $\sigma' = 0{\cdot}4$ in Fig. 5 is seen to be nearly coincident with $\beta(C_l)_s/(2\pi\alpha_0) = 1$ and, for a porous tunnel with wall porosity given by (66), no correction need be applied to measured steady lift coefficients.

Similarly, the interference on the mid-chord moment coefficient is zero if $\sigma' = \pi^2/48$. Thus, while the lift and moment coefficients are interference-free at $\sigma' = \pi^2/24$ and $\sigma' = \pi^2/48$ respectively, the pressure distribution over the aerofoil at these porosities is changed. Further, the curve in Fig. 1 for $\sigma' = 0{\cdot}4$ ($\simeq \pi^2/24$) and the curve in Fig. 2 for $\sigma' = 0{\cdot}2$ ($\simeq \pi^2/48$) lie surprisingly close to the closed tunnel ($\sigma' = 0$) curves.

Some insight into the magnitude of the error due to neglecting terms $O(1/y_1^3)$ may be obtained in the steady case by including terms $O(1/y_1^3)$ in the solution. Then, it is found that

$$(C_l)_s = \frac{2\pi\alpha_0}{\beta}\left\{1 - \frac{1}{2\beta y_1}\tan^{-1}\left(\frac{\sigma}{\beta}\right) + \frac{1}{8\beta^2 y_1^2}\left[\tan^{-1}\left(\frac{\sigma}{\beta}\right)\right]^2 + \right.$$

$$\left. + \frac{\pi^2}{96\beta^2 y_1^2} - \frac{\pi^2}{384\beta^2 y_1^2}\tan^{-1}\left(\frac{\sigma}{\beta}\right) - \frac{3}{96\beta^3 y_1^3}\left[\tan^{-1}\left(\frac{\sigma}{\beta}\right)\right]^3\right\} \quad . \quad (67)$$

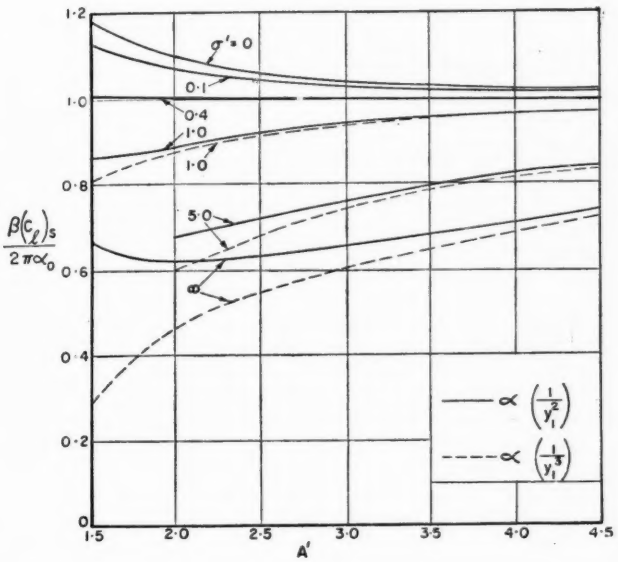

FIGURE 5. Variation of $\beta(C_l)_s/(2\pi\alpha_0)$ with A'. $y_1=2{\cdot}5$.

The effect of including terms $O(1/y_1^3)$ is shown in Fig. 5. It is seen that the higher order terms are probably only important for very large values of σ' and then only for Mach numbers approaching the transonic régime.

5. Conclusion

The quasi-steady derivatives for the subsonic flow past an oscillating aerofoil in a porous wind tunnel have been found. Comparison with the unbounded stream results show that for low frequency oscillations the resultant effect of the interference of the walls on the derivatives l_α and m_α is zero for all Mach numbers for particular values of the porosity, whereas the effect of the walls on the derivatives $l_{d\alpha/dt}$ and $m_{d\alpha/dt}$ is large for all values of the Mach number and porosity. It appears unlikely, at least for low frequency oscillations, that wind-tunnel wall interference is eliminated or substantially reduced when using porous wind tunnels.

ACKNOWLEDGMENT

The author is indebted to Dr. G. N. Lance, under whose supervision this work was carried out, and to the Department of Scientific and Industrial Research for a maintenance award.

Appendix

The sums of the infinite series

$$\sum_{n=0}^{\infty} \exp\left\{-\frac{a_n}{\beta}(x-z)\right\} a_n^{-m}, \qquad m=0,\ 1,\ 2,\ .\ .\ .\ . \tag{68}$$

where $a_n y_1=\tan^{-1}(\beta/\sigma)+n\pi$, are found in this Appendix.

(*a*) When $m=0$ the sum of the infinite series

$$\sum_{n=0}^{\infty} \exp\left\{-\frac{a_n}{\beta}(x-z)\right\} \quad . \quad . \quad . \quad . \quad . \quad (69)$$

is required, neglecting terms $O(1/y_1^2)$. This is a geometric series and it is seen that

$$\sum_{n=0}^{\infty} \exp\left\{-\frac{a_n}{\beta}(x-z)\right\} = \exp\left\{-\frac{(x-z)}{\beta y_1}\tan^{-1}\left(\frac{\beta}{\sigma}\right)+\frac{(x-z)\,\pi}{2\beta y_1}\right\} \frac{1}{2\sinh\left[(x-z)\,\pi/(2\beta y_1)\right]}$$

. . . . . (70)

and, neglecting terms $O(1/y_1^2)$,

$$\sum_{n=0}^{\infty} \exp\left\{-\frac{a_n}{\beta}(x-z)\right\} = \frac{1}{2}\left\{\frac{2\beta y_1}{\pi(x-z)}+\frac{2}{\pi}\tan^{-1}\left(\frac{\sigma}{\beta}\right)-\frac{\pi(x-z)}{12\beta y_1}+\frac{(x-z)}{\pi y_1\beta}\left[\tan^{-1}\left(\frac{\sigma}{\beta}\right)\right]^2\right\}$$

. . . . . (71)

(*b*) When $m=1$, the infinite series

$$\sum_{n=0}^{\infty} \exp\left\{-\frac{a_n}{\beta}(x-z)\right\} a_n^{-1} \quad . \quad . \quad . \quad . \quad (72)$$

is to be summed.

Letting $$\alpha=\frac{1}{\pi}\tan^{-1}\left(\frac{\beta}{\sigma}\right) \quad . \quad . \quad . \quad . \quad . \quad . \quad (73)$$

and $$\varepsilon=\frac{(x-z)\pi}{\beta y_1}, \quad . \quad . \quad . \quad . \quad . \quad (74)$$

the sum of the series $$\frac{y_1}{\pi}\sum_{n=0}^{\infty}\frac{1}{(\alpha+n)}\exp\{-\varepsilon(\alpha+n)\}=\frac{y_1}{\pi}S(\varepsilon,\alpha) \quad . \quad . \quad . \quad (75)$$

is required, where $$S(\varepsilon,\alpha)=\sum_{n=0}^{\infty}\frac{1}{(\alpha+n)}\exp\{-\varepsilon(\alpha+n)\}. \quad . \quad . \quad . \quad . \quad (76)$$

Now, differentiating (76) with respect to ε,

$$\frac{\partial S}{\partial \varepsilon} = -\sum_{n=0}^{\infty}\exp\{-\varepsilon(\alpha+n)\}$$

$$= -\exp(-\alpha\varepsilon)\frac{1}{1-\exp(-\varepsilon)}$$

$$= -\frac{1}{\varepsilon}+\left(\alpha-\frac{1}{2}\right)-\left(\frac{\alpha^2-\alpha}{2}+\frac{1}{12}\right)\varepsilon+ \quad . \quad (77)$$

neglecting terms $O(\varepsilon^2)$.

On integrating (77),

$$S(\varepsilon, \alpha) = -\log \varepsilon + \left(\alpha - \frac{1}{2}\right)\varepsilon - \left(\frac{\alpha^2-\alpha}{2} + \frac{1}{12}\right)\frac{\varepsilon^2}{2} + C(\alpha) + \ldots\ldots \quad (78)$$

where $C(\alpha)$ is a function independent of ε.

Now, differentiating (76) and (78) with respect to α gives

$$\frac{\partial S}{\partial \alpha} = -\varepsilon S(\varepsilon, \alpha) - \sum_{n=0}^{\infty} \frac{1}{(\alpha+n)^2} \exp\{-\varepsilon(\alpha+n)\} \quad (79)$$

and

$$\frac{\partial S}{\partial \alpha} = \frac{dC}{d\alpha} + \varepsilon - \left(\frac{2\alpha-1}{4}\right)\varepsilon^2 + \ldots\ldots \quad (80)$$

Equating the expressions (79) and (80) for $\partial S/\partial \alpha$ and letting ε tend to zero gives

$$\frac{dC}{d\alpha} = -\sum_{n=0}^{\infty} \frac{1}{(\alpha+n)^2} \quad (81)$$

and, in the usual notation[5],

$$\frac{dC}{d\alpha} = -\frac{d^2}{d\alpha^2} \log \Gamma(\alpha) \quad (82)$$

On integrating (82),

$$C(\alpha) = -\frac{d}{d\alpha} \log \Gamma(\alpha) + K_1, \quad (83)$$

where K_1 is independent of α. Now, by (77),

$$\frac{\partial S(\varepsilon, 1)}{\partial \varepsilon} = -\exp(-\varepsilon) \frac{1}{1-\exp(-\varepsilon)}, \quad (84)$$

and integrating,

$$S(\varepsilon, 1) = -\log\{1-\exp(-\varepsilon)\} + K_2 \quad (85)$$

where K_2 is a constant. Also, by (76),

$$\lim_{\varepsilon \to 0} S(\varepsilon, 1) = 0 \quad (86)$$

and letting $\varepsilon \longrightarrow \infty$ in (85) and using (86) leads to

$$K_2 = 0. \quad (87)$$

Thus, using (87), the expression (85) for $S(\varepsilon, 1)$ becomes

$$S(\varepsilon, 1) = -\log\{1-\exp(-\varepsilon)\}$$

$$= -\log \varepsilon + \frac{\varepsilon}{2} + \ldots\ldots \quad (88)$$

Comparing (88) with the result obtained on putting $\alpha=1$ in (78) gives

$$C(1)=0. \quad . \quad . \quad . \quad . \quad . \quad . \quad (89)$$

Now, the first logarithmic derivative of the gamma function is given by[5]

$$-\frac{d}{d\alpha}\log\Gamma(\alpha)=C+\frac{1}{\alpha}-\sum_{n=1}^{\infty}\frac{\alpha}{n(\alpha+n)} \quad . \quad . \quad . \quad . \quad (90)$$

where C is Euler's constant and, putting $\alpha=1$,

$$-\frac{d}{d\alpha}\log\Gamma(1)=C \quad . \quad . \quad . \quad . \quad . \quad . \quad (91)$$

Thus, by (83), (89) and (91),

$$K_1=-C \quad . \quad . \quad . \quad . \quad . \quad . \quad . \quad . \quad (92)$$

and
$$C(\alpha)=-\frac{d}{d\alpha}\log\Gamma(\alpha)-C \quad . \quad . \quad . \quad (93)$$

$$=\frac{1}{\alpha}+\sum_{n=1}^{\infty}\left(\frac{1}{n+\alpha}-\frac{1}{n}\right) \quad . \quad . \quad . \quad . \quad . \quad (94)$$

Substituting for $C(\alpha)$ into (78) gives

$$S(\varepsilon,\alpha)=-\log\varepsilon+\left(\alpha-\frac{1}{2}\right)\varepsilon-\left(\frac{\alpha^2-\alpha}{2}+\frac{1}{12}\right)\frac{\varepsilon^2}{2}-\frac{d}{d\alpha}\log\Gamma(\alpha)-C+\ldots\ldots \quad (95)$$

and the sum of the infinite series (72) becomes

$$\sum_{n=0}^{\infty}\exp\left\{-\frac{a_n}{\beta}(x-z)\right\}a_n^{-1}=\frac{y_1}{\pi}\left\{-\log\left[\frac{(x-z)\pi}{\beta y_1}\right]-\frac{d}{d\alpha}\log\Gamma(\alpha)-C+\right.$$
$$\left.+\frac{\pi}{\beta y_1}\left(\alpha-\frac{1}{2}\right)\left(x-z\right)-\left(\frac{\alpha^2-\alpha}{4}+\frac{1}{24}\right)\frac{(x-z)^2\pi^2}{\beta^2 y_1^{\,2}}\right\} \quad (96)$$

where terms $O(1/y_1^{\,2})$ are neglected.

(*c*) The sum of the infinite series

$$\sum_{n=0}^{\infty}\exp\left\{-\frac{a_n}{\beta}(x-z)\right\}a_n^{-2} \quad . \quad . \quad . \quad . \quad (97)$$

may easily be obtained from the expression (95) for $S(\varepsilon,\alpha)$.

Letting
$$S'(\varepsilon,\alpha)=\sum_{n=0}^{\infty}\exp\{-\varepsilon(\alpha+n)\}\frac{1}{(\alpha+n)^2} \quad . \quad . \quad . \quad . \quad (98)$$

and differentiating (98) with respect to ε,

$$\frac{\partial S'}{\partial \varepsilon} = -S(\varepsilon, \alpha) = \log \varepsilon - \left(\alpha - \frac{1}{2}\right)\varepsilon + \left(\frac{\alpha^2-\alpha}{2} + \frac{1}{12}\right)\frac{\varepsilon^2}{2} + \frac{d}{d\alpha}\log \Gamma(\alpha) + C. \quad . \quad (99)$$

Then, on integrating (99),

$$S'(\varepsilon, \alpha) = \varepsilon \log \varepsilon - \varepsilon + \frac{d}{d\alpha}\log \Gamma(\alpha)\,\varepsilon + C\varepsilon - \left(\frac{\alpha}{2} - \frac{1}{4}\right)\varepsilon^2 + \left(\frac{\alpha^2-\alpha}{12} + \frac{1}{72}\right)\varepsilon^3 + K_3, \quad . \quad . \quad . \quad . \quad (100)$$

where K_3 is independent of ε. Letting $\varepsilon \longrightarrow 0$ in (100) and using the relation

$$\lim_{\varepsilon \to 0} \varepsilon \log \varepsilon = 0 \quad . \quad . \quad . \quad . \quad . \quad . \quad (101)$$

gives

$$K_3 = \sum_{n=0}^{\infty} \frac{1}{(\alpha+n)^2}$$

$$= \frac{d^2}{d\alpha^2}\log \Gamma(\alpha). \quad . \quad . \quad . \quad . \quad (102)$$

Thus, by (100) and (102),

$$S'(\varepsilon, \alpha) = \varepsilon \log \varepsilon - \varepsilon + \varepsilon\left[\frac{d}{d\alpha}\log \Gamma(\alpha) + C\right] - \left[\frac{\alpha}{2} - \frac{1}{4}\right]\varepsilon^2 + \frac{d^2}{d\alpha^2}\log \Gamma(\alpha) + \ldots\ldots \quad . \quad . \quad . \quad (103)$$

and the sum of the infinite series (97) becomes

$$\sum_{n=0}^{\infty} \exp\left\{-\frac{a_n}{\beta}(x-z)\right\} a_n^{-2} = \frac{y_1^2}{\pi^2}\left\{\frac{(x-z)\pi}{\beta y_1}\log\frac{(x-z)\pi}{\beta y_1} - \frac{(x-z)\pi}{\beta y_1} + \right.$$

$$\left. + \frac{\pi(x-z)}{\beta y_1}\left[\frac{d}{d\alpha}\log \Gamma(\alpha) + C\right] - \frac{\pi^2(x-z)^2}{2\beta^2 y_1^2}\left(\alpha - \frac{1}{2}\right) + \frac{d^2}{d\alpha^2}\log \Gamma(\alpha)\right\}, \quad . \quad (104)$$

neglecting terms $O(1/y_1)$.

References

1. Drake, D. G. The Oscillating Two-Dimensional Aerofoil between Porous Walls. *The Aeronautical Quarterly*, Vol. VIII, August 1957.
2. Woods, L. C. On the Lifting Aerofoil in a Wind Tunnel with Porous Walls. *Proc. Roy. Soc.* A, Vol. 242, 1957.
3. Howarth, L. (Editor). *Modern Developments of Fluid Dynamics.* High Speed Flow. Vol 1, Chapter IX. Clarendon Press, Oxford, 1953.
4. Baldwin, B. S., Turner, J. B. and Knechtel, E. D. Wall Interference in Wind Tunnels with Slotted and Porous Boundaries at Subsonic Speeds. N.A.C.A. T.N. 3176, 1954.
5. Jahnke, E. and Emde, F. *Tables of Functions.* pp. 16-17. Dover, New York, 1954.
6. Jones, W. P. Wind-Tunnel Wall Interference Effects on Oscillating Aerofoils in Subsonic Flow. R. & M. 2943, 1958.

Plasto-Elastic Stress Distributions in Lugs

H. FESSLER, M.Sc.(Eng.), Ph.D., A.M.I.Mech.E. and D. J. HAINES, B.Sc.

(*The University of Nottingham*)

SUMMARY: A photoelastic layer was bonded to the face of aluminium alloy lugs and the strain distribution in the lugs was determined from the photoelastic fringe patterns which were recorded in a reflection-type polariscope. The semi-circularly-ended lugs were loaded through neat fitting hardened steel pins. Assuming the maximum shear stress criterion of yield, the region of yielding under different loads was determined from the fringe patterns. Yield contours are shown for each of the four ratios of (hole diameter)/(lug width) tested. The greatest shear strains in the lugs were related to the applied loads. The extent of yield across the section normal to the direction of loading was measured for different loads and it was found that the progress of yield across this section is independent of the (hole diameter)/(lug width) ratio. The residual stresses on this section were also estimated. Complete yielding across the lug was related to the properties of the material and to the fracture strength of the lugs. Local yielding due to surface irregularities remained local, showing that "bedding in" does not weaken the component under static loading conditions.

1. Introduction

Static tests of lugs have been carried out by many investigators (*see*, for example, Refs. 1 and 2), in attempts to relate the nominal stresses and the strength of the material to the permanent deformation of the loading hole and to the failure load of the lug. The available information on fatigue strength of the lugs has been analysed by Heywood[3]. Linge[4] used a photoelastic reflection technique to study the effect of pin clearances in lugs.

This paper is a study of the strain distributions in lugs. The regions of plastic deformation were determined by assuming the maximum shear stress criterion of yield to apply.

NOTATION

b width of lug

d diameter of hole

t_1 thickness of layer

t_m thickness of metal

Received August 1958.

y force to yield net normal section in pure tension

P force

$$U = \frac{\text{load to fracture lug}}{\text{force to fracture net normal section in pure tension}}$$

$$Y = \frac{\text{lowest force to cause yield across one limb of a lug}}{\text{force to yield net section in pure tension}}$$

Definitions

NORMAL SECTION of a lug is the section normal to the direction of loading passing through the centre of the pin hole.

YIELD FRONT is the boundary between elastic and plastic regions.

2. Experimental Technique

A photoelastic reflection method [5, 6, 7] was used. This consists in bonding a thin layer of photoelastic material to the metal surface and observing the fringe pattern in the layer caused by the strains applied to the component. These fringes are proportional to the difference of principal strains or maximum shear strain at any point.

In this invesugation lugs made of aluminium alloy D.T.D. 646B (Ref. 8) were tested by bonding a layer of the epoxy resin Araldite Casting Resin B (Ref. 9) to the surface with the adhesive Araldite 102 (Ref. 10). The joints withstood strains of more than four per cent. Because the stiffness of the layer was never greater than 1/80 of the elastic stiffness of the metal, the layer did not appreciably affect the behaviour of the metal for moderate strains and thus underwent the same strains as the metal lug.

Figure 1 shows the reflection polariscope and parts of the tensile testing machine used in the experiments.

All lugs were manufactured from one $\frac{1}{4}$ in. thick sheet of D.T.D. 646 B and had their axes parallel to the grain of the sheet. All lugs were $\frac{3}{4}$ in. wide and, except where otherwise stated, $\frac{1}{8}$ in. thick. All surfaces were surface ground, the photoelastic layer being ground to the required thickness after bonding. The thickness of the layers, which was constant on each specimen, varied from 0·012 in. to 0·034 in. This variation was necessary to obtain convenient fringe orders for predetermined strain differences. The thickness of the adhesive varied between 0·001 in. and 0·002 in. but was constant for each lug. The ends of the lugs were semi-circular, concentric with the neat-fitting, air-hardened, steel loading pins. The loading system used was self-aligning, thereby eliminating any applied bending moment on the specimens. The lug fixing was by means of a $\frac{5}{16}$ in. diameter pin, positioned $1\frac{1}{4}$ in. from the loading pin.

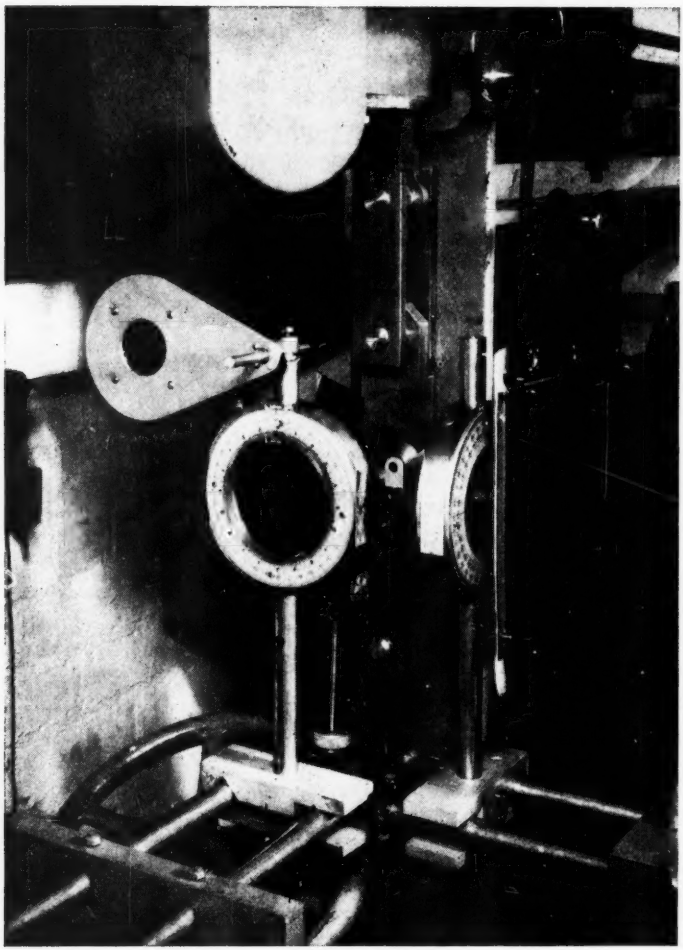

FIGURE 1. The apparatus.

To avoid errors due to creep in the adhesive, the testing time was kept to a minimum by photographing the fringe patterns. Most of the tests avoided unloading of the lugs, but it was found that repeated loading (up to 20 cycles) did not alter the strain distribution.

3. Calibrations

To evaluate the results of any plasto-elastic investigation, a knowledge of the stress-strain relationship of the material is essential. Conventional tensile tests were carried out on specimens loaded along and across the grain of the aluminium alloy sheet. The results are shown in Fig. 2. Young's modulus for both specimens

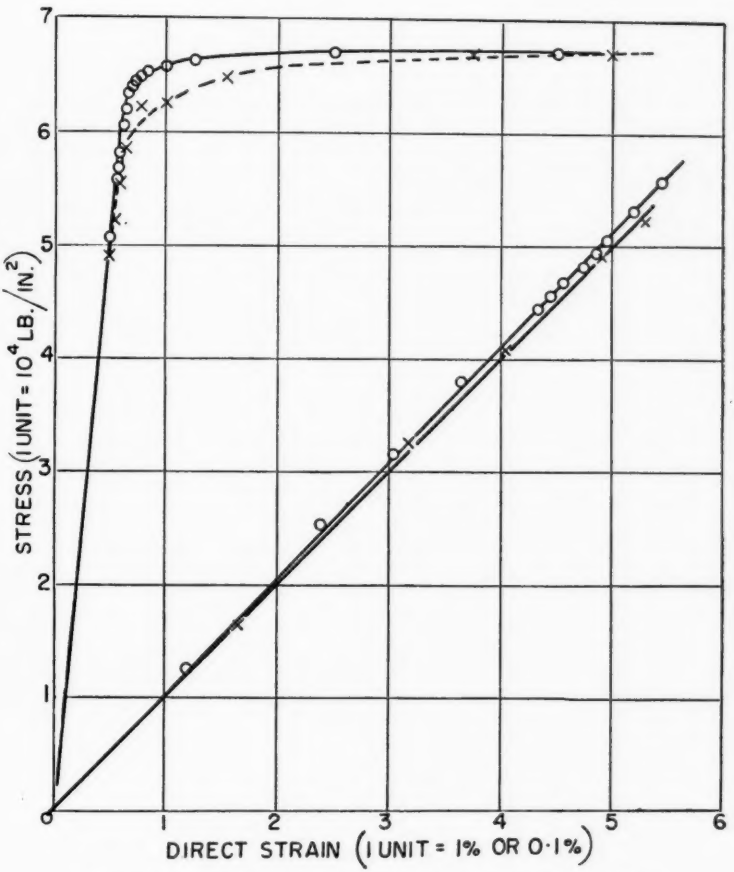

FIGURE 2. Stress-strain relation for D.T.D. 646B in pure tension.
○—test in direction of grain. ×—test perpendicular to grain.

was $10{\cdot}1 \times 10^6$ lb./in.^{2} and Poisson's ratio was 0·30 for the elastic state and 0·50 for the plastic range.

Araldite Casting Resin B, the material of the photoelastic layer, behaves elastically over the test range. Young's modulus was found to be $0{\cdot}48 \times 10^6$ lb./in.^{2}, Poisson's ratio 0·38, and the strain fringe coefficient 11,020 fringes/in. for unit strain difference.

The adhesive, Araldite 102, has a Young's modulus which is never greater than 20,000 lb./in.^{2}, and a strain fringe coefficient of 2,200 fringes/in. for unit strain difference. Because the thickness of the adhesive was only 0·001 in. to 0·002 in., it contributed little to the optical and mechanical behaviour of the layer, which varied between 0·012 in. and 0·034 in. for the specimens tested.

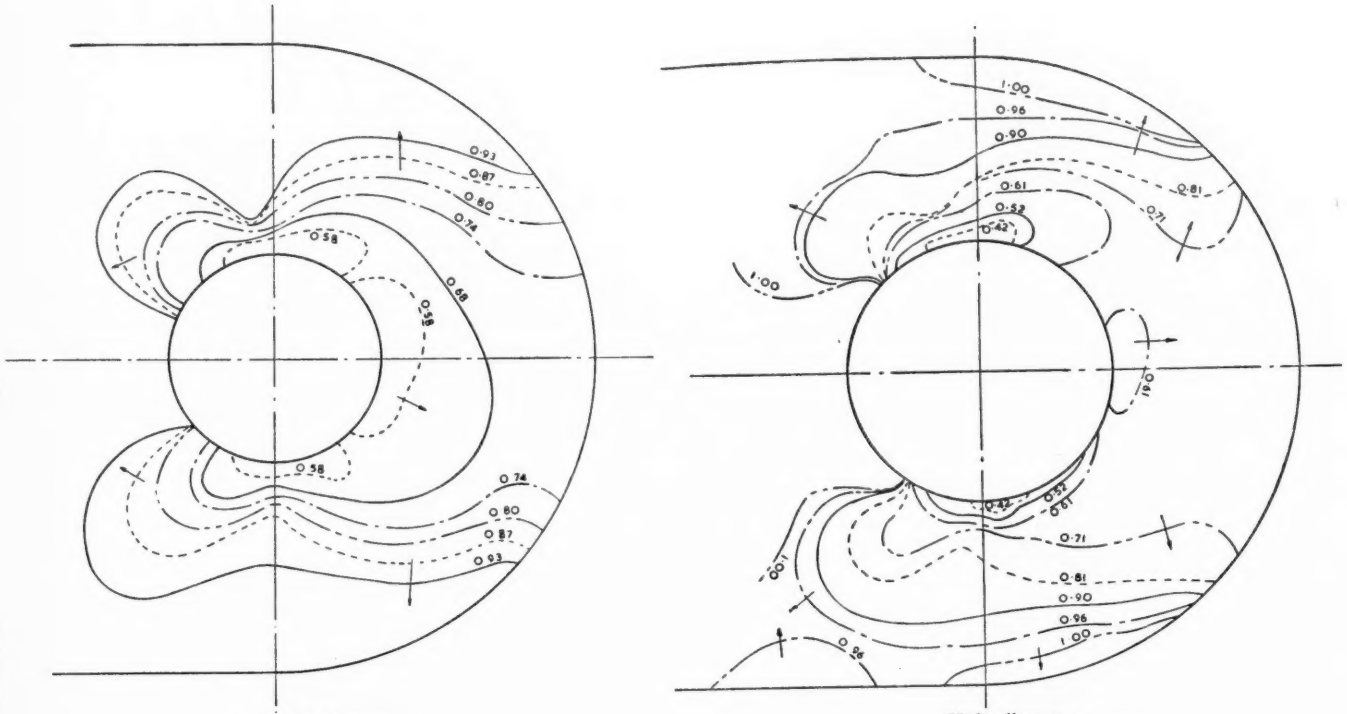

(*a*) $\frac{\text{Hole diameter}}{\text{lug width}} = 1/3$ (*b*) $\frac{\text{Hole diameter}}{\text{lug width}} = 5/12$

FIGURE 4. Yield contours showing the extent of yield for the stated fraction of the ultimate load of the lug.

FIGURE 4. Yield contours showing the extent of yield for the stated fraction of the ultimate load of the lug.

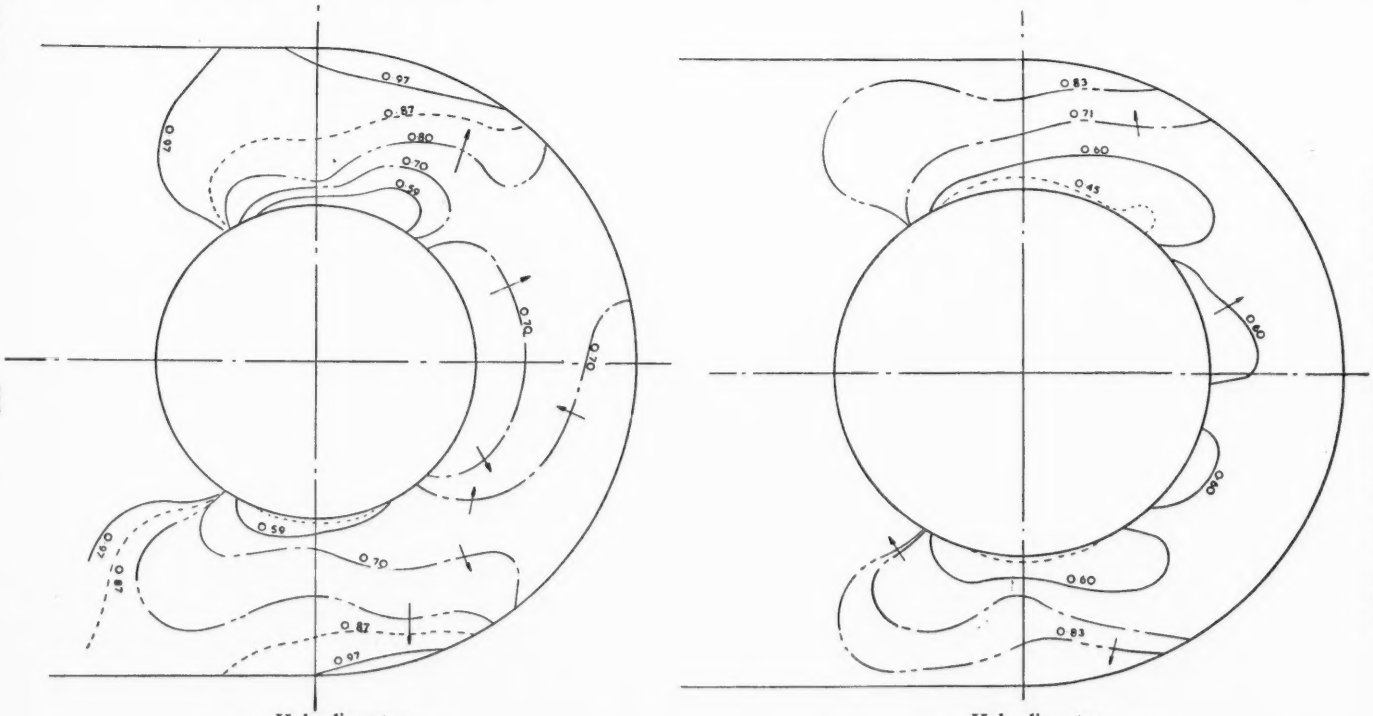

(*c*) $\frac{\text{Hole diameter}}{\text{lug width}} = 1/2$ (*d*) $\frac{\text{Hole diameter}}{\text{lug width}} = 7/12$

FIGURE 4. Yield contours, showing the extent of yield for the stated fraction of the ultimate load of the lug.

Part of the load applied to the lug is carried by the photoelastic layer and this introduces an error in the stress distributions. If it is assumed that the strains in the layer and metal are equal, because the widths are the same, the error

$$e = \frac{\text{load carried by layer}}{\text{total load}} = \frac{1}{1+P_m/P_l} = \frac{1}{1+(E_m t_m)/(E_l t_l)}$$

In the elastic range the error e was never greater than 1·2 per cent. At 4½ per cent strain the error e is 5 per cent if the thickness of the layer is 1/6 of the metal thickness.

The elastic strains at the edge of the hole in the plane normal to the direction of loading were measured for three hole sizes and the elastic stress concentration factors were compared with values interpolated from the results of Frocht and Hill[11] for square-ended lugs (Table I). The differences were attributed to the difference between round and square-ended lugs and to errors in both sets of experiments and in interpolation.

TABLE I

COMPARISON OF STRESS CONCENTRATION FACTORS

d/b	5/12	1/2	7/12
Authors	2·78	2·76	2·42
Frocht and Hill[7]	3·1	2·74	2·45

4. Strain Distributions

Figure 3 shows the fringe pattern in a typical lug after the application of the stated loads. It was thought most useful to express the loads as fractions of y, the force needed to cause yield in a uniform tensile specimen of the same material and the same net section, $(b-d)\,t_m$. For this purpose a yield stress of 65,000 lb./in.² was decided on from the test data, shown in Fig. 2. The maximum shear stress criterion of yield is the justification for the assumption that yielding in the bi-axial stress system on the surface of a lug occurs at the same stress difference of 65,000 lb./in.² This corresponds to a direct strain of 0·65 per cent and to a strain difference of 0·8 per cent. The strain differences are measured by the photoelastic layer and the thickness of this layer determines the fringe order which corresponds to yielding.

The photographs in Fig. 3 show, typically, general yield originating at the inner edge of the lug at positions inclined at 60° to 90° from the axis of loading when viewed from the centre of the pin. The "yield front," that is the boundary between the elastic and the plastic region, advances radially and circumferentially under increasing load, as may be seen by studying the position of the second order fringe.

This advance is most conveniently shown by the yield contours in Fig. 4. It may be seen that a region "behind" the pin remains elastic. As expected, the outer portions of the "small pin lug" in Fig. 4(*a*) remain elastic up to its failure by shear. Fig. 4(*c*) shows unsymmetrical behaviour. Yield first occurs in the right

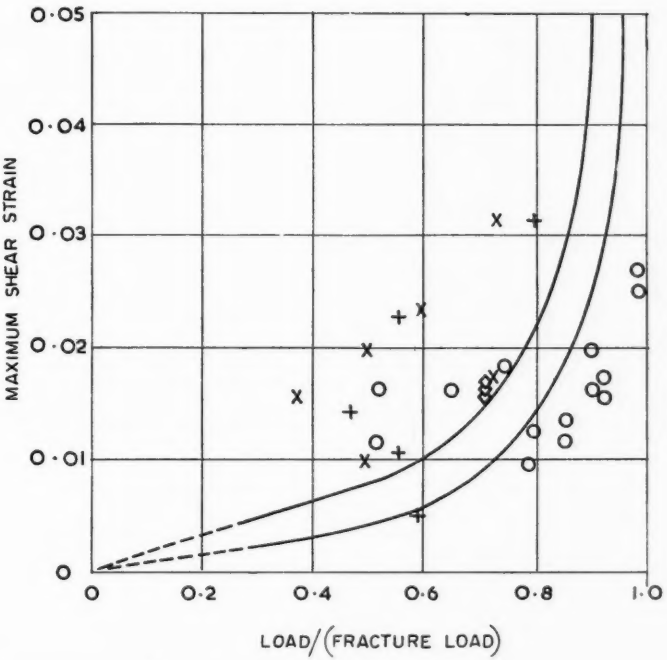

FIGURE 6. Maximum shear strains in all lugs.

d/b	1/3	5/12	1/2	7/12
Symbol	○	×	+	◇

hand limb and spreads across the limb at a load of 0·7, when most of the left hand limb is elastic. The yield front becomes slightly more symmetrical under greater loads. The last photograph for Fig. 4(*b*) was taken when straining was halted before failure under the ultimate load. This explains the 1·00 contour.

Initial yielding always occurred at the loaded pin-lug interface, but the position of this yielding and the load at which it occurred varied greatly. This was attributed to local surface irregularities of the components in contact. Figure 5 shows an example of such localised yield. If it occurred in regions of low nominal shear stress, *e.g.* near the axis of loading, this yielding was confined to a small area until the general stress level caused widespread yield in the lug. This proves the common belief that local surface irregularities are not detrimental to the static strength of components because the consequent "bedding in" causes only local yielding.

The greatest shear strains were determined from the recorded fringe patterns and related to the loads causing them. 129 readings were obtained from the lugs tested. 101 of these lie within the scatter band shown in Fig. 6. The remaining 28 values are shown individually. The points which lie above the scatter band correspond to observed local irregularities near the axis of loading. The only

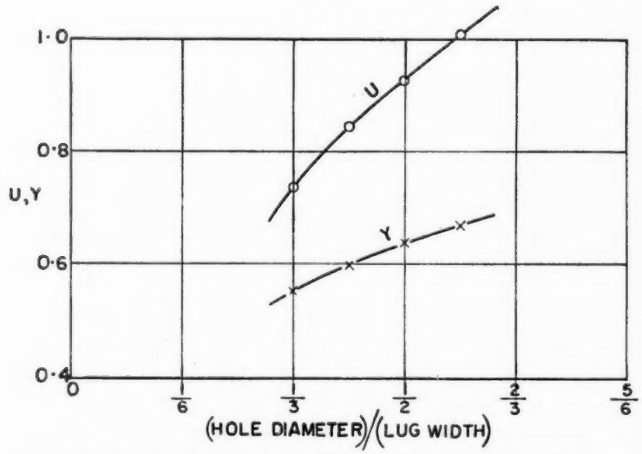

FIGURE 7. Static strength based on properties of the material.

significant difference between the different shapes of lugs is the lower strain difference in the small pin lugs under very large loads.

Figure 6 gives a guide to the ratio of the "repeated loading strength" to static strength of lugs. From the upper boundary of the scatter band the yield shear strain of 0·4 per cent corresponds to a quarter of the fracture load. If it is assumed that reverse yielding occurs when unloading after twice the yield strain has been attained on loading, this would occur at 0·8 per cent shear strain or half of the fracture load. Hence it may be suggested that lugs remain fully elastic if loaded to no more than a quarter of their static strength, yield unidirectionally if loaded to a half of their static strength and are likely to yield twice during every loading cycle if the variation in load exceeds half the static strength.

The usual measurements of permanent deformation were made on one lug ($d/b=1/3$) after the application of a load of 2,900 lb. (which subsequently caused failure). The loading pin was in single shear and its elastic deflection and its plastic deformation ($0{\cdot}0013d$) caused a variation in the elongation of the pin hole. The elongation of the hole was 1·19 per cent at the back face and 1·08 per cent at the front face of the lug. This does not affect the other results presented in this paper, because these variations through the thickness of the lug occur at large strains only.

The effect of thickness variation was studied with two thin lugs. These had a (limb width)/thickness ratio of $(b-d)/(2t)=1{\cdot}95$ instead of the normal $(b-d)/(2t)=1\frac{1}{4}$ for the narrowest limbs tested, but the results showed no significant difference from the lugs of standard thickness.

5. Ultimate Loads

Because it is easy to determine the ratio (U) of the ultimate load carried by a lug at fracture to the ultimate strength of the net section subject to pure tension,

(*a*) load/y=0·51 (*b*) load/y=0·57 (*c*) load/y=0·65

(*d*) load/y=0·70 (*e*) load/y=0·76 (*f*) load/y=0·82

FIGURE 3. Fringe patterns under increasing loads. $d/b=5/12$. Onset of yield corresponds to 1·8 fringes. Figure 3(*f*) shows the effect of a crack in the layer caused by the high local strains.

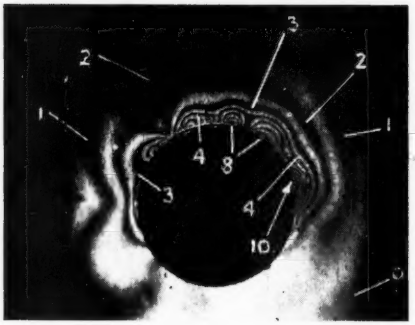

FIGURE 5. Example of local yielding due to surface irregularities. $d/b = 1/2$, load $= 0{\cdot}53y$.

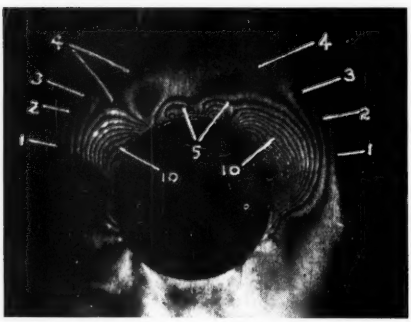

FIGURE 11(*a*). Fringe pattern under a load of $0{\cdot}80y$.

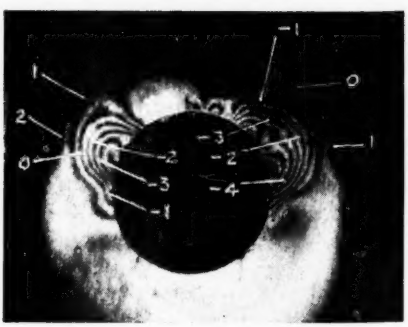

FIGURE 11(*b*). Fringe pattern after removal of load of $0{\cdot}80y$.

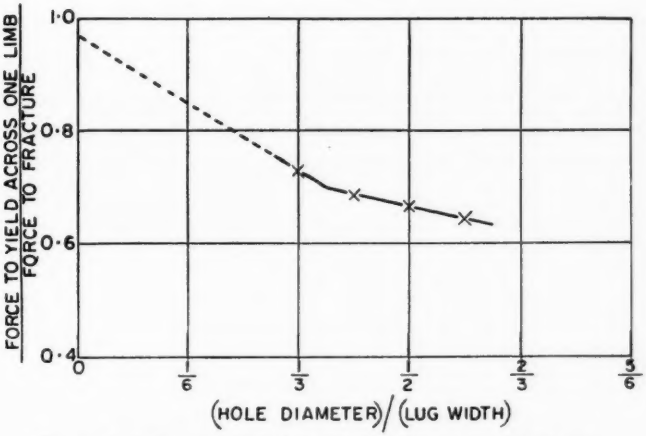

FIGURE 8. Safe static strength based on ultimate strength of lugs.

an attempt was made to relate this ratio with some yield characteristic of the lugs tested. Figure 7 shows the mean values of U and the mean values of Y, (force to cause yield to spread across one limb of a lug)/(force to yield the net section in pure tension). It is evident that both graphs are of the same form. Values of Y could only be determined as the mean of the last load before, and the first load after yield has spread across a section. The greatest divergence of any point from the Y curve was estimated as $\pm 0{\cdot}025Y$.

Figure 8 is approximately equivalent to a plot of Y/U, because the yield strength of the material is almost equal to the ultimate tensile strength (65,000 lb./in.^{2} and 67,000 lb./in.^{2} respectively). It was assumed that for zero hole size the yield fracture ratio would be the same as for a uniform bar. Linear relationships are not claimed, but are convenient because the change of slope coincides with the transition from "shear failure" to "tensile failure" (*see* Fig. 4). It may be concluded from Fig. 8 that, for practicable designs of lugs, complete yield across a section is unlikely to occur at less than 0·6 of the force required to fracture the lug. The authors believe that it is inadvisable to rely on the strain-hardening characteristics of the material and therefore suggest that the force which causes yielding across the whole section of one limb of the lug should not be exceeded. Figure 7, or Fig. 8 in connection with the ultimate load of the lug, thus give the static strength of semi-circularly-ended lugs.

6. Section Normal to Direction of Loading

Figure 9 shows typical plots of fringe order (proportional to maximum shear strain) across the normal section of one of the lugs tested. Each graph was obtained from a photograph of the fringe pattern for a particular load. The curves for the small loads are similar for all sizes of lugs and show an increase of strain gradient towards the pin hole. The horizontal lines denote the fringe order which

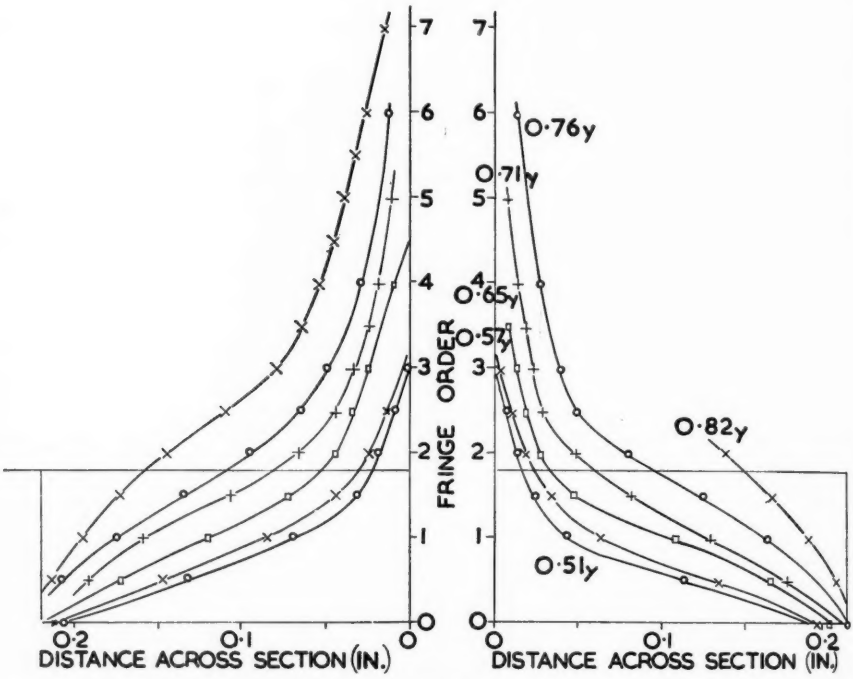

FIGURE 9. Fringe plots across normal section of a lug. $d/b = 5/12$. The numbers against the curves indicate the applied loads.

corresponds to the strain difference which is assumed to cause yielding. In many cases the strain gradient becomes fairly constant across the section under large plastic strains. This represents a strain distribution analogous to the stress distribution caused by an eccentric tension.

Fringe distance curves similar to those in Fig. 9 were plotted for fifteen lugs, and the position of the yield front was measured in each case. These positions were related to the load on the lug. Figure 10 is a record of all the results. The scatter band contains 120 points randomly distributed. This shows that yield progresses across the normal section as shown, independent of the (hole diameter)/(lug width) ratio and is not affected by variations in the load and position of the onset of yielding. The difference between small hole lugs ($d/b = 1/3$) and the other sizes tested ($d/b = 5/12, 1/2, 7/12$) is that the small hole lugs failed in shear when yield had progressed 0·6 of the distance across the normal section. The other lugs yielded across the whole normal section before failure.

7. Residual Strains and Stresses

The residual fringe pattern after the load has been removed can be recorded and these fringes are, of course, proportional to the residual difference of principal

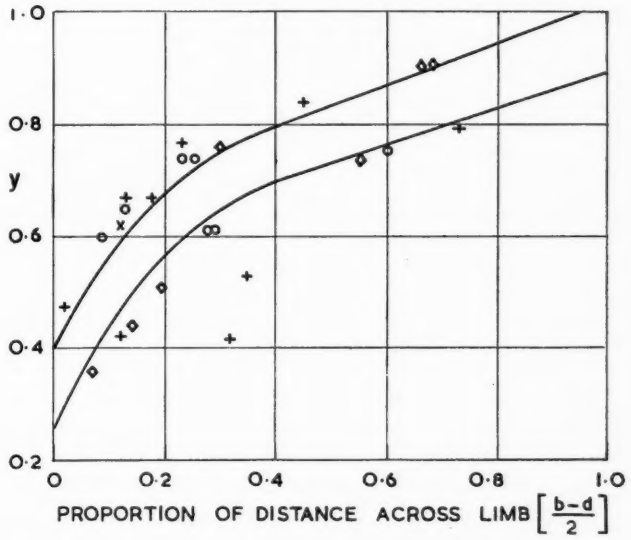

FIGURE 10. Position of yield front on normal section of all lugs.

d/b	1/3	5/12	1/2	7/12
Symbol	○	×	+	◇

strains. The residual stresses cannot readily be determined from this because, in general,

(*a*) the directions of the original and the residual stresses do not coincide,

(*b*) the residual stresses act in the same directions as the last plastic strain increment, not in the direction of overall plastic strain,

(*c*) plastic stress-strain relationships are not uniquely determined by any simple test.

In spite of these theoretical objections the attempt was made to determine the residual stresses on a section normal to the direction of loading.

It was assumed that the applied and residual strains and stresses in the normal section are parallel to the direction of loading and that the strain at right angles to the direction of loading is negligible (or constant). This assumption was necessary because it was not possible to record the directions of the residual strains reliably. The directions of the strains under elastic and considerable plastic deformation were determined for one lug. These results suggested that the foregoing assumption may be a fair approximation.

Figure 11(*a*) shows the fringe distribution in a lug of $d/b=\frac{1}{2}$ under a load of $0{\cdot}80y$. Figure 11(*b*) shows the fringe pattern after removal of that load. The negative fringe orders indicate a reversal of the sign of the strain difference.

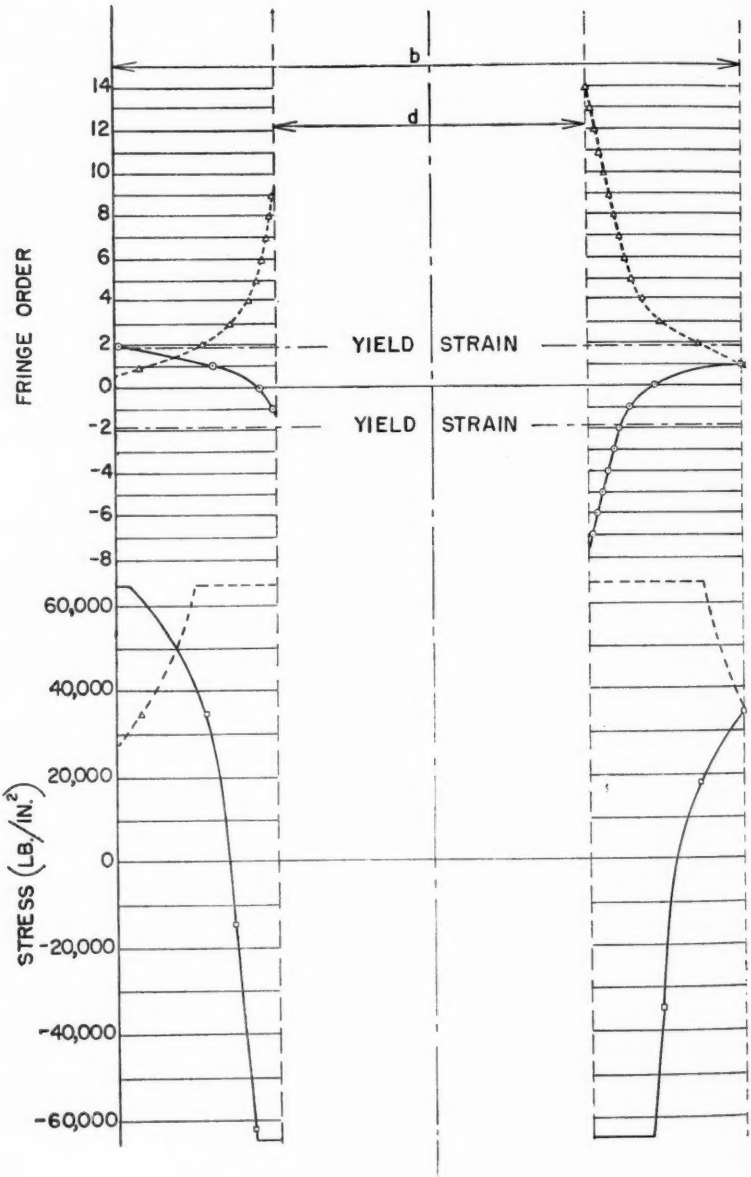

FIGURE 12. Residual strains and stresses on a normal section.
Residual distribution ——— Distribution under load of 0·80y - - - - - - -

The fringe or strain distributions across the normal section under load and after removal of the load, shown in Fig. 12, were plotted from Fig. 11. To obtain an approximate stress distribution from this information it is necessary to know the stress-strain relationship for the material in tension and compression and to assume that these relations also apply for the lug considered. From Fig. 2 it was assumed that yield occurred at a stress of 65,000 lb./in.^{2} in tension and compression and that this stress is not exceeded (*i.e.* no work-hardening). With these assumptions it is possible to plot the stress distributions shown in Fig. 12. At any point, the fringe order under load which corresponds to plastic strain must be subtracted from the residual fringe order to obtain the residual stresses.

It may be seen that reverse yield has occurred on unloading. From the graph of residual stress, the ratio of the positive area under the graph to the negative area is 0·97. This indicates the overall error due to the measurements and assumptions made. A test on another lug gave a similar result.

8. Conclusions

The results should apply approximately to semi-circularly-ended lugs of any material which has a stress-strain relationship similar to that shown in Fig. 2.

The greatest shear strains occurred at the loaded surface of the hole, usually at 60° to 85° from the axis of loading. This shear strain depends on the load only and is independent of the (hole diameter)/(lug width) ratio. If shear strain is considered a suitable fatigue criterion, Fig. 6 gives relevant information for the greatest possible value of fatigue strength.

The force required to cause yielding to spread across the whole section of one limb was related to the ultimate load in Fig. 8. Because it is inadvisable to exceed this force, Fig. 8 gives the safe static strength.

The normal section is not the most highly stressed region of a lug. The progress of yielding across this section (shown in Fig. 10) is independent of the (hole diameter)/(lug width) ratio. The residual strains after removal of a load of 0·80y showed extensive reverse yielding.

Acknowledgments

The authors wish to thank Professor J. A. Pope, who as Head of the Department of Mechanical Engineering, provided all necessary facilities for this work. Thanks are also due to Mr. I. L. G. Baillie of Bristol Aircraft Ltd. and to Mr. F. Tyson and other members of the technical staff of Handley Page Ltd. for their advice on current practice in the aircraft industry.

References

1. Howard, R. M. Strength Tests on Lugs in Sheet Materials. M.A.P. Scientific and Technical Memorandum No. 23/24, June 1945.

2. Baillie, I. L. G. Design of Lugs in Bar Materials. Bristol Aircraft Ltd., Admin. Note. No. 12, J.A.C. 418/303, November 1958.

3. HEYWOOD, R. B. The Strength of Lugs in Fatigue. R.A.E. Technical Note Structures 182, January 1956.

4. LINGE, J. R. Investigations into a Photoelastic Method for Direct Measurement of Surface Strains in Metal Components. College of Aeronautics Report 97, 1956.

5. FESSLER, H. and HAINES, D. J. A Photoelastic Technique for Strain Measurement on Flat Aluminium Alloy Surfaces. *British Journal of Applied Physics*, Vol. 9, p. 282, July 1958.

6. D'AGASTINO, J., DRUCKER, D. C., LIU, C. K. and MYLONAS, C. An Analysis of Plastic Behaviour of Metals with Bonded Birefringent Plastic. *Proceedings of the Society for Experimental Stress Analysis*, Vol. XII, No. 2, p. 115, 1955.

7. ZANDMAN, F. Stress Analysis by Photo-Elastic Varnishes. Acier Stahl Steel No. 9, p. 356, 1956.

8. Noral Data Sheet, Northern Aluminium Co. Ltd., Banbury.

9. Instruction Sheet C1. CIBA (A.R.L.) Ltd., Duxford, Cambridge.

10. Instruction Sheet A4. CIBA (A.R.L.) Ltd., Duxford, Cambridge.

11. FROCHT, M. M. and HILL, H. N. Stress Concentration Factors around a Central Circular Hole in a Plate Loaded through a Pin in the Hole. *American Society of Mechanical Engineers*, Vol. 62, p. A5, 1940.

Notes on Thin Wing Theory at Low Supersonic Speeds

Part I. The Design of Lifting Surfaces

G. J. HANCOCK

(Queen Mary College, University of London)

Summary: On the basis of the linearised theory, the integral relationship for the incidence distribution in terms of the velocity potential is established for wings with subsonic leading edges. Some analytical problems are analysed. A simple general numerical method is given for this design problem which compares favourably with exact linear theories. In Part II, to be published, a further numerical method is developed, for calculating the loading on *any* specified thin wing with subsonic leading edges, which again agrees favourably with exact linear theory. Both of these numerical techniques can be easily accommodated on desk calculating machines.

1. Introduction

Most of the effort devoted to wing theories in supersonic motion has been concentrated on the problem of determining the loading on a specified finite thin wing. This problem may be considered as solved for the majority of practical cases on the basis of the linearised theory, either by analytical or numerical techniques. However, the inverse problem of determining a wing surface which conforms to a specified loading distribution has attracted far less attention, although the relevant formulae are presented in Ref. 5.

In this part of the paper the emphasis is on the design problem for wings with subsonic leading edges. The relevant formulae are deduced from the well-known lifting surface equation for the sake of completeness. Although these formulae can be applied analytically to any particular design consideration, the integrals become intractable for complicated plan forms and loading distributions; therefore a general numerical method is developed. This method can be applied with reasonable accuracy for the whole range of wing parameters (curved or straight, subsonic trailing and leading edges) and loadings.

No mention is made in this paper of the type of loading required to optimise some aspect of performance; this is left to those who might wish to apply the method.

Received June 1958.

NOTATION

x, y, z
ξ, η, ζ — Cartesian co-ordinates

$\mathbf{q}$ velocity vector

V free stream velocity

M free stream Mach number

u, v oblique Mach co-ordinates

w downwash velocity

$u = f(v),\ v = f(u),$
$x = l(y)$ — equations of wing leading edge

c_0 centre chord of wing

s semi-span

d length of mesh system

$K^2 = (\cot\theta - \beta)/(\cot\theta + \beta)$

$K_1^2 = Mc_0/\beta$

$b_1 = K_1^2/(1+K^2)$

$b_2 = K_1^2(1-K^2)/(1+K^2)$

$b_3 = (K_1^2/2)(1-K^2)$

p_0 constant, representing uniform loading

$p_1 = p_0(\cot\theta + \beta)/M$

$A_{(i,j)(k,l)}$ coefficients for numerical method

ϕ velocity potential

$\phi_{i,j}$ the mean velocity potential between the lines $\{(i-1)d \leqslant u \leqslant id,\ (j-1)d \leqslant v \leqslant jd\}$

α wing incidence

$\alpha_{i,j}$ mean wing incidence between the lines $\{(i-1)d \leqslant u \leqslant id,\ (j-1)d \leqslant v \leqslant jd\}$

$$\gamma_{k,l} = \sum_{\substack{i=0\ldots k \\ j=0\ldots l}} A_{(i,j)(k,l)}\phi_{(i,j)}$$

$f(x, y)$ equation of wing camber surface

ρ density of free stream

δ distance from edge singularity

θ half the wing apex angle

$\beta = (M^2-1)^{1/2}$

2. Design of Camber Surfaces

On the basis of the linearised theory of supersonic flow, the perturbation velocity $q\,(u, v, w)$, relative to a set of Cartesian axes, is superimposed on a steady supersonic stream $(V, 0, 0)$ and satisfies the condition of irrotational motion. Hence a velocity potential ϕ exists such that $\mathbf{q}=\text{grad}\,\phi$. Taking the origin of the axes of reference at the leading apex of a swept wing (the x-axis is in the direction of the main stream, the y-axis is in the spanwise direction and the z-axis completes a right-handed set), the physical problem of the calculation of the loading distribution over a thin wing is resolved mathematically by the determination of the discontinuity of ϕ across the plan form of the wing on the plane $z=0$ which satisfies the condition that the downwash is continuous and makes the flow tangential to the wing surface. That is,

$$\left(\frac{\partial\phi}{\partial z}\right)_{z=0} = w\,(x, y, 0) = -V\alpha\,(x, y) = -V\,\frac{\partial\zeta\,(x, y)}{\partial x},$$

where $z=\zeta\,(x, y)$ is the equation of the wing camber surface and $\alpha\,(x, y)$ is the wing incidence distribution. The loading is equal to $2\rho V\partial\phi\,(x, y, +0)/\partial x$.

The well-known fundamental formula[1] applying this principle is

$$\phi\,(x, y, +0) = -\frac{1}{\pi}\iint_S \frac{w\,(\xi, \eta)\,d\xi\,d\eta}{[(x-\xi)^2-\beta^2\,(y-\eta)^2]^{1/2}} \quad . \quad . \quad . \quad (1)$$

where S is the fore Mach sector on the plane $z=0$ upstream of the point $(x, y, 0)$, *i.e.* for $(x-\xi)^2 \geqslant \beta^2\,(y-\eta)^2$, where $\beta^2=M^2-1$.

When the wing has supersonic leading edges and the Mach sector S does not intersect the wing tips, $w\,(\xi, \eta)$ is known over the whole of S, being specified on the wing and zero ahead of the leading edge. Equation (1) can then be applied directly. If S intersects the wing tips it will also include some of the upwash field off the wing; however, this is related directly to the incidence of the wing by Evvard's technique[2], so equation (1) is again readily applicable. For wings with subsonic leading edges S will include the upwash regions ahead of the leading edges but so far it has not been possible to relate analytically these regions to conditions on the wing, although approximate methods have been devised[3, 4].

In the design problem we wish to specify the loading over a given plan form and to calculate the incidence and camber surface of the wing. Since the loading distribution is defined in terms of $\phi\,(x, y, +0)$ we wish to invert equation (1) to obtain an integral relationship for $w\,(x, y)$ in terms of $\phi\,(\xi, \eta, +0)$. In this paper the investigation is restricted to cases of wings with subsonic leading edges only, although the methods of inversion can be applied more generally.

Consider a wing with subsonic leading edges, as shown in Fig. 1, symmetrical about the x-axis.

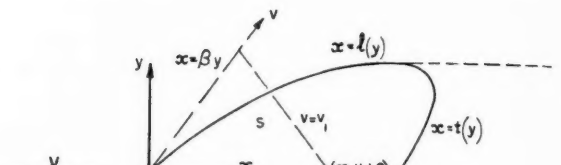

FIGURE 1. Notation.

On transforming the Cartesian co-ordinates (x, y) to oblique Mach co-ordinates (u, v), on the plane $z = +0$, defined by

$$u = \frac{M}{2\beta}(x - \beta y), \quad v = \frac{M}{2\beta}(x + \beta y),$$

as shown in Fig. 1, equation (1) becomes

$$\phi(u_1, v_1) = -\frac{1}{\pi M} \int_{u=0}^{u=u_1} \int_{v=0}^{v=v_1} \frac{w(u, v)\, du dv}{\sqrt{[(u_1 - u)(v_1 - v)]}} \quad . \quad . \quad . \quad (2)$$

As already pointed out, $w(u, v)$ is known only within the part of S on the wing surface and is unknown ahead of the leading edges. However, taking $w(u, v)$ to be an integrable function throughout the whole of area S, equation (2) may be written as the two simultaneous equations

$$\left.\begin{aligned} -\pi M \phi(u_1, v_1) &= \int_0^{u_1} \frac{F(u, v_1)\, du}{\sqrt{(u_1 - u)}} \\ F(u, v_1) &= \int_0^{v_1} \frac{w(u, v)\, dv}{\sqrt{(v_1 - v)}} \end{aligned}\right\} \quad . \quad . \quad . \quad . \quad . \quad (3)$$

These are both Abel type integral equations, so that, if

$$f(x) = \int_k^x \frac{u(\xi)\, d\xi}{(x - \xi)^{\mu}}, \quad \text{where} \quad \begin{cases} 0 \leqslant \mu \leqslant 1 \\ k \leqslant x \leqslant k_1 \end{cases}$$

$$\text{then} \quad u(x) = \frac{\sin \mu\pi}{\pi} \frac{d}{dx} \int_k^x \frac{f(\xi)\, d\xi}{(x - \xi)^{1-\mu}}.$$

Applying the inversion formula to both equations of (3) and combining them, remembering that $\alpha(u, v) = -\dfrac{w(u, v)}{V}$,

$$\alpha(u_1, v_1) = \frac{M}{\pi V} \frac{\partial^2}{\partial u_1 \partial v_1} \int_{u=0}^{u=u_1} \int_{v=0}^{v=v_1} \frac{\phi(u, v)\, du dv}{\sqrt{[(u_1 - u)(v_1 - v)]}} \quad . \quad . \quad (4)$$

This is therefore the basic design formula which gives the incidence distribution on the wing from a known distribution of $\phi(u, v)$. Since loading only occurs on the wing surface, $\partial\phi(x, y, +0)/\partial x$ is zero off the wing plan form, and the discontinuity $\phi(x, y, +0)$ occurs only on the wing surface, together with the trailing vortex wake, as in subsonic wing theory. Furthermore, the discontinuity in the wake is determined by the conditions at the trailing edge and is a function of y only. Specification of the loading on a wing implies specification of $\phi(u, v)$ on the wing and the wake, while $\phi(u, v)$ is zero outside these regions. Therefore in this case equation (4) can be applied, directly the loading is stated, over the whole wing; the wing tip and subsonic trailing edge regions have no special significance in this case.

It should be mentioned that equation (4) is not new but is essentially one of the fundamental formulae in supersonic wing theory, derived from first principles by Heaslet and Lomax[5], but it appears to be not very well known. The author thought that the present method of obtaining equation (4) from the familiar equation (1) would be the most satisfactory introduction for most readers. In any case, the application of equation (4) (to which the rest of this paper is devoted) is not investigated in Ref. 5. Goldsworthy[6] has shown that equation (4) is applicable for the symmetrical problem of the design of the thickness distribution with a specified surface pressure distribution at zero lift when the leading edges are supersonic.

3. Form of the Velocity Potential

In the present design problem the loading will be assumed over a given wing and therefore the discontinuity $\partial\phi/\partial x$ is known across the wing plan form. It is worth reviewing at this stage some of the main points to be included in any assumption of $\partial\phi(x, y, +0)/\partial x$.

At the leading edge:—

(*i*) If the incidence at the leading edge is finite, then $\partial\phi/\partial x = O(\delta^{-1/2})$, where δ is the distance from the leading edge, except at a unique value of the incidence (equivalent to the ideal angle of incidence in two-dimensional subsonic theories) when $\partial\phi/\partial x = O(\delta^{1/2})$.

(*ii*) If the loading is assumed to be $O(1)$ at the leading edge, the incidence there will be logarithmically infinite.

At the wing tips:—

(*i*) If the incidence is finite at the wing tips (assuming that they exist), $\partial\phi/\partial x = O(\delta_1^{1/2})$, where δ_1 is the distance from the wing tips.

(*ii*) If $\partial\phi/\partial x = O(1)$ at the wing tips, the incidence there will be infinite, of the order δ_1^{-1}.

At the trailing edge:—

(*i*) If the trailing edge is supersonic, then $\partial\phi/\partial x = O(1)$ for a finite incidence.

(*ii*) If the trailing edge is subsonic, then $\partial\phi/\partial x = O(\delta_2^{1/2})$, where δ_2 is the distance from the trailing edge, thus satisfying the Kutta-Joukowski hypothesis.

On assuming the distribution of $\partial\phi(x, y, +0)/\partial x$, the velocity potential follows immediately from

$$\phi(x, y, +0) = \int_{\xi=l(y)}^{\xi=x} \frac{\partial\phi}{\partial\xi}(\xi, y, +0)\, d\xi, \quad . \quad . \quad . \quad . \quad (5)$$

where $\xi = l(y)$ is the equation of the leading edge, so ensuring that $\phi(x, y, +0)$ is zero along this edge. It is seen that, when x lies in the wake, where $\partial\phi/\partial\xi$ is zero, ϕ is a function of y only.

A further consideration is now introduced, namely, if $\partial\phi(x, y, +0)/dy$ is discontinuous anywhere within the wing area, while the loading $\partial\phi(x, y, +0)/\partial x$ remains finite, the downwash will be infinite along the discontinuity. This follows basically from continuity considerations since, if $\partial\phi/\partial x$ is finite and $\partial\phi/\partial y$ is infinite, then $w = \partial\phi/\partial z$ is infinite. There are two common examples of this type of discontinuity. The first occurs on the centre line of swept wings with uniform loading. The second occurs when the lines of constant loading (or isobars) are kinked.

4. Wings with Uniform Loading

Two simple examples are worked out to illustrate Section 3. The camber surfaces of a delta and of a swept wing with subsonic leading edges are calculated to give uniform loading over the wings.

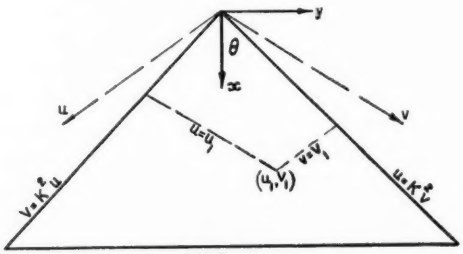

FIGURE 2. Co-ordinate system of delta wing.

4.1. Delta Wing

This wing is shown in Fig. 2 and is defined in terms of the Mach co-ordinates (u, v). The leading edges are $v=K^2u$ and $u=K^2v$ where $K^2=(\cot\theta-\beta)/(\cot\theta+\beta)$. The trailing edge $x=c_0$ is therefore $u+v=Mc_0/\beta=K_1^2$, say.

The condition of uniform loading is

$$\frac{\partial\phi}{\partial x}=\text{constant}=p_0.$$

On application of equation (5),

$$\phi=p_0\,(x-|y|\cot\theta),$$

which becomes, on transformation to the (u, v) system,

$$\left.\begin{aligned}\phi&=p_1\,(u-K^2v)\ \text{ for }\ y\geqslant 0\\ &=p_1\,(v-K^2u)\ \text{ for }\ y\leqslant 0\end{aligned}\right\}\qquad\ldots\qquad(6)$$

$$\text{where}\quad p_1=p_0\,\frac{\cot\theta+\beta}{M}\,.$$

The incidence distribution is found by substituting equation (6) in equation (4), that is

$$\alpha(u_1,v_1)=\frac{Mp_1}{\pi V}\,\frac{\partial^2}{\partial u_1\partial v_1}\left\{\int_{u=0}^{u=u_1}\frac{du}{\sqrt{(u_1-u)}}\int_{v=K^2u}^{v=u}\frac{v-K^2u}{\sqrt{(v_1-v)}}\,dv+\int_{u=0}^{u=u_1}\frac{du}{\sqrt{(u_1-u)}}\int_{v=u}^{v=\frac{v_1}{u_1}u}\frac{u-K^2v}{\sqrt{(v_1-v)}}\,dv+\right.$$

$$\left.+\int_{v=0}^{v=v_1}\frac{dv}{\sqrt{(v_1-v)}}\int_{u=K^2v}^{u=\frac{u_1}{v_1}v}\frac{u-K^2v}{\sqrt{(u_1-u)}}\,du\right\}$$

$$=\frac{Mp_1}{\pi V}\left\{-(1+K^2)\log\frac{1-u'}{1+u'}+K\log\left(\frac{1-Ku'}{1+Ku'}\right)\left(\frac{u'-K}{u'+K}\right)\right\}\qquad\ldots\qquad(7)$$

where $u'=\sqrt{(u_1/v_1)}$.

This example illustrates some of the points raised in Section 3. Since the loading is assumed to be finite at the leading edges ($u'=K,\ 1/K$), the incidence there tends to $-\infty$ like $\log\delta$. Also the assumption that $\partial\phi/\partial y$ is discontinuous across the wing centre line ($u'=1$) gives an infinite downwash on this line. Diagrams are given in Fig. 3 for the incidence distribution and camber surface of a 45° swept delta when $K^2=1/4$ ($M=1{\cdot}2$) at the spanwise positions of $s/4$, $s/2$ and $3s/4$. The camber surface $\zeta(x, y)$ is derived from the standard linearised formula $d\zeta/dx=\alpha(x, y)$.

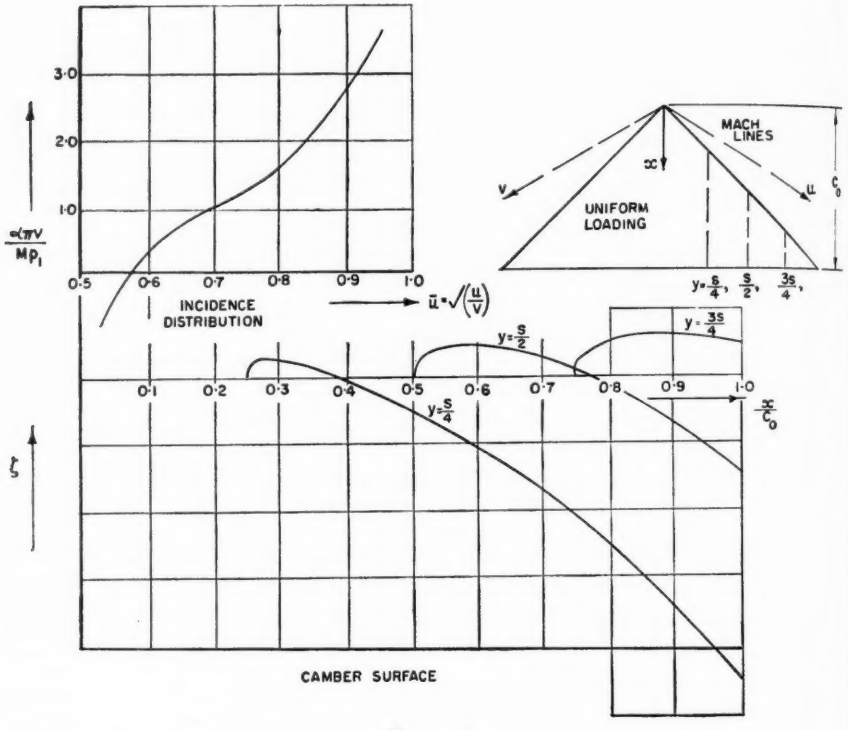

FIGURE 3.

4.2. SWEPT WING WITH SUBSONIC TRAILING EDGES

In this example the delta wing is extended to have a subsonic trailing edge (parallel to the leading edge), as shown in Fig. 4.

The assumption of uniform loading is

$$\frac{\partial \phi}{\partial x} = \text{constant} = p_0,$$

so that

$$\phi = p_0 (x - |y| \cot \theta) \qquad \text{on the wing} \begin{cases} |y| \leqslant s = c_0 \\ c_0 + |y| \cot \theta \geqslant x \geqslant |y| \cot \theta \end{cases}$$

$$= p_0 c_0 \qquad \text{on the wake} \begin{cases} x \geqslant c_0 + |y| \cot \theta \\ |y| \leqslant s = c_0 \end{cases}$$

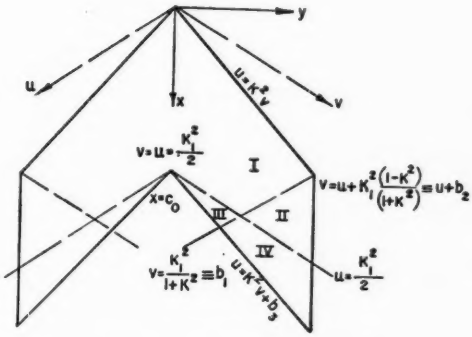

FIGURE 4. Swept wing notation.

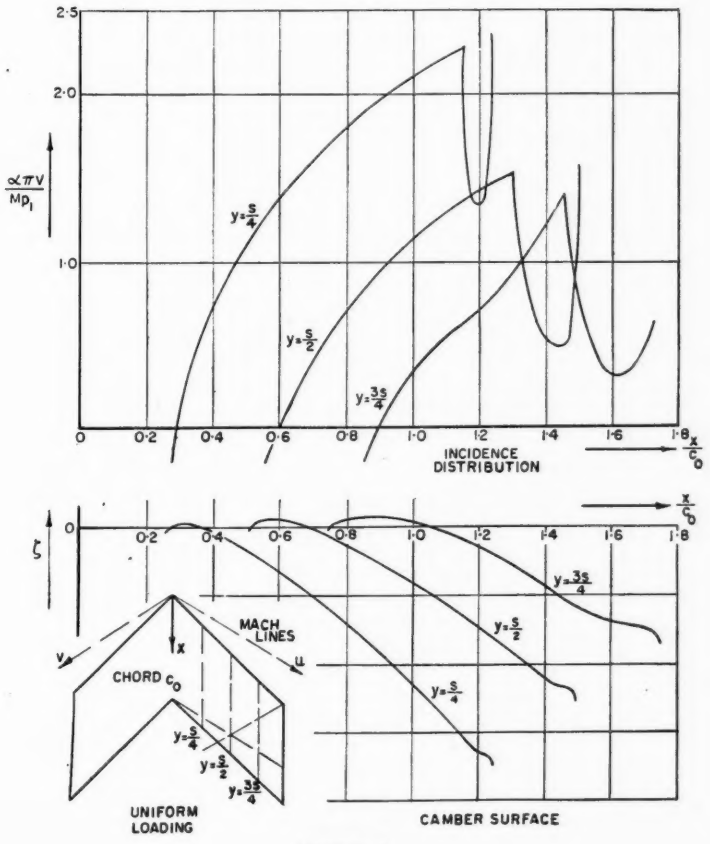

FIGURE 5.

Hence, using the (u, v) co-ordinates,

$$\left.\begin{aligned}\phi &= p_1(u-K^2v) \quad \text{for } y \geqslant 0\\ &= p_1(v-K^2u) \quad \text{for } y \leqslant 0\end{aligned}\right\} \quad \text{on the wing}$$

$$\left.\begin{aligned}&= p_0 c_0\\ &= p_1 b_3\end{aligned}\right\} \quad \text{on the wake.}$$

Four areas of influence are denoted in Fig. 4 and the incidence distributions are given for:—

Area I:—this is given by equation (7) and is denoted by $\alpha_{\mathrm{I}}(u_1, v_1)$.

Area II:—

$$\alpha_{\mathrm{II}}(u_1, v_1) = \alpha_{\mathrm{I}} - \frac{Mp_1}{\pi V}\frac{\partial^2}{\partial u_1 \partial v_1}\int_{v=b_1}^{v=v_1}\frac{dv}{\sqrt{(v_1-v)}}\int_{u=K^2v}^{u=v-b_2}\frac{u-K^2v}{\sqrt{(u_1-u)}}\,du$$

$$= \alpha_{\mathrm{I}} - \frac{Mp_1}{\pi V}\left\{-K\cosh^{-1}\left(\frac{u_1+K^2v_1-2b_1K^2}{u_1-K^2v_1}\right)+\right.$$

$$\left.+\frac{1}{2}(1+K^2)\cosh^{-1}\left(\frac{u_1+b_2+v_1-2b_1}{u_1+b_2-v_1}\right)-(1-K)\frac{\sqrt{[(v_1-b_1)(u_1-K^2b_1)]}}{u_1+b_2-v_1}\right\}.$$

Area III:—

$$\alpha_{\mathrm{III}}(u_1, v_1) = \alpha_{\mathrm{I}} - \frac{Mp_1}{\pi V}\frac{\partial^2}{\partial u_1 \partial v_1}\left\{\int_{u=K_1^2/2}^{u=u_1}\frac{du}{\sqrt{(u_1-u)}}\int_{v=K_1^2u+b_3}^{v=u}\frac{v-K^2u-b_3}{\sqrt{(v_1-v)}}\,dv+\right.$$

$$\left.+\int_{u=K_1^2/2}^{u=u_1}\frac{du}{\sqrt{(u_1-u)}}\int_{v=u}^{v=(u-b_3)/K^2}\frac{u-K^2v-b_3}{\sqrt{(v_1-v)}}\,dv\right\}$$

$$= \alpha_{\mathrm{I}} - \frac{Mp_1}{\pi V}\left\{\frac{2(1-K^2)}{v_1-u_1}\sqrt{\left[(u_1-K_1^2/2)(v_1-K_1^2/2)\right]}-\right.$$

$$-K\cosh^{-1}\left(\frac{v_1-b_3+K^2u_1-K^2K_1^2}{v_1-b_3-u_1K^2}\right)-$$

$$\left.-K\cosh^{-1}\left(\frac{K^2v+b_3+u_1-K_1^2}{K^2v_1+b_3-u_1}\right)+2\cosh^{-1}\left(\frac{v_1+u_1-K_1^2}{v_1-u_1}\right)\right\}$$

Area IV:—

$$\alpha_{\mathrm{IV}}(u_1, v_1) = \alpha_{\mathrm{II}}(u_1, v_1) + \alpha_{\mathrm{III}}(u_1, v_1) - \alpha_{\mathrm{I}}(u_1, v_1).$$

This example also illustrates some further points of Section 3 in the respect that the incidence tends to infinity at the wing tips and the trailing edge because of the assumption that the loading is finite at these edges.

The incidence and camber surface distribution is given in Fig. 5 for the spanwise stations $y=s/4,\ s/2,\ 3s/4$.

5. A Numerical Technique

In general the analytical approach of specifying the loading, substituting in equation (4) and evaluating the numerous integrals for the incidence becomes more tedious and difficult as the loadings and plan forms become more complex. Therefore the next step is the investigation of a numerical computation of equation (4) to cover all cases with equal facility and to any desired accuracy. There are several ways of attempting to do this. These depend on the extent to which the differentiation process is taken under the integral sign analytically before resorting to computation, with the idea of increasing the accuracy for a minimum of computation. The author investigated these possibilities but came finally to the conclusion that the direct numerical evaluation is the simplest approach, giving sufficient accuracy. This direct method is the only one discussed any further.

First it is assumed that the loading is known either as an analytic function or a discrete function over the plan form. Therefore the velocity potential may be regarded as specified over the wing and wake. On forming a mesh across the wing plan form and trailing wake, composed by oblique Mach co-ordinates ($u=0,\ d,\ 2d,\ \ldots\ nd$; $v=0,\ d,\ 2d\ \ldots\ nd$, where d is a small distance), it is assumed that the velocity potential ϕ is constant within each area of the mesh. Denoting by $\phi_{i,j}$ the constant velocity potential enclosed within the lines $\{(i-1)\,d \leqslant u \leqslant id,\ (j-1)\,d \leqslant v \leqslant jd\}$ it is assumed that $\phi_{i,j}$ is the value of the specified function at the centre point of the area, that is

$$\phi_{i,j}=\phi\,[(i-\tfrac{1}{2})\,d,\ (j-\tfrac{1}{2})\,d].$$

These points are illustrated in Fig. 6.

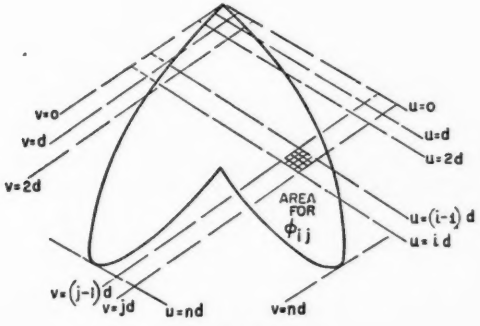

FIGURE 6. Notation.

Now consider the integral

$$\delta\gamma_{k,l} = \int_{u=(i-1)d}^{u=id} \frac{du}{\sqrt{(u_k-u)}} \int_{v=(j-1)d}^{v=jd} \frac{\phi_{i,j}}{\sqrt{(v_l-v)}}\,dv$$

$$= 4\phi_{i,j}\{\sqrt{[u_k-(i-1)d]}-\sqrt{[u_k-id]}\}\{\sqrt{[v_l-(j-1)d]}-\sqrt{[v_l-jd]}\}$$

$$= 4d\phi_{i,j}\{\sqrt{(k-i+1)}-\sqrt{(k-i)}\}\{\sqrt{(l-j+1)}-\sqrt{(l-j)}\}$$

$$= 4d\,A_{(i,j)(k,l)}\,\phi_{i,j}, \qquad (8)$$

assuming that $u_k = kd$, $v_l = ld$ is a point on the wing affected by $\phi_{i,j}$. Thus the coefficient $A_{(i,j)(k,l)}$, defined by equation (8), is finite when $k \geqslant i$ and $l \geqslant j$, but zero for other conditions.

On summation over the wing, extending equation (8),

$$\gamma_{k,l} = 4d \sum_{\substack{i=0,\ldots k \\ j=0,\ldots l}} \phi_{i,j}\; A_{(i,j)(k,l)} \qquad (9)$$

If $\alpha_{k,l}$ is the average incidence over the area $\{(k-1)d \leqslant u \leqslant kd,\ (l-1)d \leqslant v \leqslant ld\}$, remembering that equation (4) states that

$$\alpha(u_1, v_1) = \frac{M}{\pi V}\frac{\partial^2}{\partial u_1 \partial v_1}\int_{u=0}^{u=u_1}\int_{v=0}^{v=v_1} \frac{\phi(u,v)\,du\,dv}{\sqrt{[(u_1-u)(v_1-v)]}},$$

$$\text{then} \quad \alpha_{k,l} = \frac{M}{\pi V d^2}\left\{\gamma_{k,l}+\gamma_{k-1,l-1}-\gamma_{k-1,l}-\gamma_{k,l-1}\right\}. \qquad (10)$$

Although equations (9) and (10) can be combined, it is better, from a numerical point of view, to leave them separate.

Once the table of $A_{(i,j)(k,l)}$ has been established (depending only on the integers $k-i$, $l-j$), operation (9) is easily applied on a desk machine, provided, of course, that the mesh is not too fine.

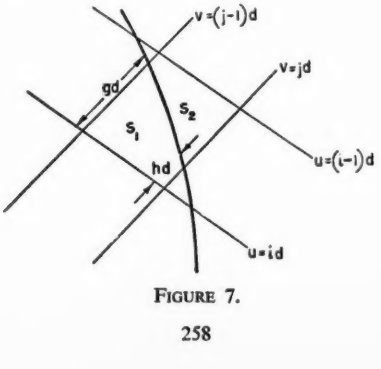

FIGURE 7.

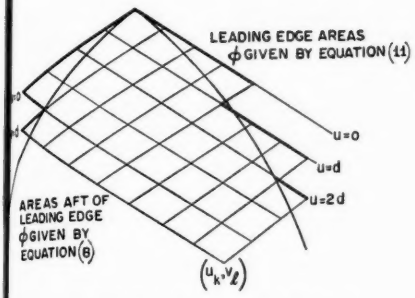

FIGURE 8. Mesh pattern with leading edge modified for numerical evaluation.

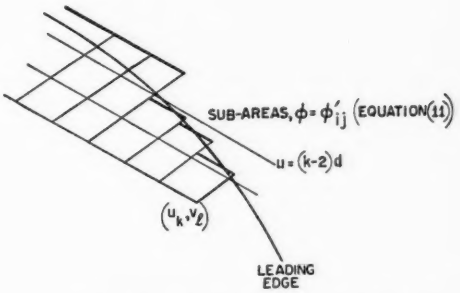

FIGURE 9. Sub-division of mesh pattern for (u_k, v_l) near the leading edge.

Refinements of this method need to be introduced for areas near the leading edges. The author has adopted the following procedures.

(*i*) If the point (u_k, v_l) is not "near to the leading edge" (this point is clarified later) the value of $\phi_{i,j}$ for an area intersected by the leading edge is taken as

$$\left.\begin{aligned} \phi_{i,j} &= \phi'_{i,j}\,\frac{S_1}{S_1+S_2} \\ \text{where}\quad \phi'_{i,j} &= \phi\left[\left(i-\frac{g+h}{4}\right)d,\,(j-\tfrac{1}{2})\,d\right] \end{aligned}\right\} \quad . \quad . \quad . \quad . \quad (11)$$

using the notation shown in Fig. 7.

This means that, for a point (u_k, v_l) inboard of the leading edge, the leading edge is effectively modified, as shown in Fig. 8, with the velocity potential given by equation (11) at the leading edge areas and by equation (8) for those areas aft of the leading edge.

The introduction of this sub-mesh introduces the need for a further table $A_{(i,j)(k,l)}$ for small non-integral values of $k-i$, $l-j$, depending on the shape of the leading edge.

The final point concerns whether or not (u_k, v_l) belongs to case (*i*) or (*ii*). The author assumed that if u_k or v_l is less than the distance $2d$ away from its nearest leading edge, then (u_k, v_l) belongs to case (*ii*), and if farther away it belongs to case (*i*).

(*ii*) If the point (u_k, v_l) is near the leading edge the mesh is subdivided locally with the velocity potential calculated on the same principles as before (*i.e.*, the value of ϕ is ϕ', defined in equation (11), at the centre of the sub-area, and it is assumed that this value holds over the whole sub-area). This is shown in Fig. 9.

This technique has been applied to three examples, which are discussed in the following section. The full numerical computation of the first example is given in the Appendix.

6. Numerical Examples

Three examples have been worked out. These are:—

(*i*) To check that the loading of a flat plate delta wing gives a uniform incidence distribution.

(*ii*) The application of the numerical technique to the uniform loading over a delta wing, and comparison with the analytical solution given in Fig. 3. This is designed to check the accuracy of the numerical method when singularities of the incidence distribution are expected at the leading edge.

(*iii*) The application to the uniform loading over a swept wing with subsonic leading and trailing edges and comparison with the analytical solution given in Fig. 4. This will check the accuracy of the numerical method when singularities are expected at the trailing edge.

Example (*i*)

It is well known that the velocity potential on the upper surface of a flat plate delta wing with 45° sweep is

$$\phi(x, y+0) = \frac{V\alpha}{E'(\beta)}(x^2 - y^2)^{1/2},$$

$$\text{where} \quad E'(\beta) = \int_0^{\pi/2} [1 - (1-\beta^2)\sin^2\theta]^{1/2} d\theta.$$

In this example $\beta = 0{\cdot}6$ is assumed, so that

$$\phi(x, y) = \frac{V\alpha}{1{\cdot}28}(x^2 - y^2)^{1/2}$$

$$= \frac{V\alpha}{1{\cdot}28}\left[\left(u - \frac{v}{4}\right)\left(v - \frac{u}{4}\right)\right]^{1/2} \frac{1+\beta}{M} \quad . \quad . \quad (12)$$

in oblique co-ordinates.

The potential equation (12) is now assumed over a 45° swept delta wing and the incidence is calculated numerically by the method of Section 5. The mesh is specified in this case to give 10 points (or areas) at the centre span and 5 areas at the quarter span, as shown in Fig. 10.

The numerical method for this example is presented more fully in the Appendix.

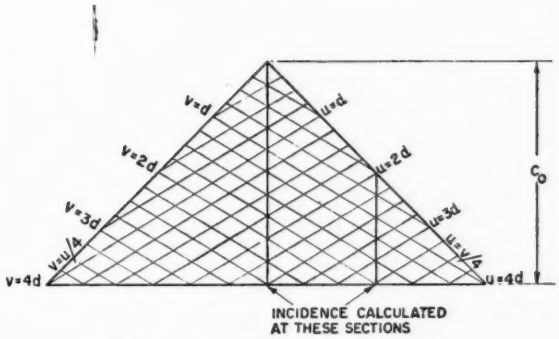

FIGURE 10. Mesh system for computation.

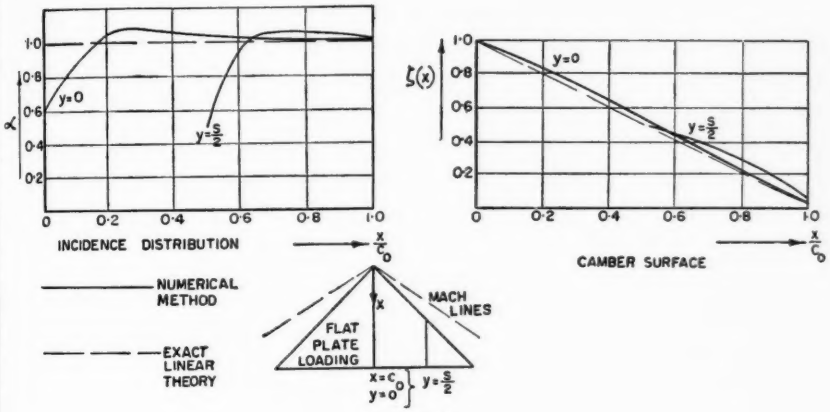

FIGURE 11.

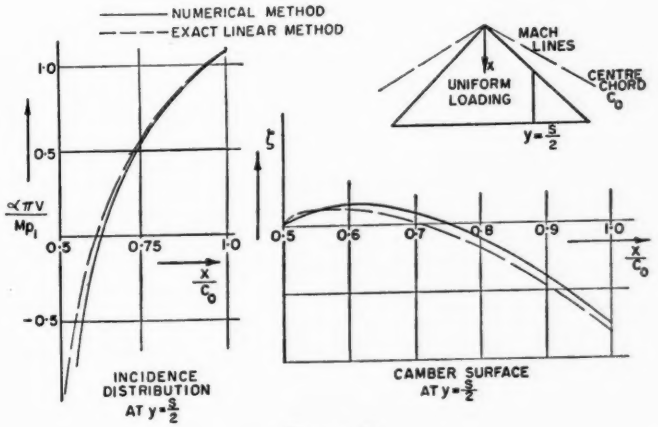

FIGURE 12.

It is seen that, although the mesh is comparatively wide, the error for the incidence is only appreciable in the area at the leading edge; otherwise the agreement is good. However, on integration of the incidence distribution for the camber surface, the effective error is less near the leading edge, so that the agreement with the flat plate is good over most of the wing surface.

The incidence distribution and wing shape has been calculated at the centre section and the quarter-span section and is compared with the flat plate distribution in Fig. 11.

Example (ii)

In this case a uniform loading is assumed over the same delta wing as in the previous example, moving at the same speed. The mesh system of Fig. 10 is again used as the basis for the computation.

Equation (6) states that, in this case,

$$\left.\begin{aligned} \phi &= p_1\left(u-\frac{v}{4}\right) \quad \text{for} \quad y \geqslant 0 \\ &= p_1\left(v-\frac{u}{4}\right) \quad \text{for} \quad y \leqslant 0 \end{aligned}\right\} \qquad \ldots \ldots \quad (13)$$

where p_1 is a constant.

The downwash distribution and the camber line have been computed for $y=s/2$ and are compared with the exact theory, presented in Section 4, in Fig. 12.

Again the error is greatest near the leading edge, but the characteristics of the camber line are brought out, even allowing for the infinite leading edge downwash.

Example (iii)

Example (*ii*) has been extended to the 45° swept wing with uniform loading, discussed analytically in Section 4 (leading and trailing edges parallel, aspect ratio 2). The velocity potential is again given by equation (13), remembering that it remains constant aft of the trailing edge. The comparison of theory and numerical approximation is shown in Fig. 13, for both the downwash distribution and the camber line at the section $y=s/2$.

The regions of error for this example are confined to both the leading and trailing edges, although the overall characteristics of the wing are obtained. The conditions at the trailing edge do not satisfy the Kutta-Joukowski hypothesis, but more orthodox distributions in this region should give better results.

7. Conclusions

The numerical method suggested in Section 5 has been applied to three examples, which include between them the various edge singularities that might be encountered in practice. It has been seen that with a fairly wide mesh distribution errors are appreciable only for the edge areas of the mesh. There are two ways of avoiding these errors. The first is not to try to calculate the incidence

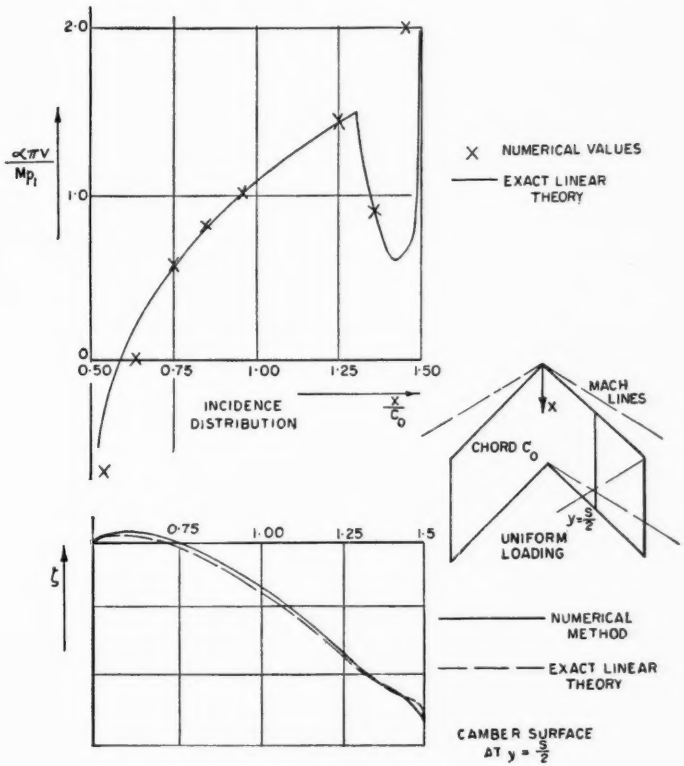

FIGURE 13.

at the singular edge areas, but to extrapolate the values calculated at the inboard areas, bearing in mind the types of singularities expected. The second method is to decrease the mesh areas locally in the edge regions and so approach the conditions at these edges more accurately. However, it is debatable whether the extra work in the second method is justified, since it must be realised that the derivation is based on a linearised approximation to real conditions, together with the fact that the main camber and twist characteristics are given for the wing as a whole to conform to a specified loading.

Appendix

The numerical method of Example (*i*) of Section 6 is now discussed in more detail.

The velocity potential distribution is taken to be

$$\phi(u, v) = \frac{V\alpha}{0{\cdot}933}\left[\left(u-\frac{v}{4}\right)\left(v-\frac{u}{4}\right)\right]^{1/2} \quad . \quad . \quad . \quad . \quad (14)$$

where $\beta = 0{\cdot}6$ is assumed.

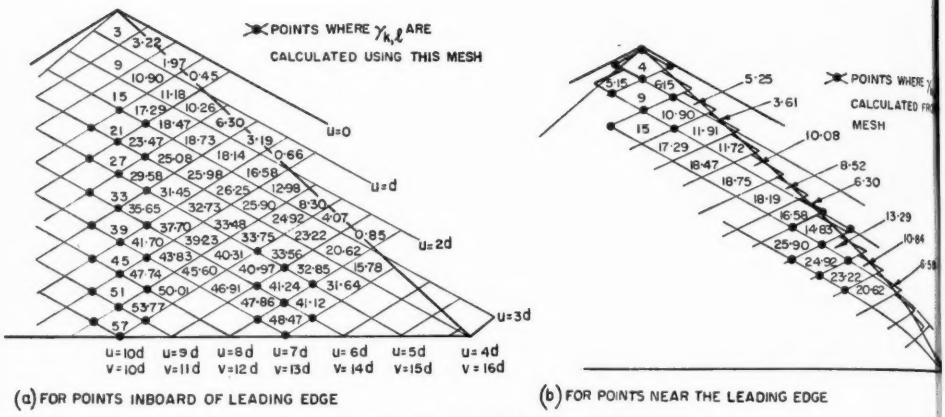

FIGURE 14. Values of $8\,\phi_{i,j}\,(0{\cdot}933)/(v_{\infty}d)$.

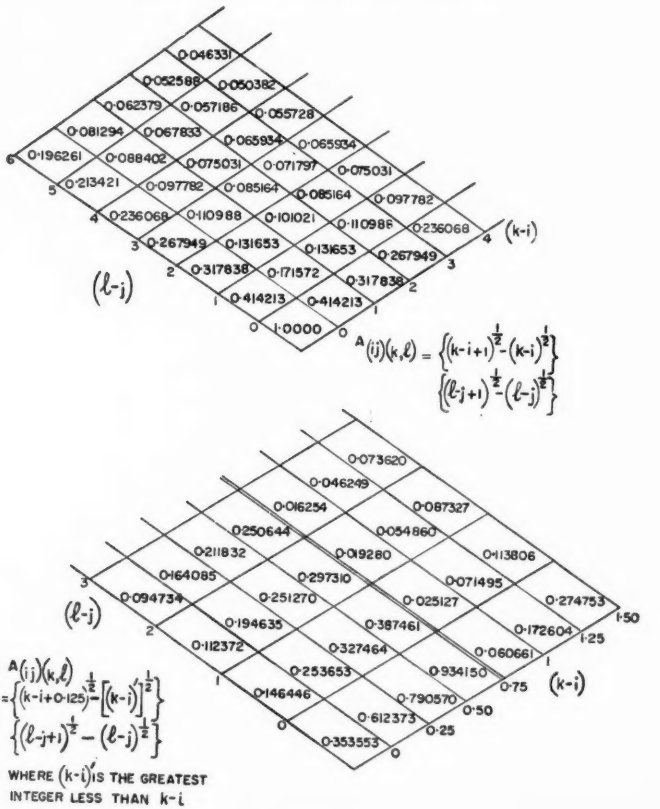
(k-i)
(ℓ-j)
$A_{(ij)(k,\ell)} = \left\{(k-i+1)^{\frac{1}{2}} - (k-i)^{\frac{1}{2}}\right\}\left\{(\ell-j+1)^{\frac{1}{2}} - (\ell-j)^{\frac{1}{2}}\right\}$
$A_{(ij)(k,\ell)} = \left\{(k-i+0{\cdot}125)^{\frac{1}{2}} - [(k-i)']^{\frac{1}{2}}\right\}\left\{(\ell-j+i)^{\frac{1}{2}} - (\ell-j)^{\frac{1}{2}}\right\}$
WHERE $(k-i)'$ IS THE GREATEST INTEGER LESS THAN $k-i$

FIGURE 15.

The distribution of $8\phi_{i,j}(0{\cdot}933)/(V\alpha d)$ in the mesh pattern chosen for this example is shown in Fig. 14, where the incidence is to be calculated for areas inboard from the leading edge from Fig. 14(*a*) and for areas near the leading edge from Fig. 14(*b*).

The table of values for $A_{(i,j)(k,l)}$ is shown in Fig. 15. It is presented in the form of a V-matrix to ease the computation of $\sum_{i,j} \phi_{i,j} A_{(i,j)(k,l)}$.

The operation of equation (9) for the calculation of $\gamma_{k,l}$ can now be applied directly and has been applied to the points indicated in Fig. 14.

From these the average incidence of each of the indicated areas is obtained by equations (10) and the results are presented in Fig. 11.

References

1. Puckett, A. E. Supersonic Wave Drag of Thin Aerofoils. *Journal of the Aeronautical Sciences*, Vol. 13, September 1946.

2. Evvard, J. C. Use of Source Distributions for Evaluating Theoretical Aerodynamics of Thin Finite Wings at Supersonic Speeds. N.A.C.A. Report 951, 1950.

3. Etkin, B. and Woodward, F. A. Lift Distribution on Supersonic Wings with Subsonic Leading Edges and Arbitrary Angles of Attack. *Proceedings of the Second Canadian Symposium on Aerodynamics*, Institute of Aerophysics, University of Toronto, 1954.

4. Hancock, G. J. Note on the Extension of Evvard's Method to Wings with Subsonic Leading Edges Moving at Supersonic Speeds. *The Aeronautical Quarterly*, Vol. VIII, February 1957.

5. Heaslet, M. A. and Lomax, H. *High Speed Aerodynamics and Jet Propulsion.* Vol. VI. General Theory of High Speed Aerodynamics, pp. 148-157. Edited by W. R. Sears. Princeton University Press, 1954. Oxford University Press, 1955.

6. Goldsworthy, F. A. Supersonic Flow over Thin Symmetrical Wings with given Surface Distribution. *The Aeronautical Quarterly*, Vol. III, February 1952.

Symmetrically Loaded Circular Plates under the Combined Action of Lateral and End Loading

RAYMOND HICKS

(G.E.C. Simon-Carves Atomic Energy Group)

SUMMARY: Expressions are obtained for the radial and tangential bending moments in a circular plate under the combined action of (*a*) a lateral load concentrated on the circumference of a circle and an end tension or compression, and (*b*) a uniformly distributed lateral load, having a diameter less than the diameter of the plate, and an end tension or compression. For both types of loading, solutions are obtained for plates which are simply-supported and for plates with an arbitrary end rotation.

In addition, the following limiting cases are considered: (*i*) concentrated lateral load with end tension or compression, and (*ii*) an infinite plate under the simultaneous action of an end tension and a lateral load concentrated on the circumference of a circle of finite diameter.

1. Introduction

For a laterally loaded plate having small deflections, the bending stress distribution is linearly related to the applied load system. That is, any increase in the intensity of the applied loading results in a corresponding increase in the intensity of stress, with no resulting change in the stress distribution. This implies that for a plate under the simultaneous action of two or more lateral load systems, the resultant stress distribution can be obtained by adding the stress distribution associated with each type of lateral loading.

For a plate under the combined action of lateral and end loading, the principle of superposition is no longer applicable, so that the resultant stress distribution is not obtained by simple addition of the stress distributions associated with the lateral and end load systems when acting separately. In general the bending stresses due to the lateral load are decreased by the application of a tensile end load, and increased by the application of a compressive end load. Furthermore, the change in the bending stress distribution is not linearly related to the change in the intensity of end loading, the relative effect of the end loading being more severe as its intensity increases.

Received January 1959.

The deflection and vibration of a circular plate under the simultaneous action of lateral and end loading has been considered by Bickley[1]. He confined his attention to a plate with a clamped boundary and considered several important applied symmetrical load systems as well as a concentrated load at an arbitrary point. Bickley was particularly interested in the behaviour of a diaphragm used in the construction of a condenser microphone; possibly for this reason he does not reduce his solutions to forms which give explicitly the stress distributions when the end loading is compressive.

In the absence of lateral loadings, Bryan[2] and Nadai[3] considered the effect of end compression and determined the load necessary to buckle the plate. They found that the critical compressive stress for a plate with a clamped edge is about 50 per cent greater than the corresponding stress necessary to buckle a strut having a length equal to the diameter of the plate.

For an end-loaded plate with a hole at its centre, the compressive load necessary to cause buckling has been determined by Meissner[4]. For a plate with a clamped outer edge, he found that the buckling stress is a minimum when the diameter of the plate is approximately five times the diameter of the hole.

This paper considers a further series of problems dealing with a symmetrically loaded plate under the combined action of lateral and end loading. General expressions are obtained for the radial and tangential bending moments and for the deflection surface of the plate. It is found that these expressions can be written in terms of the modified Bessel functions I_n and K_n when the end load is tensile, and in terms of the ordinary Bessel functions J_n and Y_n when the end load is compressive. In all cases the order of the Bessel functions is zero or unity, so that numerical values for these functions can be obtained readily from standard tables, for example, Refs. 5, 6, 7 and 8.

For a plate under the action of a load concentrated on the circumference of a circle of arbitrary diameter, the general solution has been used to obtain the moment distribution in a circular plate with a concentrated load at its centre. Furthermore, this solution has been used to obtain the transcendental equation which defines the stress necessary to buckle the plate. Also, the general solution has been used to consider the case of an infinite plate under the combined action of an end tension and a lateral load concentrated on the circumference of a circle. A solution is also obtained for an end-loaded circular plate with a lateral load uniformly distributed over a circle of arbitrary diameter; this solution is used to consider the case where the load completely covers the plate. For a particular example considered, it is found that the effect of an end compression of 4·47 tons/in.^{2} is to increase the maximum bending moment by 36 per cent. A further example is used to show the attenuation of the bending moment in an infinite plate under the simultaneous action of an end tension and a uniform load distributed over a circle of finite diameter.

Finally, where applicable, it is shown that for limiting cases the solutions obtained in this paper reduce to those given in Refs. 1, 2 and 3.

NOTATION

w deflection
r radial co-ordinate
a radius of lateral load
b radius of plate
h thickness of plate
Q_r radial shear per unit length
Q total external shear
M_r radial moment
M_θ tangential moment
L lateral load
q intensity of lateral loading
p end load stress
D flexural rigidity
ν Poisson's ratio
E Young's modulus
θ end rotation
J_n, Y_n Bessel functions
I_n, K_n modified Bessel functions
$H_n^{(2)}$ Hankel function
$\alpha = \sqrt{(ph/D)}$
$x = r\sqrt{\alpha}$
$\psi = dw/dr$
C_n constant

2. Fundamental Equation for Small Deflections

For a symmetrically loaded circular plate having small deflections, the radial shear per unit circumferential length is given by the following well known expression:—

$$Q_r = D\frac{d}{dr}\left(\frac{d^2w}{dr^2} + \frac{1}{r}\frac{dw}{dr}\right).$$

Referring to the outer section of the plate shown in Figs. 1 and 2, around its inner boundary the total external shear acting in a vertical direction is given by

$$Q = L - 2\pi aph\left(\frac{dw}{dr}\right)_a.$$

The negative sign has been inserted to be consistent with the convention that a downward deflection is positive and corresponds to a negative radial slope.

Also, at any arbitrary point in the plate, the external shear is in equilibrium with the radial shear Q_r. In this case, it follows that

$$Q_r = \frac{Q}{2\pi r} + ph\frac{dw}{dr}.$$

Combining the expressions for Q_r, the equation defining the deflection surface of the plate is given by

$$\frac{d}{dr}\left(\frac{d^2w}{dr^2} + \frac{1}{r}\frac{dw}{dr}\right) - \frac{ph}{D}\frac{dw}{dr} = \frac{Q}{2\pi rD}.$$

For convenience let

$$\alpha = \frac{ph}{D}$$

$$x = r\sqrt{\alpha} = r\sqrt{\left(\frac{ph}{D}\right)}$$

$$\psi = \frac{dw}{dr}.$$

Using these parameters, the fundamental equation becomes

$$x^2\frac{d^2\psi}{dx^2} + x\frac{d\psi}{dx} - (x^2+1)\psi = \frac{Qx}{2\pi\sqrt{(\alpha)}\,D} \quad . \quad . \quad . \quad . \quad (1)$$

Except for the term containing the external shear due to the lateral loading, equation (1) is identical to the equation used by Meissner[4].

3. Load Concentrated on the Circumference of a Circle (i.e. Concentric Loading)

For the outer section of the plate shown in Fig. 1, it can be verified that the necessary solution of (1) is given by

$$\psi = \frac{dw}{dr} = C_1 I_1(r\sqrt{\alpha}) + C_2 K_1(r\sqrt{\alpha}) - \frac{Q}{2\pi r\alpha D}, \quad . \quad . \quad . \quad (2)$$

so that

$$w = \frac{C_1}{\sqrt{\alpha}} I_0(r\sqrt{\alpha}) - \frac{C_2}{\sqrt{\alpha}} K_0(r\sqrt{\alpha}) - \frac{Q}{2\pi\alpha D}\log(r\sqrt{\alpha}) - \frac{B}{\sqrt{\alpha}}, \quad . \quad (3)$$

where

$$B = C_1 I_0(b\sqrt{\alpha}) - C_2 K_0(b\sqrt{\alpha}) - \frac{Q}{2\pi\alpha D}\log(b\sqrt{\alpha}).$$

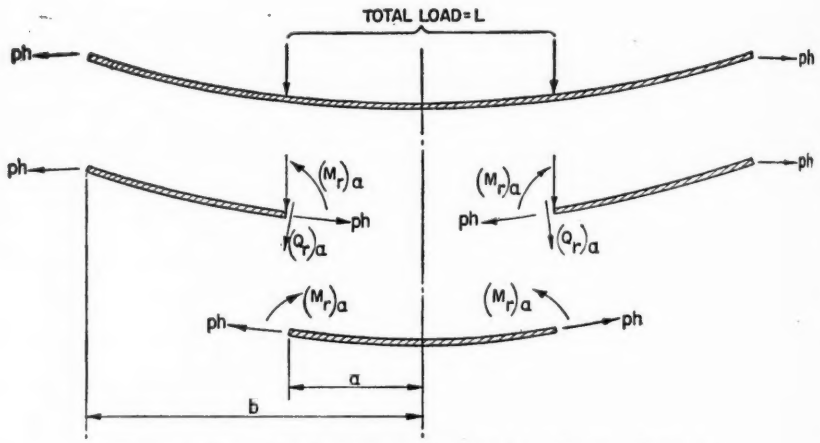

FIGURE 1. Lateral load concentrated on the circumference of a circle.

Tables and formulae for this Bessel function can be obtained from Refs. 5, 6, 7 and 8.

$$\text{Now} \quad Q = L - 2\pi aph\left(\frac{dw}{dr}\right)_a \quad . \quad . \quad . \quad . \quad . \quad . \quad (4)$$

Thus, from (2) and (4),

$$C_1 I_1(a\sqrt{\alpha}) + C_2 K_1(a\sqrt{\alpha}) - \frac{L}{2\pi a\alpha D} = 0. \quad . \quad . \quad . \quad (5)$$

This is the first boundary condition for the outer portion of the plate.

4. Simply-Supported Plate with Concentric Loading and End Tension

The radial bending moment is given by the well-known relationship

$$M_r = -D\left(\frac{d^2w}{dr^2} + \frac{\nu}{r}\frac{dw}{dr}\right).$$

Substituting (2) and (4) in this expression, two further boundary conditions are given by

$$(M_r)_b = -D\sqrt{\alpha}\left\{C_1\left[I_1'(b\sqrt{\alpha}) + \frac{\nu}{b\sqrt{\alpha}} I_1(b\sqrt{\alpha})\right] + \right.$$

$$\left. + C_2\left[K_1'(b\sqrt{\alpha}) + \frac{\nu}{b\sqrt{\alpha}} K_1(b\sqrt{\alpha})\right] - \frac{(1-\nu)\,a\psi_a}{b^2\sqrt{\alpha}} + \frac{(1-\nu)\,L}{2\pi b^2\alpha^{3/2}D}\right\} = 0 \quad . \quad (6)$$

$$(M_r)_a = -D\sqrt{\alpha}\left\{C_1\left[I_1'(a\sqrt{\alpha}) + \frac{\nu}{a\sqrt{\alpha}} I_1(a\sqrt{\alpha})\right] + \right.$$

$$\left. + C_2\left[K_1'(a\sqrt{\alpha}) + \frac{\nu}{a\sqrt{\alpha}} K_1(a\sqrt{\alpha})\right] - \frac{(1-\nu)\psi_a}{a\sqrt{\alpha}} + \frac{(1-\nu)L}{2\pi a^2 \alpha^{3/2} D}\right\} \quad . \quad . \quad (7)$$

where primes (') denote differentiation with respect to r. Similarly, for the inner portion of the plate,

$$\psi = \frac{dw}{dr} = C_0 I_1(r\sqrt{\alpha}) \quad . \quad . \quad . \quad . \quad . \quad . \quad . \quad (8)$$

$$\text{so that} \quad (M_r)_a = -DC_0\sqrt{\alpha}\left[I_1'(a\sqrt{\alpha}) + \frac{\nu}{a\sqrt{\alpha}} I_1(a\sqrt{\alpha})\right] . \quad . \quad . \quad (9)$$

Using the identities

$$\left.\begin{aligned} z[I_1'(z) K_1(z) - I_1(z) K_1'(z)] &= 1 \\ zI_1'(z) + I_1(z) &= zI_0(z) \\ zK_1'(z) + K_1(z) &= -zK_0(z), \end{aligned}\right\} \quad . \quad . \quad . \quad (10)$$

consideration of boundary conditions gives

$$\left.\begin{aligned} C_0 &= \frac{-C}{(a\sqrt{\alpha}) K_1(a\sqrt{\alpha})}\left\{\frac{(1-\nu)a}{b^2\sqrt{\alpha}} K_1(a\sqrt{\alpha}) + (a\sqrt{\alpha}) SK_0(a\sqrt{\alpha}) - \right. \\ &\qquad \left. - \left[K_0(b\sqrt{\alpha}) + \frac{(1-\nu)}{b\sqrt{\alpha}} K_1(b\sqrt{\alpha})\right]\right\} \\ C_1 &= -C\left\{\frac{(1-\nu)}{b^2\alpha} - \left[K_0(b\sqrt{\alpha}) + \frac{(1+\nu)}{b\sqrt{\alpha}} K_1(b\sqrt{\alpha})\right] I_0(a\sqrt{\alpha})\right\} \\ C_2 &= C\left[I_0(b\sqrt{\alpha}) - \frac{(1-\nu)}{b\sqrt{\alpha}} I_1(b\sqrt{\alpha})\right] I_0(a\sqrt{\alpha}), \end{aligned}\right\} \quad . \quad (11)$$

where

$$\left.\begin{aligned} \frac{1}{C} &= \frac{2\pi a\alpha D}{L}\left[SI_0(a\sqrt{\alpha}) - \frac{(1-\nu)}{b^2\alpha} I_1(a\sqrt{\alpha})\right] \\ S &= K_1(a\sqrt{\alpha})\left[I_0(b\sqrt{\alpha}) - \frac{(1-\nu)}{b\sqrt{\alpha}} I_1(b\sqrt{\alpha})\right] + \\ &\qquad + I_1(a\sqrt{\alpha})\left[K_0(b\sqrt{\alpha}) + \frac{(1-\nu)}{b\sqrt{\alpha}} K_1(b\sqrt{\alpha})\right], \end{aligned}\right\}$$

also $Q = L - 2\pi aphC_0 I_1(a\sqrt{\alpha})$.

Finally, the radial and tangential bending moments are given by equations (12) which follow.

$$
\left.\begin{aligned}
M_r &= -\sqrt{(\alpha)}\,DC_0\left[I_0(r\sqrt{\alpha})-\frac{(1-\nu)}{r\sqrt{\alpha}}I_1(r\sqrt{\alpha})\right] && (0\leqslant r\leqslant a)\\
M_r &= -\sqrt{(\alpha)}\,D\left\{C_1\left[I_0(r\sqrt{\alpha})-\frac{(1-\nu)}{r\sqrt{\alpha}}I_1(r\sqrt{\alpha})\right]-C_2\left[K_0(r\sqrt{\alpha})+\right.\right.\\
&\quad\left.\left.+\frac{(1-\nu)}{r\sqrt{\alpha}}K_1(r\sqrt{\alpha})\right]+\left[\frac{L}{2\pi\sqrt{(\alpha)}\,D}-(a\sqrt{\alpha})\,C_0I_1(a\sqrt{\alpha})\right]\frac{(1-\nu)}{r^2\alpha}\right\} && (a\leqslant r\leqslant b)\\
M_\theta &= -\sqrt{(\alpha)}\,DC_0\left[\nu I_0(r\sqrt{\alpha})+\frac{(1-\nu)}{r\sqrt{\alpha}}I_1(r\sqrt{\alpha})\right] && (0\leqslant r\leqslant a)\\
M_\theta &= -\sqrt{(\alpha)}\,D\left\{C_1\left[\nu I_0(r\sqrt{\alpha})+\frac{(1-\nu)}{r\sqrt{\alpha}}I_1(r\sqrt{\alpha})\right]-C_2\left[\nu K_0(r\sqrt{\alpha})-\right.\right.\\
&\quad\left.\left.-\frac{(1-\nu)}{r\sqrt{\alpha}}K_1(r\sqrt{\alpha})\right]-\left[\frac{L}{2\pi\sqrt{(\alpha)}\,D}-(a\sqrt{\alpha})\,C_0I_1(a\sqrt{\alpha})\right]\frac{(1-\nu)}{r^2\alpha}\right\} && (a\leqslant r\leqslant b)
\end{aligned}\right\}\quad(12)
$$

Expressions (11) and (12) show that, for a fixed value of the direct stress p, the bending moments in the plate are proportional to the lateral concentric loading.

5. Simply-Supported Plate with a Concentrated Load and End Tension

When the diameter of the concentric loading approaches zero, the solution (12) is applicable to a circular plate under the action of a concentrated load L at its centre.

Thus, since
$$
\left.\begin{aligned}
&[\psi_a=C_0I_1(a\sqrt{\alpha})=0]_{a=0}\\
&[(a\sqrt{\alpha})\,K_1(a\sqrt{\alpha})=I_0(a\sqrt{\alpha})=1]_{a=0}
\end{aligned}\right\}\quad\ldots\quad(13)
$$

it can be shown that

$$
\left.\begin{aligned}
M_r &= \frac{LC}{2\pi}\left\{\frac{(1-\nu)}{b^2\alpha}-\left[K_0(b\sqrt{\alpha})+\frac{(1-\nu)}{b\sqrt{\alpha}}K_1(b\sqrt{\alpha})\right]\right\}\left[I_0(r\sqrt{\alpha})-\right.\\
&\quad\left.-\frac{(1-\nu)}{r\sqrt{\alpha}}I_1(r\sqrt{\alpha})\right]-\frac{LC}{2\pi}\left|\left\{\frac{(1-\nu)}{r^2\alpha}-\left[K_0(r\sqrt{\alpha})+\right.\right.\right.\\
&\quad\left.\left.\left.+\frac{(1-\nu)}{r\sqrt{\alpha}}K_1(r\sqrt{\alpha})\right]\right\}\left[I_0(b\sqrt{\alpha})-\frac{(1-\nu)}{b\sqrt{\alpha}}I_1(b\sqrt{\alpha})\right]\right.\\
M_\theta &= \frac{LC}{2\pi}\left\{\frac{(1-\nu)}{b^2\alpha}-\left[K_0(b\sqrt{\alpha})+\frac{(1-\nu)}{b\sqrt{\alpha}}K_1(b\sqrt{\alpha})\right]\right\}\left[\nu I_0(r\sqrt{\alpha})+\right.\\
&\quad\left.+\frac{(1-\nu)}{r\sqrt{\alpha}}I_1(r\sqrt{\alpha})\right]+\frac{LC}{2\pi}\left\{\frac{(1-\nu)}{r^2\alpha}+\left[\nu K_0(r\sqrt{\alpha})-\right.\right.\\
&\quad\left.\left.-\frac{(1-\nu)}{r\sqrt{\alpha}}K_1(r\sqrt{\alpha})\right]\right\}\left[I_0(b\sqrt{\alpha})-\frac{(1-\nu)}{b\sqrt{\alpha}}I_1(b\sqrt{\alpha})\right]
\end{aligned}\right\}\quad(14)
$$

where $\dfrac{1}{C}=\left[I_0(b\sqrt{\alpha})-\dfrac{(1-\nu)}{b\sqrt{\alpha}}I_1(b\sqrt{\alpha})\right]$.

Now $K_0(z) = -[\gamma + \log(z/2)]\, I_0(z) + \sum_{r=1}^{\infty} \frac{(0{\cdot}5z)^{2r}}{(r!)^2}\left[1 + \frac{1}{2} + \frac{1}{3} + \ldots \frac{1}{r}\right]$

$$K_1(z) = -K_0'(z)$$

$$I_n(z) = \sum_{r=0}^{\infty} \frac{(0{\cdot}5z)^{n+2r}}{n!\,(n+r)} \quad (n \text{ integer})$$

$$\gamma = 0{\cdot}5772.$$

Thus, for sufficiently small values of z,

$$K_0(z) = -\log(z/2)$$

$$K_1(z) = \frac{z}{2}\log\frac{z}{2} + \frac{1}{z} - \frac{z}{4}.$$

Using these expressions for $K_n(z)$ and the series for $I_n(z)$, in the limit when p is zero, it is found that

$$M_r = \frac{L}{4\pi}(1+\nu)\log\frac{b}{r}$$

$$M_\theta = \frac{L}{4\pi}\left[(1+\nu)\log\frac{b}{r} + (1-\nu)\right].$$

These are well-known expressions for the moments in a laterally loaded plate with no end load.

6. Simply-Supported Plate with a Concentrated Load and End Compression

For a plate under the action of a compressive end load, p is negative, so that the modified Bessel functions have imaginary arguments. This implies that for a compressive end load the radial and tangential bending moments are functions of the ordinary Bessel functions $J_n(z)$ and $Y_n(z)$.

Now $K_n(z\,e^{\pi i/2}) = K_n(iz) = -\frac{1}{2}\pi e^{-\pi(n-1)i/2} H_n^{(2)}(z)$

and $H_n^{(2)}(z) = J_n(z) - iY_n(z)$.

Thus $K_0(iz) = -\frac{\pi}{2}[iJ_0(z) + Y_0(z)]$.

Also, it can be shown that

$$I_0(iz) = J_0(z)$$

$$I_1(iz) = iJ_1(z).$$

Using these relationships, for a compressive end load, it is found that

$$\left.\begin{aligned} M_r = &-\frac{LC}{2\pi}\left\{\frac{(1-\nu)}{b^2\alpha}-\frac{\pi}{2}\left[Y_0(b\sqrt{\alpha})-\frac{(1-\nu)}{b\sqrt{\alpha}}Y_1(b\sqrt{\alpha})\right]\right\}\left[J_0(r\sqrt{\alpha})-\right.\\ &\left.-\frac{(1-\nu)}{r\sqrt{\alpha}}J_1(r\sqrt{\alpha})\right]+\frac{LC}{2\pi}\left\{\frac{(1-\nu)}{r^2\alpha}-\frac{\pi}{2}\left[Y_0(r\sqrt{\alpha})-\right.\right.\\ &\left.\left.-\frac{(1-\nu)}{r\sqrt{\alpha}}Y_1(r\sqrt{\alpha})\right]\right\}\left[J_0(b\sqrt{\alpha})-\frac{(1-\nu)}{b\sqrt{\alpha}}J_1(b\sqrt{\alpha})\right]\\ M_\theta = &-\frac{LC}{2\pi}\left\{\frac{(1-\nu)}{b^2\alpha}-\frac{\pi}{2}\left[Y_0(b\sqrt{\alpha})-\frac{(1-\nu)}{b\sqrt{\alpha}}Y_1(b\sqrt{\alpha})\right]\right\}\left[\nu J_0(r\sqrt{\alpha})+\right.\\ &\left.+\frac{(1-\nu)}{r\sqrt{\alpha}}J_1(r\sqrt{\alpha})\right]-\frac{LC}{2\pi}\left\{\frac{(1-\nu)}{r^2\alpha}+\frac{\pi}{2}\left[\nu Y_0(r\sqrt{\alpha})+\right.\right.\\ &\left.\left.+\frac{(1-\nu)}{r\sqrt{\alpha}}Y_1(r\sqrt{\alpha})\right]\right\}\left[J_0(b\sqrt{\alpha})-\frac{(1-\nu)}{b\sqrt{\alpha}}J_1(b\sqrt{\alpha})\right] \end{aligned}\right\}. \quad (15)$$

where $\dfrac{1}{C}=\left[J_0(b\sqrt{\alpha})-\dfrac{(1-\nu)}{b\sqrt{\alpha}}J_1(b\sqrt{\alpha})\right]$.

It is worth noting that the moments given by equations (15) become infinite when

$$b\sqrt{(\alpha)}\,J_0(b\sqrt{\alpha})-(1-\nu)\,J_1(b\sqrt{\alpha})=0.$$

This is the well-known transcendental equation which defines the critical compressive stress for an end-loaded circular plate with a simply-supported boundary (*see*, for example, Ref. 9, p. 369).

7. Arbitrary End Rotation, Concentric Load and End Tension

This problem is of practical interest, since it has an application in the analysis of a cylindrical pressure vessel with a flat head. Also, as a particular example, it gives the solution for a plate with clamped edges.

Referring to equation (3), if θ is the radial slope of the plate at $r=b$, the outer boundary condition is given by

$$C_1I_1(b\sqrt{\alpha})+C_2K_1(b\sqrt{\alpha})-\frac{Q}{2\pi b\alpha D}-\theta=0. \quad . \quad . \quad . \quad (16)$$

Substituting the appropriate expression for Q, the condition (16) becomes

$$C_1I_1(b\sqrt{\alpha})+C_2K_1(b\sqrt{\alpha})+\frac{a}{b}C_0I_1(a\sqrt{\alpha})-\frac{L}{2\pi b\alpha D}-\theta=0. \quad . \quad (17)$$

Proceeding as before it is found that the following expressions are obtained for C_0, C_1 and C_2.

$$\left.\begin{aligned} C_0 &= \frac{1}{G}\left\{\frac{L}{2\pi a\alpha D I_1(a\sqrt{\alpha})}\left[G - \frac{b}{a} I_1(b\sqrt{\alpha})\right] + \frac{b\theta}{a}\right\} \\ C_1 &= \frac{1}{G}\left\{\frac{L}{2\pi a\alpha D}\left[1 - (b\sqrt{\alpha}) K_1(b\sqrt{\alpha}) I_0(a\sqrt{\alpha})\right] + (b\sqrt{\alpha})\theta I_0(a\sqrt{\alpha}) K_1(a\sqrt{\alpha})\right\} \\ C_2 &= \frac{b}{G}\sqrt{(\alpha)}\, I_0(a\sqrt{\alpha})\left\{\frac{L}{2\pi a\alpha D} I_1(b\sqrt{\alpha}) - \theta I_1(a\sqrt{\alpha})\right\} \end{aligned}\right\} \quad (18)$$

where

$$G = \{I_1(a\sqrt{\alpha}) + (b\sqrt{\alpha}) I_0(a\sqrt{\alpha})[K_1(a\sqrt{\alpha}) I_1(b\sqrt{\alpha}) - K_1(b\sqrt{\alpha}) I_1(a\sqrt{\alpha})]\}$$

Using these values for the constants, the radial and tangential bending moments are given by (12). For a concentrated load at the centre of the plate,

$$\left.\begin{aligned} M_r = -\frac{L}{2\pi}\Bigg\{ & \frac{1}{I_1(b\sqrt{\alpha})}\left[\frac{1}{b\sqrt{\alpha}} - K_1(b\sqrt{\alpha}) + \frac{2\pi\sqrt{(\alpha)}\, D\theta}{L}\right]\left[I_0(r\sqrt{\alpha}) - \frac{(1-\nu)}{r\sqrt{\alpha}} I_1(r\sqrt{\alpha})\right] - \\ & - \left[K_0(r\sqrt{\alpha}) + \frac{(1-\nu)}{r\sqrt{\alpha}} K_1(r\sqrt{\alpha})\right] + \frac{(1-\nu)}{r^2\alpha}\Bigg\} \\ M_\theta = -\frac{L}{2\pi}\Bigg\{ & \frac{1}{I_1(b\sqrt{\alpha})}\left[\frac{1}{b\sqrt{\alpha}} - K_1(b\sqrt{\alpha}) + \frac{2\pi\sqrt{(\alpha)}\, D\theta}{L}\right]\left[\nu I_0(r\sqrt{\alpha}) + \frac{(1-\nu)}{r\sqrt{\alpha}} I_1(r\sqrt{\alpha})\right] - \\ & - \left[\nu K_0(r\sqrt{\alpha}) - \frac{(1-\nu)}{r\sqrt{\alpha}} K_1(r\sqrt{\alpha})\right] - \frac{(1-\nu)}{r^2\alpha}\Bigg\} . \end{aligned}\right\} \quad (19)$$

When p and θ are both zero, these can be reduced to the following well-known expressions.

$$M_r = \frac{L}{4\pi}\left[(1+\nu)\log\frac{b}{r} - 1\right]$$

$$M_\theta = \frac{L}{4\pi}\left[(1+\nu)\log\frac{b}{r} - \nu\right].$$

For an end compression, these expressions for the bending moments can be rewritten in terms of the Bessel functions J_n and Y_n by using the relationships previously given.

8. Infinite Plate with a Finite Concentric Load and End Tension

When the stresses acting at the middle plane of the plate are sufficiently large, the radial and tangential moments are confined mainly to a region of the plate in the vicinity of the concentric lateral loading. This implies that the solution for an infinite plate is applicable to a plate of finite size, provided that its least lateral dimension is several times the diameter of the concentric loading. It is clear that for any particular problem the degree of approximation introduced into the analysis, by assuming the plate to be infinite, can be determined readily by comparing the stresses and displacements applied to the boundary of the finite plate with the stresses and displacements around the corresponding contour in the infinite plate.

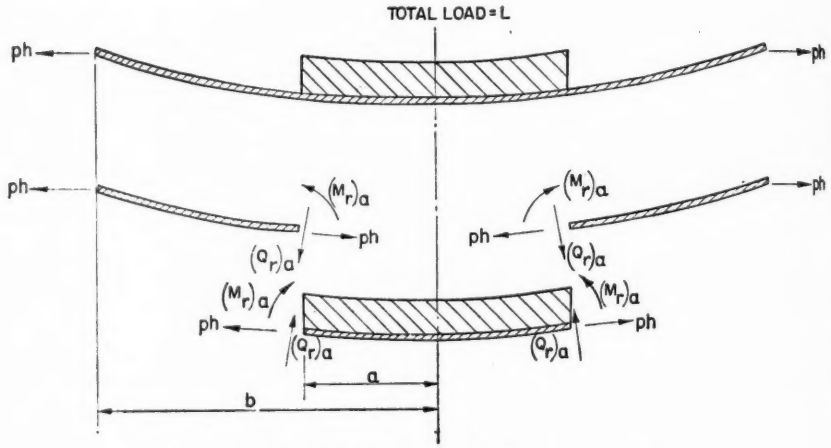

FIGURE 2. Lateral load uniformly distributed over a circle.

Considering (19), if θ is zero and b is made infinite, it is found that

$$M_r=\frac{LK_0(a\sqrt{\alpha})}{2\pi(a\sqrt{\alpha})K_1(a\sqrt{\alpha})I_0(a\sqrt{\alpha})}\left[I_0(r\sqrt{\alpha})-\frac{(1-\nu)}{r\sqrt{\alpha}}I_1(r\sqrt{\alpha})\right] \qquad (0\leqslant r\leqslant a)$$

$$M_r=\frac{L}{2\pi(a\sqrt{\alpha})K_1(a\sqrt{\alpha})}\left\{\left[K_0(r\sqrt{\alpha})+\frac{(1-\nu)}{r\sqrt{\alpha}}K_1(r\sqrt{\alpha})\right]-\frac{(1-\nu)}{r^2\alpha I_0(a\sqrt{\alpha})}\right\} (a\leqslant r\leqslant\infty)$$

$$M_\theta=\frac{LK_0(a\sqrt{\alpha})}{2\pi(a\sqrt{\alpha})K_1(a\sqrt{\alpha})I_0(a\sqrt{\alpha})}\left[\nu I_0(r\sqrt{\alpha})+\frac{(1-\nu)}{r\sqrt{\alpha}}I_1(r\sqrt{\alpha})\right] \qquad (0\leqslant r\leqslant a)$$

$$M_\theta=\frac{L}{2\pi(a\sqrt{\alpha})K_1(a\sqrt{\alpha})}\left\{\left[\nu K_0(r\sqrt{\alpha})-\frac{(1-\nu)}{r\sqrt{\alpha}}K_1(r\sqrt{\alpha})\right]+\right.$$
$$\left.+\frac{(1-\nu)}{r^2\alpha I_0(a\sqrt{\alpha})}\right\} (a\leqslant r\leqslant\infty) \qquad (20)$$

A practical example showing the distribution of the radial moment in an infinite plate is considered later.

9. Uniformly Distributed Load

Let L be the total load uniformly distributed over the centre portion of the plate, as shown in Fig. 2.

The radial shear at any arbitrary point is given by

$$Q_r=\frac{Lr}{2\pi a^2}+ph\frac{dw}{dr}. \qquad (21)$$

Thus, for the centre portion of the plate, it can be shown that

$$\psi = C_0 I_1(r\sqrt{\alpha}) - \frac{Lr}{2\pi a^2 \alpha D} \quad . \quad . \quad . \quad . \quad (22)$$

Also, the following expressions give the radial and tangential bending moments in the plate:—

$$\left.\begin{aligned}
M_r &= -\sqrt{(\alpha)}D\left\{C_0\left[I_0(r\sqrt{\alpha}) - \frac{(1-\nu)}{r\sqrt{\alpha}} I_1(r\sqrt{\alpha})\right] - \frac{L(1+\nu)}{2\pi a^2 \alpha^{3/2} D}\right\} \quad (0 \leqslant r \leqslant a) \\
M_r &= -\sqrt{(\alpha)}D\left\{C_1\left[I_0(r\sqrt{\alpha}) - \frac{(1-\nu)}{r\sqrt{\alpha}} I_1(r\sqrt{\alpha})\right] - C_2\left[K_0(r\sqrt{\alpha}) + \frac{(1-\nu)}{r\sqrt{\alpha}} K_1(r\sqrt{\alpha})\right] + \right. \\
&\qquad \left. + \left[\frac{L}{\pi\sqrt{(\alpha)}D} - (a\sqrt{\alpha})C_0 I_1(a\sqrt{\alpha})\right]\frac{(1-\nu)}{r^2\alpha}\right\} \quad (a \leqslant r \leqslant b) \\
M_\theta &= -\sqrt{(\alpha)}D\left\{C_0\left[\nu I_0(r\sqrt{\alpha}) + \frac{(1-\nu)}{r\sqrt{\alpha}} I_1(r\sqrt{\alpha})\right] - \frac{L(1+\nu)}{2\pi a^2 \alpha^{3/2} D}\right\} \quad (0 \leqslant r \leqslant a) \\
M_\theta &= -\sqrt{(\alpha)}D\left\{C_1\left[\nu I_0(r\sqrt{\alpha}) + \frac{(1-\nu)}{r\sqrt{\alpha}} I_1(r\sqrt{\alpha})\right] - C_2\left[\nu K_0(r\sqrt{\alpha}) - \right.\right. \\
&\qquad \left.\left. - \frac{(1-\nu)}{r\sqrt{\alpha}} K_1(r\sqrt{\alpha})\right] - \left[\frac{L}{\pi\sqrt{(\alpha)}D} - (a\sqrt{\alpha})C_0 I_1(a\sqrt{\alpha})\right]\frac{(1-\nu)}{r^2\alpha}\right\} \quad (a \leqslant r \leqslant b)
\end{aligned}\right\} \quad . \quad . \quad . \quad . \quad . \quad (23)$$

10. Simply-Supported Plate with a Uniformly Distributed Load and End Tension

For a simply-supported plate, the boundary conditions correspond to the following set of equations:—

$$\left.\begin{aligned}
&C_1 I_1(a\sqrt{\alpha}) + C_2 K_1(a\sqrt{\alpha}) - \frac{L}{2\pi a \alpha D} = 0 \\
&C_1\left[I_1'(b\sqrt{\alpha}) + \frac{\nu}{b\sqrt{\alpha}} I_1(b\sqrt{\alpha})\right] + C_2\left[K_1'(b\sqrt{\alpha}) + \frac{\nu}{b\sqrt{\alpha}} K_1(b\sqrt{\alpha})\right] - \\
&\qquad - \frac{(1-\nu)}{b^2\sqrt{\alpha}} a C_0 I_1(a\sqrt{\alpha}) + \frac{L(1-\nu)}{\pi b^2 \alpha^{3/2} D} = 0 \\
&C_1\left[I_1'(a\sqrt{\alpha}) + \frac{\nu}{a\sqrt{\alpha}} I_1(a\sqrt{\alpha})\right] + C_2\left[K_1'(a\sqrt{\alpha}) + \frac{\nu}{a\sqrt{\alpha}} K_1(a\sqrt{\alpha})\right] - \\
&\qquad - C_0 I_0(a\sqrt{\alpha}) + \frac{(3-\nu)L}{2\pi a^2 \alpha^{3/2} D} = 0.
\end{aligned}\right\} \quad . \quad (24)$$

Solving these equations, it is found that C_0, C_1 and C_2 are given by the following expressions.

$$\left.\begin{aligned}
C_0 &= \frac{C}{(a\sqrt{\alpha})\,K_1(a\sqrt{\alpha})}\left\{\left[K_0(b\sqrt{\alpha})+\frac{(1-\nu)}{b\sqrt{\alpha}}K_1(b\sqrt{\alpha})\right]-\right.\\
&\qquad\left.-(a\sqrt{\alpha})\,SK_0(a\sqrt{\alpha})+2\left[S-\frac{a(1-\nu)}{b^2\sqrt{\alpha}}\right]K_1(a\sqrt{\alpha})\right\}\\
C_1 &= C\left\{\left[K_0(b\sqrt{\alpha})+\frac{(1-\nu)}{b\sqrt{\alpha}}K_1(a\sqrt{\alpha})\right]I_1(a\sqrt{\alpha})-\frac{(1-\nu)}{b^2\alpha}+\right.\\
&\qquad\left.+\frac{(1-\nu)}{b^2\alpha}K_1(a\sqrt{\alpha})\,[2I_1(a\sqrt{\alpha})-(a\sqrt{\alpha})\,I_0(a\sqrt{\alpha})]\right\}\\
C_2 &= C\left\{\left[I_0(b\sqrt{\alpha})-\frac{(1-\nu)}{b\sqrt{\alpha}}I_1(b\sqrt{\alpha})\right]I_0(a\sqrt{\alpha})-\right.\\
&\qquad\left.-\frac{(1-\nu)}{b^2\alpha}I_1(a\sqrt{\alpha})[2I_1(a\sqrt{\alpha})-(a\sqrt{\alpha})\,I_0(a\sqrt{\alpha})]\right\},
\end{aligned}\right\} \quad . \quad . \quad (25)$$

where C and S are constants defined by (11).

When $a=b$, so that the load completely covers the plate,

$$\left.\begin{aligned}
M_r &= -\frac{L(1+\nu)C}{2\pi a^2\alpha}\left\{\left[I_0(r\sqrt{\alpha})-\frac{(1-\nu)}{r\sqrt{\alpha}}I_1(r\sqrt{\alpha})\right]-\right.\\
&\qquad\left.-\left[I_0(a\sqrt{\alpha})-\frac{(1-\nu)}{a\sqrt{\alpha}}I_1(a\sqrt{\alpha})\right]\right\}\\
M_\theta &= -\frac{L(1+\nu)C}{2\pi a^2\alpha}\left\{\left[\nu I_0(r\sqrt{\alpha})+\frac{(1-\nu)}{r\sqrt{\alpha}}I_1(r\sqrt{\alpha})\right]-\right.\\
&\qquad\left.-\left[I_0(a\sqrt{\alpha})-\frac{(1-\nu)}{a\sqrt{\alpha}}I_1(a\sqrt{\alpha})\right]\right\},\\
&\text{where } \frac{1}{C}=\left[I_0(a\sqrt{\alpha})-\frac{(1-\nu)}{a\sqrt{\alpha}}I_1(a\sqrt{\alpha})\right].
\end{aligned}\right\} \quad . \quad . \quad (26)$$

Substituting the appropriate series for the Bessel functions, it can be shown that when p is zero the bending moments are given by the following well-known expressions:—

$$M_r = q\,\frac{(3+\nu)}{16}(a^2-r^2)$$

$$M_\theta = \frac{q}{16}\left[(3+\nu)\,a^2-(1+3\nu)\,r^2\right],$$

where q is the intensity of the lateral loading.

For many practical problems the parameter $(a\sqrt{\alpha})$ is appreciably less than two, in this case it is convenient to write the expressions (26) in a series form.

Now $$I_0(z)=1+\sum_{m=1}\frac{z^{2m}}{2^{2m}(m!)^2}$$

$$I_1(z)=\frac{z}{2}+\sum_{m=1}\frac{z^{2m+1}}{2^{2m+1}(m!)(m+1)!}$$

so that

$$I_0(z)-\frac{(1-\nu)}{z}I_1(z)=\frac{(1+\nu)}{2}+\sum_{m=1}\frac{z^{2m}}{2^{2m+1}(m!)^2}\left[\frac{2m+1+\nu}{m+1}\right] \tag{25}$$

$$\nu I_0(z)+\frac{(1-\nu)}{z}I_1(z)=\frac{(1+\nu)}{2}+\sum_{m=1}\frac{z^{2m}}{2^{2m+1}(m!)^2}\left[\frac{2m\nu+1+\nu}{m+1}\right].$$

Substituting these series in (26), it is found that

$$M_r=\frac{(1+\nu)}{2}CM_{r0}\left\{1+\frac{16}{(3+\nu)(a^2-r^2)}\sum_{m=2}\frac{(2m+1+\nu)(a^{2m}-r^{2m})}{2^{2m+1}(m!)^2(m+1)}\alpha^{m-1}\right\}$$

$$M_\theta=\frac{(1+\nu)}{2}CM_{\theta 0}\left\{1+\frac{16}{[a^2(3+\nu)-r^2(1+3\nu)]}\times\right.$$

$$\left.\times\sum_{m=2}\frac{[(2m\nu+1+\nu)a^{2m}-(2m+3-\nu)r^{2m}]}{2^{2m+1}(m!)^2(m+1)}\alpha^{m-1}\right\},$$

where $$\frac{1}{C}=\frac{(1+\nu)}{2}+\sum_{m=1}\frac{a^{2m}\alpha^m(2m+1+\nu)}{2^{2m+1}(m!)^2(m+1)}$$

and M_{r0} and $M_{\theta 0}$ are the corresponding moments in a plate with no end load. (26)

Provided that $(a\sqrt{\alpha})$ is reasonably small, the bending moments can be evaluated by considering the first few terms in the series. For example, suppose the end tension is 4·47 tons/in.², $E=13{,}400$ tons/in.², $\nu=0{\cdot}3$, and $a=15h$. Then $(a\sqrt{\alpha})\simeq 1$ and the maximum radial bending moment is given with sufficient accuracy by taking the first term in the series. Thus if $M_{\max 0}$ is the maximum moment in a similarly loaded plate with no end load, then

$$(M_r)_{\max}=M_{\max 0}\left(\frac{1+0{\cdot}067a^2\alpha+\ldots}{1+0{\cdot}317a^2\alpha+\ldots}\right),$$

where the end load is tensile; this gives $(M_r)_{\max}=0{\cdot}81M_{\max 0}$.

Similarly, when the end load is compressive, $(M_r)_{\max}=1{\cdot}36M_{\max 0}$.

It can be verified that, for a plate with end tension, the maximum moment acts in a radial direction; while, for a plate with end compression, the maximum moment acts in a tangential direction. For the particular example considered, the maximum tangential moment with end compression is given by

$$(M_\theta)_{\max}=1{\cdot}43\,M_{\max}.$$

11. Arbitrary End Rotation, Uniform Distributed Load, and End Tension

For an arbitrary rotation of the plate at $r=b$, the boundary conditions correspond to the following set of equations:—

$$\left.\begin{aligned}
&C_1 I_1(a\sqrt{\alpha})+C_2 K_1(a\sqrt{\alpha})-\frac{L}{2\pi a\alpha D}=0\\
&C_1 I_1(b\sqrt{\alpha})+C_2 K_1(b\sqrt{\alpha})+\frac{a}{b}C_0 I_1(a\sqrt{\alpha})-\frac{L}{\pi b\alpha D}-\theta=0\\
&C_1\left[I_1'(a\sqrt{\alpha})+\frac{\nu}{a\sqrt{\alpha}}I_1(a\sqrt{\alpha})\right]+C_2\left[K_1'(a\sqrt{\alpha})+\frac{\nu}{a\sqrt{\alpha}}K_1(a\sqrt{\alpha})\right]-\\
&\qquad -C_0 I_0(a\sqrt{\alpha})+\frac{(3-\nu)L}{2\pi a^2\alpha^{3/2}D}=0.
\end{aligned}\right\} \quad (27)$$

Solving these equations,

$$\left.\begin{aligned}
C_0&=\frac{L}{2G\pi a\alpha D I_1(a\sqrt{\alpha})}\left[G-\frac{b}{a}I_1(b\sqrt{\alpha})\right]+\frac{b\theta}{aG}-\\
&\quad -\frac{L}{2G\pi a^2\alpha^{3/2}D I_0(a\sqrt{\alpha})}\left\{\left[2I_1(a\sqrt{\alpha})-(a\sqrt{\alpha})I_0(a\sqrt{\alpha})\right]-2G\right\}\\
C_1&=\frac{L}{2G\pi a\alpha D}\left\{1-(b\sqrt{\alpha})K_1(a\sqrt{\alpha})I_0(a\sqrt{\alpha})-K_1(a\sqrt{\alpha})[2I_1(a\sqrt{\alpha})-\right.\\
&\qquad \left.-(a\sqrt{\alpha})I_0(a\sqrt{\alpha})]+\frac{b}{G}\sqrt{(\alpha)}\,\theta I_0(a\sqrt{\alpha})K_1(a\sqrt{\alpha})\right\}\\
C_2&=\frac{b\sqrt{\alpha}}{G}I_0(a\sqrt{\alpha})\left[\frac{LI_1(b\sqrt{\alpha})}{2\pi a\alpha D}-\theta I_1(a\sqrt{\alpha})\right]+\\
&\qquad +\frac{LI_1(a\sqrt{\alpha})}{2G\pi a\alpha D}[2I_1(a\sqrt{\alpha})-(a\sqrt{\alpha})I_0(a\sqrt{\alpha})],
\end{aligned}\right\} \quad (28)$$

where G is given by (18).

For a load uniformly distributed over the whole area of the plate,

$$\left.\begin{aligned}
M_r&=\frac{-\sqrt{(\alpha)}D}{I_1(a\sqrt{\alpha})}\left\{\left[\frac{L}{2\pi a\alpha D}+\theta\right]\left[I_0(r\sqrt{\alpha})-\frac{(1-\nu)}{r\sqrt{\alpha}}I_1(r\sqrt{\alpha})\right]-\frac{L(1+\nu)I_1(a\sqrt{\alpha})}{2\pi a^2\alpha^{3/2}D}\right\}\\
M_\theta&=-\frac{-\sqrt{(\alpha)}D}{I_1(a\sqrt{\alpha})}\left\{\left[\frac{L}{2\pi a\alpha D}+\theta\right]\left[\nu I_0(r\sqrt{\alpha})+\frac{(1-\nu)}{r\sqrt{\alpha}}I_1(r\sqrt{\alpha})\right]-\right.\\
&\qquad \left.-\frac{L(1+\nu)I_1(a\sqrt{\alpha})}{2\pi a^2\alpha^{3/2}D}\right\}
\end{aligned}\right\} \quad (29)$$

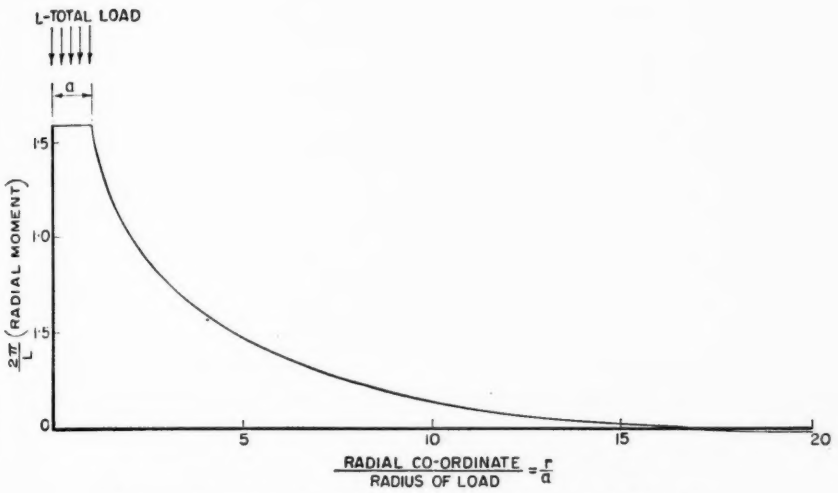

FIGURE 3. Example of a radial moment attenuation in an infinite plate.

When p and θ are zero, it can be verified that

$$M_r = \frac{q}{16}[(1+\nu)a^2-(3+\nu)r^2], \qquad M_\theta = \frac{q}{16}[(1+\nu)a^2-(1+3\nu)r^2],$$

where q is the intensity of loading.

12. Infinite Plate with End Tension and a Uniformly Distributed Circular Load

For a load distributed over a finite circular area having a diameter $2a$, the limiting values of (28) can be reduced to

$$\left.\begin{aligned} C_0 &= L\frac{[2K_1(a\sqrt{\alpha})-(a\sqrt{\alpha})K_0(a\sqrt{\alpha})]}{2\pi a^2\alpha^{3/2}DI_0(a\sqrt{\alpha})K_1(a\sqrt{\alpha})} \\ C_1 &= 0 \\ C_2 &= \frac{L}{2\pi a\alpha DK_1(a\sqrt{\alpha})} \end{aligned}\right\} \quad . \quad . \quad . \quad (30)$$

Substituting these values for the constants in (23), the resulting expressions give the radial and tangential bending moments in the infinite plate.

When the diameter of the applied loading is small and the stress at the middle plane of the plate is reasonably high, the arguments of the Bessel functions become small compared with unity.

In this case reduction of expressions (23) and (30) gives

$$\left.\begin{aligned} M_r = M_\theta &\simeq -L\frac{(1+\nu)}{4\pi}\log\left(\frac{a\sqrt{\alpha}}{2}\right) && (0 \leqslant r \leqslant a) \\ M_r &= \frac{L}{2\pi}\left\{\left[K_0(r\sqrt{\alpha}) + \frac{(1-\nu)}{r\sqrt{\alpha}}K_1(r\sqrt{\alpha})\right] - \frac{(1-\nu)}{r^2\alpha}\right\} && (a \leqslant r \leqslant \infty) \\ M_\theta &= \frac{L}{2\pi}\left\{\left[\nu K_0(r\sqrt{\alpha}) - \frac{(1-\nu)}{r\sqrt{\alpha}}K_1(r\sqrt{\alpha})\right] + \frac{(1-\nu)}{r^2\alpha}\right\} && (a \leqslant r \leqslant \infty). \end{aligned}\right\} \quad . \quad (31)$$

Also, for small values of $r > a$, it can be shown that

$$M_r = M_\theta \simeq -\frac{L}{4\pi}(1+\nu)\log\left(\frac{r\sqrt{\alpha}}{2}\right). \quad . \quad . \quad . \quad (32)$$

To illustrate the attenuation of the radial bending moment in an infinite plate, consider the example where the diameter of the loading is three times the thickness of the plate, $p = 4{\cdot}47$ tons/in.^{2}, $E = 13{,}400$ tons/in.^{2}, and $\nu = 0{\cdot}3$. Thus, in this example $a\sqrt{\alpha} = 0{\cdot}1$, so that the approximate expressions (31) can be used to determine the moment distribution. This is plotted in Fig. 3.

Acknowledgments

The author wishes to express his indebtedness to Dr. K. J. Wootton, Manager of the G.E.C. Simon-Carves Atomic Energy Group, for permission to publish this paper.

References

1. Bickley, W. G. Deflection and Vibration of a Circular Plate under Torsion, *Phil. Mag.*, Vol. 15, p. 776, 1933.
2. Bryan, G. H. On the Stability of a Plane Plate under Thrust in its own Plane with Application to the Buckling of the Sides of the Ship. *Proceedings of the London Mathematical Society*, Vol. 22, p. 54, 1891.
3. Nadai, A. Uber das Ausbeulen von Kreisformigen Platten. *V. D. I. Zeitschrift*, Vol. 59, p. 169, 1915.
4. Meissner, E. Uber das Knicken Kreisformiger Scheiben. *Schweizerische Bauzeitung*, Vol. 101, p. 87, 1933.
5. British Association Mathematical Tables. Cambridge University Press, 1950.
6. McLachlan, N. W. *Bessel Functions for Engineers*. Second Edition. Clarendon Press, Oxford, 1955.
7. Jahnke, E. and Emde, F. *Funktionentafeln*. Teubmer, Leipzig, 1933; Dover Publications, New York, 1943.
8. Dwight, H. D. *Tables of Integrals and other Mechanical Data*. Macmillan, 1953.
9. Timoshenko, S. *Theory of Elastic Stability*. McGraw-Hill, New York, 1936.

The Drag of Ducted Bodies with Annular or Side Intakes in Supersonic Flow*

H. PORTNOY

(Royal Technical College, Salford)

SUMMARY: A slender ducted body of arbitrary cross section is studied. This possesses an annular, side or "scoop" type of intake at some streamwise station. The parts of the body forward of and behind the intake are both permitted to have discontinuities of longitudinal profile slope at streamwise stations widely separated both from each other and from the intake. The external flow is taken to be entirely supersonic and it is assumed that the intake lip is sharp and that there is no "spill over" due to choking of the internal flow, which must be supersonic for a short distance inside the duct.

The interference drag between the forebody and afterbody is calculated and, since their isolated drags are known from previous work, the drag of the whole body is then known.

The results are applied to bodies of elliptic cross section and some numerical comparisons are made between different bodies of this type.

The work of this paper is applicable only to intakes with sharp lips of small external streamwise slope (because of the slenderness requirement) under conditions of no spillage.

1. Introduction

Ducted slender bodies in supersonic flow have been considered by several authors. Lighthill[1] has dealt with bodies of revolution whose meridian section may have discontinuities of slope, and a ducted body of revolution with an open nose is a special case of these results. In a similar way the results of Fraenkel[2] cover the case of an open-nosed ducted body of elliptic cross section, the eccentricity being constant, while more general open-nosed elliptic bodies have been dealt with in Ref. 3. Finally, general open-nosed slender bodies of any cross section form a special case of the theory of Ref. 4. In Ref. 4 it was indicated how the results could be applied to other types of ducted body, such as bodies with annular or side intakes, but they were not explicitly applied to the drag problem for such configurations,

*This paper is extracted from a thesis for a Ph.D. degree in the University of London, written while the author was at the Imperial College of Science and Technology.

Received July 1958

although the external side force and moment expressions were derived. It is the purpose of this present paper, using a result of Ref. 4, to deal with the external drag problem. For the particular case of a ducted body of revolution with an annular intake, a complete set of results for the external forces, together with an expression for the internal lift force, was derived by Ward[5]. In all the other references only the forces due to external pressures were considered.

The type of configuration considered here consists of a slender forebody, in which for generality we permit a finite number of widely spaced discontinuities of longitudinal profile slope, after the manner of Ref. 4, followed by a ducted afterbody, which, similarly, may have discontinuities which are far from the intake and are widely separated from each other. This ducted afterbody may have an intake of annular type (not necessarily circular) or it may have side intakes or a "scoop" intake. Whichever configuration is considered it is assumed that the external flow is independent of the internal flow; which implies that there is no "spill-over" due to choking of the internal flow, which must be supersonic for a short distance inside the body.

As an example of the method, some results and comparisons for the case of a body of elliptic cross section are given.

NOTATION

$A(z)$	major radius of an elliptic body cross section at station z
b_0	*see* equation (4)
b_{02}, b_{0I}	*see* equation (6)
$B(z)$	minor radius of an elliptic body cross section at station z
C	contour of a section $z=$constant on body
D	drag. Various suffixes define the component in question
D_I	interference drag between forebody and afterbody
e_i	values of z at which the longitudinal surface slope of a slender body is discontinuous
$F_1(S', \beta)$	*see* equation (8)
$F_2(S', \beta)$	*see* equation (10)
$H(z)$	Heaviside unit function. $H=1$ when $z>0$; $H=0$ when $z<0$
k_I	a quantity defined as 1 when considering the drag of an afterbody in the field of a forebody and as 0 when the afterbody is isolated
l	length of a body
m	number of discontinuities in an afterbody
M	free stream Mach number
r, θ, z	cylindrical polar co-ordinates
$S(z)$	cross-sectional area of a slender body at station z
t	the complex variable $\lambda e^{i\mu}$

V_0 free stream velocity

x, y, z Cartesian co-ordinates

z_2 *see* equation (13)

$\beta = \sqrt{(M^2 - 1)}$

$\gamma_m = \gamma_{mR} + i\gamma_{mI}$. *See* equation (18)

Δ symbol indicating a jump or change in a quantity

ε slender-body thickness ratio. A slenderness parameter

ζ the complex variable $x + iy$

$\lambda_b = (A + B)/2$

ν, τ normal and circumferential variables on a contour z = constant

ρ_0 free stream density

ϕ_h two-dimensional harmonic potential

ψ *see* equation (11)

Suffixes

$i, i+1$ relates to a segment of slender body between the i^{th} and the $(i+1)^{th}$ discontinuity

a, b, c relate to the bodies a, b and c.

2. The Drag of a Segment of a Slender Body Between Two Discontinuities

Let Ox, Oy and Oz be a right-handed system of axes with Oz lying in the direction of the undisturbed stream and the origin at the nose of the forebody*.

A typical body segment is considered, lying between the streamwise stations $z = e_i$ and $z = e_{i+1}$, at which not only the body streamwise slope but also the body profile radius may be discontinuous. However, as high speed exhaust gases cannot in general be treated by the method of small perturbations which is used here, a segment influenced by such gases cannot be dealt with, and so in practice the discontinuities of body radius must be such that the radius increases with increasing z, *i.e.* we permit only intake openings, except at the base, which could coincide with $z = e_{i+1}$. However, it is convenient in writing expressions for wave drag to assume the body continued downstream of the base by an infinite cylindrical extension with the base cross section. This extension does not influence the wave drag upstream of the base in supersonic flow, but enables one to define slope discontinuities at the base and so to write wave-drag expressions in a concise manner. The normal to a body contour in a plane z = constant is denoted by ν and the circumferential variable is represented by τ, while the body cross-sectional area at station z is written $S(z)$. The slenderness parameter ε may be taken as the greatest value of the streamwise slope of the body and, for the body to be slender, $S(z) = O(\varepsilon^2)$ everywhere.

*In the most general case admissible under the present analysis, *i.e.* that where the forebody has an open nose, the origin is taken at the centroid of the nose section.

In Ref. 4 it is shown that the drag, $D_{i,\,i+1}$, of the typical segment is given by

$$\frac{D_{i,\,i+1}}{\frac{1}{2}\rho_0 V_0^{\,2}} = -\oint_{C_{(i+1)-}} \left(\phi_h \frac{dv}{dz}\right)_{z=e_{i+1}-} d\tau + \oint_{C_{i+}} \left[2\,(\phi_h)_{z=e_i-} - (\phi_h)_{z=e_i+}\right]\left(\frac{dv}{dz}\right)_{z=e_i+} d\tau +$$

$$+2\left[\int_{e_i}^{e_{i+1}} S''(z)\, b_0(z)\, dz + S'(e_i+)\, b_0(e_i-) - S'(e_{i+1}-)\, b_0(e_{i+1}-)\right] + O(\varepsilon^5), \quad . \quad (1)$$

where ϕ_h is a two-dimensional harmonic potential in a plane $z=$constant which satisfies the conditions

$$\frac{\partial \phi_h}{\partial v} = \frac{dv}{dz} \quad . \quad . \quad . \quad . \quad . \quad . \quad . \quad (2)$$

on the body contour, and

$$\lim_{r\to\infty}\left(\phi_h - \frac{S'(z)}{2\pi}\log r\right) = 0, \quad . \quad . \quad . \quad . \quad (3)$$

r being equal to $\sqrt{(x^2+y^2)}$ and

$$b_0(z) = \frac{S'(z)}{2\pi}\log \tfrac{1}{2}\beta - \frac{1}{2\pi}\int_{0-}^{z} \log(z-z_1)\, dS'(z_1). \quad . \quad . \quad (4)$$

$C_{(i+1)-}$ denotes the body contour just upstream of $z=e_{i+1}$ and so on. In equation (4), $\beta=\sqrt{(M^2-1)}$ and the integral is a Stieltjes integral.

3. The Drag of a Body with Side or Annular Intakes. Interference Between the Forebody and Afterbody

The result (1) is now used to derive the interference drag between the forebody and afterbody of a configuration with intakes at a single streamwise station as described in the Introduction (*see* also Fig. 1). The drags of the forebody and afterbody being known from Ref. 4, this is the only unknown component of the drag.

The forebody is unaffected by the afterbody in supersonic flow, and so the interference drag is the drag of the afterbody in the presence of the forebody minus its drag when isolated (at the same free stream conditions).

The afterbody has discontinuities at $z=e_i$ ($i=0, 1, 2 \ldots m$), where $z=e_0$ is the position of the intake and $z=e_m$ is the position of the base.

Thus, if base drag is ignored, the following expression for the afterbody wave drag may be obtained by summation of (1). This expression covers both the case where the forebody is present and when it is absent.

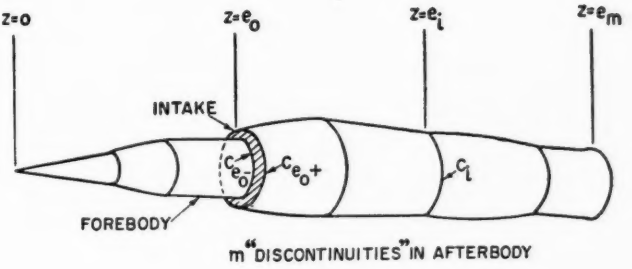

FIGURE 1.

$$\frac{\text{Wave drag of afterbody}}{\frac{1}{2}\rho_0 V_0^2} = \oint_{C_{e_0+}} \left[2k_f (\phi_b)_{z=e_0-} - (\phi_b)_{z=e_0+} \right] \left(\frac{dv}{dz} \right)_{z=e_0+} d\tau +$$

$$+ \sum_{i=1}^{m} \oint_{C_i} \left[(\phi_b)_{z=e_i-} \left(\Delta \frac{dv}{dz} \right)_i - \Delta\phi_{b_i} \left(\frac{dv}{dz} \right)_{z=e_i+} \right] d\tau +$$

$$+ 2 \left[\int_{e_0}^{e_m} S''(z)\, b_0(z)\, dz + \sum_{i=1}^{m} b_0(e_i-)\, \Delta S'_i + S'(e_0+)\, b_0(e_0-) \right] + O(\varepsilon^5), \qquad (5)$$

where k_f is defined as unity when the forebody effect is to be included and as zero otherwise. b_0 must, of course, also be defined according to the conditions. The usual notation

$$\Delta f_i = f(x, y, e_i+) - f(x, y, e_i-)$$

is used. Let

$$\left.\begin{aligned} b_{02} &= \frac{1}{2\pi} \left\{ S'(z) \log \frac{\beta}{2} H(z-e_0) - \int_{e_0+}^{z} \log(z-z_1)\, dS'(z_1) - S'(e_0+) \log(z-e_0) \right\} \\ b_{0I} &= \frac{1}{2\pi} \left\{ S'(z) \log \frac{\beta}{2} H(e_0-z) - \int_{0-}^{e_0-} \log(z-z_1)\, dS'(z_1) + S'(e_0-) \log(z-e_0) \right\} \end{aligned}\right\} \qquad (6)$$

where H is the Heaviside unit function and $\log(z-e_0)$ is taken as zero for $z < e_0$. It is evident that, for the afterbody

$b_0 = b_{02}$, when the forebody is absent;

$b_0 = b_{02} + b_{0I}$, when the forebody is present.

Hence, if D_I is the required interference drag, subtraction yields

$$\frac{D_I}{\frac{1}{2}\rho_0 V_0^2} = \oint_{C_{e_0+}} 2(\phi_h)_{z=e_0-}\left(\frac{dv}{dz}\right)_{z=e_0+} d\tau +$$

$$+2\left[\int_{e_0}^{e_m} S''(z)\, b_{0I}(z)\, dz + \sum_{i=1}^{m} b_{0I}(e_i-)\,\Delta S'_i + S'(e_0+)\, b_{0I}(e_0-)\right] + O(\varepsilon^5)$$

$$= \oint_{C_{e_0+}} 2(\phi_h)_{z=e_0-}\left(\frac{dv}{dz}\right)_{z=e_0+} d\tau + F_1(S', \beta) + O(\varepsilon^5), \quad . \quad . \quad . \quad . \quad (7)$$

where

$$F_1(S', \beta) = \frac{1}{\pi}\left\{\int_{e_0}^{e_m} S''(z)\left[S'(e_0-)\log(z-e_0) - \int_{0-}^{e_0-}\log(z-z_1)\, dS'(z_1)\right] dz - \right.$$

$$- \sum_{i=1}^{m}\left[\Delta S_i' \int_{0-}^{e_0-}\log(e_i-z_1)\, dS'(z_1) - \Delta S'_i\, S'(e_0-)\log(e_i-e_0)\right] +$$

$$\left. + S'(e_0+)\left[S'(e_0-)\log\frac{\beta}{2} - \int_{0-}^{e_0-}\log(e_0-z_1)\, dS'(z_1)\right]\right\}$$

$$= \frac{1}{\pi}\left\{\int_{e_0+}^{e_m+}\int_{0-}^{e_0-}\log\frac{1}{z-z_1}\, dS'(z_1)\, dS'(z) + S'(e_0+)\int_{0-}^{e_0-}\log\frac{1}{e_0-z}\, dS'(z) + \right.$$

$$\left. + S'(e_0+)\, S'(e_0-)\log\frac{\beta}{2} - S'(e_0-)\int_{e_0+}^{e_m+}\log\frac{1}{z-e_0}\, dS'(z)\right\}. \quad (8)$$

The drag result of Ref. 5 is readily recovered from equation (7), making use of expressions for the drag of the forebody and afterbody obtained from Ref. 1 (for example) and the fact that, for a body of revolution,

$$\phi_h = \frac{S'(z)}{2\pi}\log r.$$

Equations (7) and (8) also form an extension of equation (8.14) of Ref. 2, which gives the interference drag of an elliptic cross-sectioned configuration in which the forebody and afterbody are separated by a plane in which the longitudinal profile slope only is discontinuous (and not the body radius).

4. The Afterbody of Elliptic Cross Section

Next consider the case of a smooth afterbody having two longitudinal planes of symmetry and elliptic cross sections. For the present, no particular restrictions, apart from slenderness, will be imposed on the forebody.

The limiting case in which the elliptic intake opening is tangential to the forebody at two points is of some practical interest, as then there is something approximating to a body with side openings.

The drag of the isolated afterbody may be written down directly from the general result derived in Ref. 3, equations (10) and (11). The only "discontinuities" of the afterbody, in this case, occur at the intake end ($z=e_0$) and the base ($z=e_1$); therefore

$$\frac{D_{\text{afterbody}}}{\frac{1}{2}\rho_0 V_0^2}=\frac{1}{2\pi}\int_{e_0}^{e_1}\int_{e_0}^{e_1}\log\frac{1}{|z-z_1|}S''(z)\,S''(z_1)\,dzdz_1+\frac{1}{\pi}\left\{S'(e_0+)\int_{e_0}^{e_1}\log\frac{1}{z-e_0}S''(z)\,dz-\right.$$

$$\left.-S'(e_1-)\int_{e_0}^{e_1}\log\frac{1}{e_1-z}S''(z)\,dz-S'(e_0+)\,S'(e_1-)\log\frac{1}{e_1-e_0}\right\}+$$

$$+\frac{1}{2\pi}\left\{[S'(e_0+)]^2\log\left[\frac{4}{\beta(A+B)}\right]_{z=e_0+}+[S'(e_1-)]^2\log\left[\frac{4}{\beta(A+B)}\right]_{z=e_1-}\right\}+$$

$$+\frac{\pi}{8}\left\{\left[B^2\frac{d}{dz}\left(\frac{A}{B}\right)\right]^2_{z=e_0+}+\left[B^2\frac{d}{dz}\left(\frac{A}{B}\right)\right]^2_{z=e_1-}\right\}+O(\varepsilon^5)$$

$$=F_2(S',\beta)+\left\{\frac{[S'(e_0+)]^2}{2\pi}\log\frac{2}{A+B}+\frac{\pi B^4}{8}\left[\frac{d}{dz}\left(\frac{A}{B}\right)\right]^2\right\}_{z=e_0+}+$$

$$+\left\{\frac{[S'(e_1-)]^2}{2\pi}\log\frac{2}{A+B}+\frac{\pi B^4}{8}\left[\frac{d}{dz}\left(\frac{A}{B}\right)\right]^2\right\}_{z=e_1-}+O(\varepsilon^5), \quad . \quad (9)$$

where $A(z)$ and $B(z)$ are the major and minor radii of the section at station z, and

$$F_2(S',\beta)=\frac{1}{2\pi}\int_{e_0}^{e_1}\int_{e_0}^{e_1}\log\frac{1}{|z-z_1|}S''(z)\,S''(z_1)\,dzdz_1+\frac{1}{\pi}\left\{S'(e_0+)\int_{e_0}^{e_1}\log\frac{1}{z-e_0}S''(z)\,dz-\right.$$

$$\left.-S'(e_1-)\int_{e_0}^{e_1}\log\frac{1}{e_1-z}S''(z)\,dz-S'(e_0+)\,S'(e_1-)\log\frac{1}{e_1-e_0}\right\}+$$

$$+\frac{1}{2\pi}\left\{[S'(e_0+)]^2+[S'(e_1-)]^2\right\}\log\frac{2}{\beta} \quad . \quad . \quad (10)$$

To find the interference drag D_I it is first necessary to evaluate the contour integral appearing in (7). The body section at z on the after portion will, in this case, be given by the parametric equations

$$x=A(z)\cos\psi;\quad y=B(z)\sin\psi. \qquad (11)$$

For a body given in such a parametric form it is readily shown that, if ψ increases anticlockwise,

$$\frac{d\nu}{dz}=\frac{x_z y_\psi - y_z x_\psi}{[(x_\psi)^2+(y_\psi)^2]^{1/2}}.$$

In the present instance

$$\frac{d\nu}{dz}=\left[\frac{S'(z)}{2\pi}+\tfrac{1}{2}B^2(z)\frac{d}{dz}\left(\frac{A}{B}\right)\cos 2\psi\right]\left[A^2(z)\sin^2\psi+B^2(z)\cos^2\psi\right]^{-1/2}. \qquad (12)$$

Making the conformal transformation

$$\left.\begin{aligned} x+iy=\zeta&=t+[A^2(z_2)-B^2(z_2)]/(4t)\\ z&=z_2, \end{aligned}\right\} \qquad (13)$$

where $t=\lambda e^{i\mu}$, the body section at $z=z$ becomes a circle of radius $\lambda=\lambda_b=(A+B)/2$. Also on the body $\mu=\psi$ and

$$\left|\frac{d\zeta}{dt}\right|=\frac{1}{\lambda_b}(A^2\sin^2\mu+B^2\cos^2\mu)^{1/2}. \qquad (14)$$

The boundary condition (2) for the potential of the afterbody may now be written as

$$\frac{\partial\phi_h}{\partial\nu}=\frac{\partial\phi_h}{\partial\lambda}\left|\frac{dt}{d\zeta}\right|_{\text{body}}=\frac{d\nu}{dz},$$

$$\text{and so}\quad \frac{\partial\phi_h}{\partial\lambda}=\frac{1}{\lambda_b}\left\{\frac{S'(z_2)}{2\pi}+\tfrac{1}{2}B^2(z_2)\frac{d}{dz_2}\left(\frac{A}{B}\right)\cos 2\mu\right\} \qquad (15)$$

on the afterbody.

Now since

$$\frac{d\nu}{dz}\delta\tau=\frac{\partial\phi_h}{\partial\nu}\delta\tau=\frac{\partial\phi_h}{\partial\lambda}\left|\frac{dt}{d\zeta}\right|\left|\frac{d\zeta}{dt}\right|\lambda_b\delta\mu=\frac{\partial\phi_h}{\partial\lambda}\lambda_b\delta\mu, \qquad (16)$$

the contour integral becomes

$$\oint_{C_{e_0+}} 2(\phi_h)_{z=e_0-}\left(\frac{d\nu}{dz}\right)_{z=e_0+}d\tau=\int_0^{2\pi}2(\phi_h)_{z_2=e_0-}\left(\frac{\partial\phi_h}{\partial\lambda}\right)_{z_2=e_0+}\lambda_b d\mu. \qquad (17)$$

But, as the forebody contour lies within the ellipse at $z=e_0+$, the transformed forebody contour will lie entirely within the circle $\lambda=\lambda_b$, as do the singularities of the transformation, and hence so will all the singularities of $(\phi_b)_{z_2=e_0-}$. Therefore this potential may be expanded on the circle $\lambda=\lambda_b$ as a series in the form

$$(\phi_b)_{z_2=e_0-} = \mathscr{R}\left\{\frac{S'(e_0-)}{2\pi}\log t + \sum_{m=1}^{\infty}\frac{\gamma_m}{t^m}\right\}_{|t|=(A+B)/2} \quad . \quad . \quad (18)$$

where $\gamma_m=\gamma_{mR}+i\gamma_{mI}$, and the coefficient of $\log t$ has been immediately placed equal to $S'(e_0-)/2\pi$, as this is readily derivable using the expression analogous to (16) for the contour C_{e_0-}, together with Cauchy's theorem.

On inserting (15) and (18) in (17) one obtains

$$\oint_{C_{e_0+}} 2(\phi_b)_{z=e_0-}\left(\frac{dv}{dz}\right)_{z=e_0+} d\tau = \frac{S'(e_0+)\,S'(e_0-)}{\pi}\log\left(\frac{A+B}{2}\right)_{z=e_0+} + \\ + 4\pi\left[\gamma_{2R}\left(\frac{B}{A+B}\right)^2\frac{d}{dz}\left(\frac{A}{B}\right)\right]_{z=e_0+} \quad . \quad (19)$$

Equation (7) now gives, upon substituting this result,

$$\frac{D_I}{\frac{1}{2}\rho_0 V_0^2} = \frac{S'(e_0+)\,S'(e_0-)}{\pi}\log\left(\frac{A+B}{2}\right)_{z=e_0+} + 4\pi\left[\gamma_{2R}\left(\frac{B}{A+B}\right)^2\frac{d}{dz}\left(\frac{A}{B}\right)\right]_{z=e_0+} \\ + F_1(S',\beta)+O(\varepsilon^5). \quad . \quad . \quad (20)$$

It is worth noting two results which follow from (20).

(*i*) If the eccentricity of the afterbody sections is constant, *i.e.* $d(A/B)/dz=0$, then D_I does not depend on the cross-sectional shape of the forebody, but only on $S'(e_0-)$.

(*ii*) If the forebody is circular,

$$(\phi_b)_{z=e_0-} = \mathscr{R}\left\{\frac{S'(e_0-)}{2\pi}\log\zeta\right\} .$$

Therefore $$(\phi_b)_{z_2=e_0-} = \mathscr{R}\left\{\frac{S'(e_0-)}{2\pi}\left[\log t + \frac{A^2(e_0+)-B^2(e_0+)}{4t^2}+O\left(\frac{1}{t^4}\right)\right]\right\},$$

and so $$\gamma_{2R}=[A^2(e_0+)-B^2(e_0+)]\,\frac{S'(e_0-)}{8\pi},$$

whence $$\frac{D_I}{\frac{1}{2}\rho_0 V_0^2} = S'(e_0-)\left[\frac{S'(e_0+)}{\pi}\log\frac{A+B}{2}+\frac{1}{2}B^2\left(\frac{A-B}{A+B}\right)\frac{d}{dz}\left(\frac{A}{B}\right)\right]_{z=e_0+} + \\ + F_1(S',\beta)+O(\varepsilon^5). \quad . \quad (21)$$

5. Example

The foregoing results are now used to compare the drags of three ducted bodies having the same distribution of cross-sectional area, the same forebody, and possessing two streamwise planes of symmetry. The forebody is a circular cone of semi-angle ε, and it extends to half way along the total body length, this last quantity being denoted by l. The ratio $S(e_0+)/S(e_0-)$ is taken to be 1·5.

The three bodies differ in the shape of the after portion. The first (body *a*) has an axi-symmetric afterbody in the form of a cone frustum also of semi-angle ε. The second configuration (body *b*) has elliptic afterbody sections varying from a section tangential to the forebody at top and bottom, at the intake, to a circular base, $d(A/B)/dz$ being held constant. Finally, body *c* also has elliptic sections and an intake opening tangential to the forebody at the top and bottom, but its sections have constant eccentricity. Their drags are respectively denoted by D_a, D_b, and D_c. It is found in the Appendix, from equations (9) and (21), that

$$\frac{D_a - D_b}{\frac{1}{2}\rho_0 V_0^2} = -0{\cdot}274\pi l^2 \varepsilon^4, \qquad (22)$$

and

$$\frac{D_a - D_c}{\frac{1}{2}\rho_0 V_0^2} = 0{\cdot}042\pi l^2 \varepsilon^4, \qquad (23)$$

the errors being $O(\varepsilon^5)$, and, using the result of Ref. 5 to obtain D_a (*see* Appendix),

$$\frac{D_a - D_b}{D_a} = \frac{-0{\cdot}110}{0{\cdot}219 - \log \beta\varepsilon} + O\left(\frac{\varepsilon^2}{\log \varepsilon}\right). \qquad (24)$$

$$\frac{D_a - D_c}{D_a} = \frac{0{\cdot}017}{0{\cdot}219 - \log \beta\varepsilon} + O\left(\frac{\varepsilon}{\log \varepsilon}\right). \qquad (25)$$

These last two expressions are plotted in Fig. 2 against $\beta\varepsilon$. It should be noted that the drag differences shown in (22) and (23) are independent of Mach number, as this only enters the drag expressions through the functions $F_1(S', \beta)$ and $F_2(S', \beta)$ of equations (21) and (9), respectively, which are eliminated in subtraction, as all the bodies have the same $S'(z)$ distribution.

Evidently body *c* has the smallest drag, followed by *a* and lastly by *b*. This is similar to the result of Ref. 2, where it is shown that open-nosed elliptic bodies of constant eccentricity have less drag than the body of revolution with the same cross-sectional area distribution. It appears that changing to elliptic sections tends to decrease the drag, but varying the eccentricities of the sections has an adverse effect which can completely overcome the advantage of the elliptic sections, as here.

From Fig. 2 it is seen that neither *b* nor *c* has a drag more than a few per cent different from that of the equivalent body of revolution *a*, in the range considered (which is a reasonable working range for the theory). Thus it may be expected that the tangential elliptic opening is as good an approximation to any of the usual side opening intakes as will ever be required in practice, since these are generally closer to the tangential elliptic opening than it is itself to the circular intake.

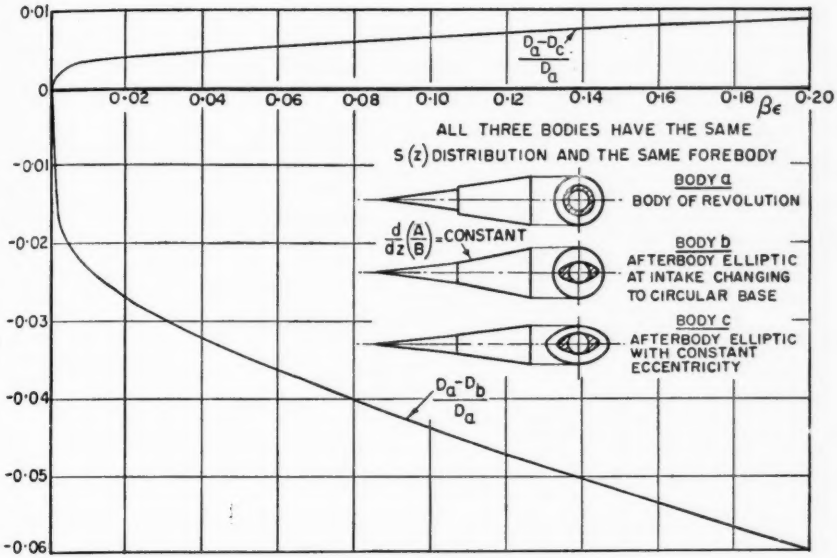

FIGURE 2.

As D_b and D_c differ so little from D_a, Ward's result[5] would be adequate practically for finding these drags except for very low values of $\beta\varepsilon$, especially since the differences are of the same order, or approaching the same order, as the error terms, except for these low values.

However, the configurations *b* and *c* are not very different from bodies of revolution and it is to be expected that for bodies diverging further from the axi-symmetric shape, *e.g.* much flatter elliptic sections with larger variations of eccentricity, or bodies carrying nacelles on narrow wings (which could be treated by the present general method if certain restrictions were fulfilled), the differences from the axi-symmetric result would not be negligible. This would also, most probably, be the case for bodies not possessing two planes of symmetry, such as bodies with "scoop" intakes.

ACKNOWLEDGMENT

The author would like to express his sincere thanks to Dr. L. E. Fraenkel, who directed this research, for his help and advice.

Appendix

All three bodies described in the example in Section 5 have the same area distribution, given by

$$\left.\begin{aligned} S(z) &= \pi\varepsilon^2 z^2, && 0 < z < l/2 \\ \text{and} \quad S(z) &= \pi\varepsilon^2 \{ l/2(\sqrt{1{\cdot}5}-1)+z \}^2, && l/2 < z < l \end{aligned}\right\} \quad . \quad . \quad . \quad (26)$$

The station $z=e_0$ is therefore at $z=l/2$.

In addition, for bodies b and c, the value of the ratio A/B for the elliptic intake opening is seen to be 1·5. For body c this value of A/B is maintained until the base, whereas for body b it varies at a constant rate to produce a circular base. Thus the constant value of $d(A/B)/dz$ equals $-1/l$.

Since all three bodies have the same axi-symmetric forebody, the difference of the drags of any two of them equals the sum of the differences of their isolated afterbody drags, as given by equation (9), and their D_1's, as given by (21). Also, since $S'(z)$ is the same for all three, the functions F_1 and F_2 disappear on subtraction as they depend only on $S'(z)$ and β.

Thus, using (26) with equations (9) and (21),

$$\frac{D_a-D_b}{\frac{1}{2}\rho_0 V_0^2}=\frac{(\sqrt{1\cdot5}\,\pi\varepsilon^2 l)^2}{2\pi}\left(\log\frac{2}{\sqrt{1\cdot5}\,\varepsilon l}-\log\frac{2}{1\cdot25\,\varepsilon l}\right)-\frac{\pi}{8l^2}\left(\frac{\varepsilon l}{2}\right)^4-\frac{\pi}{8l^2}(\sqrt{1\cdot5}+1)^4\left(\frac{\varepsilon l}{2}\right)^4+$$

$$+\frac{(\pi\varepsilon^2 l)(\sqrt{1\cdot5}\,\pi\varepsilon^2 l)}{\pi}\left(\log\frac{\sqrt{1\cdot5}\,\varepsilon l}{2}-\log\frac{1\cdot25\,\varepsilon l}{2}\right)-$$

$$-\tfrac{1}{2}(\pi\varepsilon^2 l)\left(\frac{\varepsilon l}{2}\right)^2\left(\frac{0\cdot5}{2\cdot5}\right)\left(\frac{-1}{l}\right)+O(\varepsilon^5)$$

$$=-0\cdot274\,\pi l^2\varepsilon^4+O(\varepsilon^5)\,, \qquad . \quad . \quad . \quad . \quad (27)$$

which is equation (22).

In the same way equation (23) is derived.

The result of Ref. 5 is for the drag of the whole of a ducted body of revolution of unit length without discontinuities other than those at the intake station and the base. In the present notation, and adjusted to a length l, it reads

$$\frac{D}{\frac{1}{2}\rho_0 V_0^2}=\frac{1}{2\pi}\int_0^l\int_0^l\log\frac{1}{|z-z_1|}S''(z)\,S''(z_1)\,dz_1\,dz-\frac{S'(l)}{\pi}\int_0^l\log\frac{1}{l-z}S''(z)\,dz+$$

$$+\frac{[S'(l)]^2}{2\pi}\log\frac{2}{\beta}\sqrt{\left[\frac{\pi}{S(l)}\right]}+\frac{S'(e_0+)-S'(e_0-)}{\pi}\left\{\int_0^l\log\frac{1}{|e_0-z|}S''(z)\,dz-\right.$$

$$\left.-S'(l)\log\frac{1}{l-e_0}\right\}+\frac{1}{2\pi}\left\{S'(e_0+)-S'(e_0-)\right\}^2\log\frac{2}{\beta}\sqrt{\left[\frac{\pi}{S(e_0+)}\right]}+$$

$$+\frac{[S'(e_0-)]^2}{4\pi}\log\frac{S(e_0+)}{S(e_0-)}+O(\varepsilon^5)\,. \quad (28)$$

The error term is that found in Ref. 4, as used throughout this paper, whereas Ward gives $O(\varepsilon^6\log^2\varepsilon)$.

Equation (28) can be obtained from the results of the present paper as a special case.

Substitution of (26) in (28) yields

$$\frac{D_a}{\frac{1}{2}\rho_0 V_0^2}=\pi l^2\varepsilon^4(2\cdot50\log\frac{1}{\beta\varepsilon}+0\cdot548)+O(\varepsilon^5)\,. \quad . \quad . \quad . \quad . \quad (29)$$

This result, together with (22) and (23), gives (24) and (25).

REFERENCES

1. LIGHTHILL, M. J. Supersonic Flow past Slender Bodies of Revolution, the Slope of whose Meridian Section is Discontinuous. *Quarterly Journal of Mechanics and Applied Mathematics*, Vol. I, March 1948.

2. FRAENKEL, L. E. Supersonic Flow Past Slender Bodies of Elliptic Cross-Section. R. & M. 2954, 1952.

3. PORTNOY, H. The Forces on the General Slender Body of Elliptic Cross-Section in Supersonic Flow. *Journal of the Aeronautical Sciences*, Readers' Forum, Vol. 23, January 1956.

4. FRAENKEL, L. E. and PORTNOY, H. Supersonic Flow past Slender Bodies with Discontinuous Profile Slope. *The Aeronautical Quarterly*, Vol. VI, May 1955.

5. WARD, G. N. The Supersonic Flow past a Slender Ducted Body of Revolution with an Annular Intake. *The Aeronautical Quarterly*, Vol. I, February 1950.

Review

The Potential Theory of Unsteady Supersonic Flow. J. W. Miles. Cambridge University Press, London, 1959. 220 pp. Illustrated. 45s.

"Observe how . . . the critic is invariably a tremendous specialist in the subject under review, and must at all costs be more so than the author of the book discussed. It doesn't matter if the subject is as remote as the study of Greek in Lower California, the reviewer must be there before."[1] It seems only fair to warn readers at the outset that this fundamental principle will not be upheld in the present review, for the reviewer's knowledge of unsteady supersonic flow, even though it were fortified by every gambit in the Lifeman's armoury, would still be no match for Professor Miles's complete mastery of his subject.

In a sense the problems of unsteady linearised wing theory are of a classical type, and may be viewed as an exercise (for advanced students) in the theory of sound: if the co-ordinate system is fixed in still air, one seeks solutions of the wave equation which satisfy certain mixed boundary conditions in the plane of the wing, and this may be achieved, in principle, by a suitable distribution of retarded-potential doublets in that plane. Unfortunately this approach (due to Kirchhoff[2]) leads, in general, to rather terrible integral equations for the doublet strength (although for points influenced only by a supersonic leading edge the problem is simpler: sources of known strength may be used), and modern workers have tended to explore a number of other avenues. It is this recent work which Professor Miles expounds, and one is left with the following general impression.

The choice of a best co-ordinate system is not obvious: co-ordinates fixed in still air are "natural" for the potential equation and the pressure relation, and co-ordinates moving with the wing for the boundary condition: other systems, with unnatural times, may effect a compromise. Integral transforms (one, two, or three may be used, according to the problem) are invaluable in reducing the algebra to reasonable proportions. The transformed problem is straightforward for two-dimensional wings and those with supersonic leading edges; it turns out to be an old one in diffraction theory for the semi-infinite rectangular wing; and it has a solution in Mathieu functions for the complete rectangular wing. The inversion and numerical evaluation of this last solution is not without difficulties, and for wings with subsonic side edges an extension of Evvard's method offers the best hope of success. But for the delta wing with subsonic edges one must accept defeat, and expand in powers of the frequency. Finally, if the aspect ratio

can possibly be considered "small", one is in the calmer realm of slender-wing theory, but even here high frequencies may require the addition of a time derivative to the transverse-plane Laplace equation, and thus make the problem more difficult than in steady flow.

Professor Miles steps nimbly through this material, with as much unity of method as the vagaries of the subject allow. In addition to the acoustic and slender-wing theories already mentioned, he systematically derives six other approximate equations for the velocity potential, together with the restrictions on reduced frequency, amplitude, aspect ratio, and Mach number appropriate to each. Slender non-planar bodies are also treated, non-linear problems are described briefly, and an appendix deals with reverse flow theorems. The main applications are to damping in pitch and gust loading. There is no space for such questions as accelerated flight, drag, or the calculation of all the relevant forces and derivatives, but ample references are given to papers on those topics.

The reviewer was able to detect only two minor flaws. First, the restriction to a perfect gas (p. 1) is unnecessary for the linearised approximations with which the book is mainly concerned. Secondly, the special notation $\partial n/\partial x$ and $\partial n/\partial t$ of slender-body theory (pp. 158-9) should be defined, for the function $n(x,s,t)$, which the author uses explicitly, is meaningless and does not exist in general.

The reader is expected to concentrate and to skip no pages; constant reference is made to the material in earlier chapters (usually by equation numbers only), and the pace of the mathematics may leave the reader somewhat breathless at first—but gradually a definite pattern emerges.

This authoritative account of an important subject, with its complete guide to the existing literature, is a most welcome addition to the aerodynamicist's library.

L. E. FRAENKEL.

REFERENCES

1. POTTER, S. *Lifemanship.* Hart-Davis, London, 1950.

2. KIRCHHOFF, G. Zur Theorie der Lichtstrahlen, Sitzungsberichte der Preussischen Akademie der Wissenschaften, Berlin, 1882.